Université catholique de Louvain
Ecole polytechnique de Louvain
Institute of Mechanics, Materials and Civil Engineering

Field and model investigation of flow and sediment transport in the Lower Mekong River

Thesis presented for the degree of Doctor in Engineering Sciences by

Hoang Anh Le

In partial fulfilment of the requirements for the degree of
DOCTOR IN ENGINEERING SCIENCES

Members of the Jury:

Prof. Sandra Soares-Frazão, Université catholique de Louvain, Belgium,	Promoter
Dr. Nicolas Gratiot, Université Grenoble Alpes, France,	Promoter
Prof. Eric Delersnijder, Université catholique de Louvain, Belgium	
Assoc. Prof. Alessandra Crosato, IHE Delft, The Netherlands	
Dr. Pham Van Chien, Thuyloi University, Vietnam	
Dr. Jonathan Lambrechts, Université catholique de Louvain, Belgium	Secretary
Prof. Hervé Jeanmart	President

Louvain-la-Neuve, June 2020

Acknowledgments

I would like to begin this thesis by thanking you for your contribution to the accomplishment of my work.

First of all, I wish to express the deepest appreciation to my first promoter, Prof. Sandra Soares-Frazão for her kind supports during my doctoral study processes. Her professional knowledge and valuable advices give me a good direction for pursuing my study. Without her guidance and persistent helps, this thesis would not be possible.

I would like to acknowledge my co-promotor, Dr. Nicolas Gratiot. He taught me very much, professionally and humanly. During my first trip in Laos, I was really confused with new devices and techniques as well as a hard schedule but he was very enthusiastic to give me guidance. Many long tele-discussions and also hard questions incented me to widen my research from various perspectives. It is my pleasure to work with him.

My sincere thanks go to Prof. Eric Deleersnijder, who gives me an opportunity to join in the SLIM team. His enthusiasm and meticulousness remind me passion at works and valuable results.

I greatly appreciate Dr. Jonathan Lambrechts for his patience over years. His kindness reassured me when I was facing with digital and SLIM problems, and encouraged me continuing my work.

I extend my acknowledgment to all my jury members for their meticulous readings and worth comments on my thesis as well as relative references.

This work cannot be completed without the fellowship from the Université catholique de Louvain, a support from the Centre Asiatique de Recherche sur l'Eau (CARE-Rescif), Vietnam and the Institut de Recherche pour le Développement (IRD), France to fund the field survey in Laos. I would like send my great thanks to my colleagues from the Mekong River Commission, the Vietnam Meteorological and Hydrological Administration, the Lower Mekong Delta Coastal Zone project, experts from the Danish Hydraulic Institute (DHI), Vietnam. Special thanks are sent to Assoc. Prof. Nguyen Thong from the Centre Asiatique de Recherche sur l'Eau (CARE-Rescif),

HoChiMinh city University of Technology, Vietnam for his enthusiasm when giving me fruitful guidance and comments on my works in TELEMAC-2D; and Dr. Doan Quang Tri from the Vietnam Journal of Hydrometeorology for sharing indispensable data during my study.

I'd love to show a warm thankfulness to my dear officemates, Insaf Draoui and Jovana Jezdimirović for making the most friendly working place and sharing our daily lives. Thanks to all SLIM members, especially Valentine Vallaeys and David Vincent, who create an ideal group and functional meetings to discuss about SLIM works and give me fruitful recommendations to solve my problems.

My heartfelt thanks are given to the aids and helps of my Vietnamese friends in Belgium. Thank you for being with me on special vacations and bringing me warmness of home and family.

With the deepest sense of gratitude, I would like to send my family. Even you are living so far from me but you are always besides me whenever I need and share my happiness and weakness.

The last but very important person, that I am indebted, is my beloved daughter, Thu Minh. Sometimes she gives me a lot of troubles but without her, I will lose my motivation.

June, 2020

Le Hoang Anh

Table of contents

Acronyms

a.s.l.	above sea level
CFL	Courant-Friedrichs-Lewy
LMB	Lower Mekong Basin
MRC	Mekong River Commission
PoR	Plain of Reed
LXQ	Long Xuyen Quadrangle
PSD	Particle size distribution
SCAF	System for the Characterization of Aggregates and Flocs
SLIM	Second-generation Louvain-la-Neuve Ice-ocean Model
SSC	Suspended Sediment Concentration
UMB	Upper Mekong Basin
VMD	Vietnamese Mekong Delta
W-D	Wetting - Drying

Chapter 1 Introduction

1.1 Motivations

Civilizations have been intimately connected to rivers for thousands of years (Wright et al., 1978, Wright et al., 2011 and Bianchi, 2016) because ancient people used rivers for the most basic human needs such as water, food, transportation and recreation. At present, approximately 2.7 billion people are living in major river basins in the world (Best et al., 2018). During significant socio-economic development and industrial revolution periods, rivers and their basins have been vastly modified (Goudie et al., 2018). The combination of natural disasters and anthropogenic pressures may threaten the riverine hydrology, morphology and ecosystems in massive ways. These threats are expected to continue in the coming decades (Vörösmarty et al., 2010, Varis et al., 2012).

The Mekong is one of the largest rivers in the world (Kite, 2001). It provides livelihood for approximately 70 million people (Mekong River Commission - MRC website, www.mrcmekong.org/) and plays an essential role in the socio-economic development of the Southeast Asian countries (Piman et al., 2013), where riparian people, plants and animals depend on its annual cycle of flood and drought (Kite, 2001). Although the Mekong is still one of few major river systems in the world whose water resources have yet to be developed extensively (MRC, 2009, Varis et al., 2012), it has been faced with the major issues below.

Floods and droughts

Floodings in the Mekong Basin has been caused by the operation of upstream hydropower plants, water infrastructures, tidal regimes (Le et al., 2007), heavy rains and unsustainable urbanization (Huong et al., 2013). Annual floods result in large inundation areas of approximately 2 million ha with water depth of 0.5 – 4.0 m and flooding duration of 3 – 6 months (Triet et al., 2017). Besides benefits to soil fertility and productivity, floods are responsible for disasters such as fatalities, damages to infrastructure, property, crops and disruption of social and economic activities throughout the basins (Käkönen et al., 2008, Garschagen et al., 2012). The annual average cost of the floods in the Lower Mekong Basin (LMB) is estimated to be approximately US$ 60 - 70 million (MRC, 2017).

On the other hand, drought is a natural hazard and complex phenomenon, damaging to agricultural production and livelihood of sensitive communities (Son et al., 2012). According to a report by Vietnam's Ministry of Agriculture and Rural Development (2016), the severe drought in the dry season 2015 - 2016 strongly affected 11 of the 13 provinces in the Vietnamese Mekong Delta (VMD), the damage cost is estimated to be approximately US$ 1.5 billion.

Sediment budget and erosion

The sediment flux in the Mekong Basin has already decreased by almost five folds over 35 years, from about 160 Mtons/year in 1983 (Milliman et al., 1983) to 87.4 ± 28.7 Mtons/year in 2005 (Darby et al., 2016 and Schmitt et al., 2017), 75 Mtons/year in 2009 (Kummu et al., 2010) and 40 ± 20 Mtons/year in 2015 - 2016 (Ha et al., 2018). The reduction of sediment flux is mainly caused by the construction and operation of upstream hydropower plants (Kummu and Varis, 2007, Anthony et al., 2015, Lovelock et al., 2015). The cumulative sediment trapped by reservoirs can reach up to 96 % of total volume (Kondolf et al., 2014), thus the sediment volume supplied to the delta falls to approximately 9 Mtons/year (Schmitt et al., 2019). Sand mining along the river is considered to play an additional role in the sediment budget reduction in the downstream (Brunier et al., 2014 and Anthony et al., 2015). The reduction in sediment supply would likely have profound implications for the sustainability of the river landform, it may exacerbate erosion patterns along

river banks and in the delta area (Kummu and Varis, 2007). In the period of 2003 - 2012, over 50 % of the VMD shoreline experienced erosion (Anthony et al., 2015). Even if some areas are eroded under ocean forcings, a large-scale sediment is redistributed (Marchesiello et al., 2019).

Other reasons or erosion could be intensive agricultural production, groundwater over-exploitation, land-use changes, climate changes (Anthony et al., 2015, Piman and Shrestha, 2017) and intensive waterway transports (Renaud and Kuenzer, 2012).

Salt intrusion

Salt intrusion affects approximately 45 % of the VMD in the dry season (Renaud and Kuenzer, 2012) and it has been exacerbated significantly in recent years by the modified upstream inflows, relative sea level rises as the best-known consequence of climate change (Garschagen et al., 2012) and human induced subsidence. It causes significant damages to agri- and aqua-cultural production and freshwater supplies (Duong et al., 2018b).

Severe salt intrusion often occurs in the VMD from the end of February to April, causing higher salinity in rivers and irrigation channels. Normally, seawater, with salt concentration of > 4 g/L, intrudes 45 - 60 km up-river (Wolanski et al., 1996, Wolanski et al. 1998 and Nowacki et al., 2015) in an area of 18,000 km^2 (Smajgl et al., 2015). Historically, severe salt intrusion events have occurred in the years with strong El Niño, particularly in 1998 and 2010 (Wassmann et al., 2019). Recently in the dry season 2019 - 2020, due to a short rainy season and low upstream flow, the drought came approximately 2 months earlier and resulted in the most extensive salt intrusion event during last 90 years. According to a report composed by the United Nations Resident Coordinator Office in Vietnam (2020), the salt intrusion has entered up to 110 km inland, more than 30 km beyond the highest long-term average levels of the dry season 2015 - 2016.

Water quality

Over the last 30 years, the Mekong River has been faced with environmental degradation due to multiple pressures, including rapid population growth, industrialization, intensive agricultural production (Chea et al., 2016). In

particular, several sites such as the northwestern Thailand, the Tonle Sap lake, and swamps in Laos are considered to be hotspots of water pollution, which are characterized by high concentrations of nutrient and dissolved solids (Chea et al., 2016). The water quality degradation in the VMD (Garschagen et al., 2012) is mainly due to the excessive abuse of agrochemicals (Käkönen et al., 2008) together with waste and sewage from domestic and development activities (Renaud and Kuenzer, 2012). Other contamination sources are heavy metals from mineral mining activities (Fu et al., 2012) and the geochemical origin of the basin (Buschmann et al., 2008). Water pollution also causes negative stresses on the basin ecosystem, evenly the extinction of some species. Best et al. (2018) predicted that the ecology of the Mekong Basin may likely collapse before the end of this century.

Climate change

Climate change, with a particular emphasis on sea level rise, is likely to further enhance these stresses in the medium and long-term perspectives. According to Asian Development Bank (ADB) (2009a), an area of approximately 12,300 km^2, equivalent to 31 % of the VMD area will be inundated in 2100. It would affect 9,800 km^2 of agri- and aqua-culture areas as well as 4.8 million people. Recent studies implemented by Minderhoud et al. (2019) and Kulp and Strauss (2019) pointed out the inundation area may rise upto 75 % of the whole VMD area by relative sea level rise. Contemporarily, storm surge is also considered one of the biggest hazards that threaten the Mekong coastal communities in Vietnam. The highest water elevation due to storm surges in the past six decades was estimated to approximately 1 m (Takagi et al., 2014) which constitutes a significant threat in this very flat area.

However, in such an important and transboundary river basin, the hydrodynamics and sediment transport mechanisms have not been comprehensively documented yet. Historical studies generally focused on limited regions of the delta (Hung et al., 2012, Hanington et al., 2017). Only recently researches have paid more attention to the whole domain by extensive monitoring networks (Dang et al., 2016, Gugliotta et al., 2017), satellite observations (Balica et al. 2013 and Yamazaki et al. 2014) and by applying 1D (Hoa et al., 2008, Katoush et al., 2017, Duong et al., 2018 and Dang et al., 2018a), semi/quasi 2D (Triet et al. 2017), or 1D - 2D coupled models (Le et

al. 2007, Eslami et al., 2019, Thanh et al., 2020). Other works are concentrated in the impacts of dyke systems on the hydrodynamics (Fujihara et al., 2015, Duc Tran et al., 2018, Aires et al. 2020). Even so, several studies have assessed the basin hydrodynamics on a large scale. Therefore, a comprehensive study on flow dynamics and sediment transport processes in the LMB is extremely essential for the authorities and scientists to design proper measures for the integrated water resources management.

1.2 Objectives

Since 2010, the RESCIF (Réseau d'excellence des sciences de l'ingénieur de la francophonie) network has been established. Its initiative is to promote joint scientific programmes between countries which are subject to extremely challenging climate conditions and countries of scientific excellence. Hence, the thesis is implemented under the collaboration of two member institutions of the network: the Université catholique de Louvain, Belgium and the Centre Asiatique de Recherche sur l'Eau (CARE), Vietnam. The aim is to create an academic interconnection between two institutions and conduct a comprehensive research on the flow and sediment transport in the LMB, which plays a vital role in the Southeast Asia.

The global target of the study is a better understanding of water and sediment dynamics in the Lower Mekong Basin (LMB) that may provide robust information to decision makers and stakeholders, and suggest proper governance measures for the basin. A clear knowledge and understanding of processes driving the flow and sediment regimes must be obtained before implementing further studies on unsolved issues. To this end, both field and model investigations in the domain are developed. The work is undertaken following three main directions with specific objectives related to the main objective stated before.

The first direction concerns the field and laboratory investigation of sediment properties along the LMB, with particular concentrations on particle sizes, settling velocities, flocculation index and assumption concerning sediment transport mechanics, which have not been fully documented previously. This work is conducted through three field survey campaigns in three different

environments, from the fluvial and lacustrine environments to the estuaries with the supports of the Institut de Recherche pour le Développement (IRD), France, the Lower Mekong Delta Coastal Zone (LMDCZ) project and the CARE-Rescif, an international joint laboratory (hosted by the HoChiMinh city University of Technology, Vietnam). The findings of this work aim at constituting a reliable data source for further sediment transport studies and implications for the Mekong Delta management.

The second research direction is the numerical simulation of the inundation and subsequent drying processes in the Tonle Sap lake, an integral part of the LMB, located in the Cambodia floodplain. Clearly, the accurate simulation of wetting - drying processes in floodplains has been a challenge for hydrodynamic modelers for recent decades. In order to improve the modelling of inundation and drying processes, we integrated an existing wetting - drying algorithm and implement it in two-dimensional SLIM software (the Second-generation Louvain-la-Neuve Ice-ocean Model, www.slim-ocean.be), which solves the shallow water equations by means of the (discontinuous Galerkin) finite element method, in a fully implicit way. The new technique should meet the requirements for mass conservation and computational efficiency. The simulation results were then used to assess hydraulic relations between the Tonle Sap lake and the Mekong Delta.

The third research direction concerns the spatial and temporal distribution of the flow and sediment dynamics in the Vietnamese Mekong Delta (VMD). This subject was performed during the time working in the CARE (HoChiMinh city University of Technology, Vietnam). The flow and sediment distribution are investigated by the combination of the finding results from the first objective of the thesis, available hydrological data from the CARE and an existing hydrodynamic model used by the HoChiMinh City University of Technology. This model is developed under TELEMAC-2D, a robust and well-known simulation tool. It is coupled with SISYPHE module to simulate flow and sediment transport in the VMD. Using this tool and the previous results, the objective is to evaluate the effects of the multi-channel system on the hydro- and sediment- dynamic modifications in the VMD.

1.3 The Lower Mekong Basin

1.3.1 Topography

The Mekong River is the twelfth longest river in the world. It originates from the Tibetan Plateau (China) with an elevation of more than 5000 m above sea level (a.s.l.), a length of 4400 km and a basin area of 795,000 km^2. Its mean annual discharge is approximately 475 km^3, i.e. the sixth largest in the world. The river passes through a variety of geomorphological and climatic systems (in Myanmar, Laos, Thailand and Cambodia) (Schmitt et al., 2018) and discharges to the fertile delta of Vietnam and Cambodia (with an area of 55,000 km^2), before draining into the East Sea of Vietnam (MRC website www.mrcmekong.org/) (see Fig.1.1).

To study the hydrological regime of the Mekong River, it is usually divided into two key sub-regions: the Upper Mekong Basin (UMB), covering area apart from China and Myanmar makes up 24 % of the total area, contributes to 15 - 20 % of the water volume and 50 % of the suspended sediment load (Walling et al., 2009). The area from Chiang Sean, Laos to the delta of Vietnam makes up the Lower Mekong Basin (LMB) (MRC, 2015) (see Fig. 1.2).

The LMB covers an area of approximately 606,000 km^2 in Cambodia, Laos, Thailand, and Viet Nam territories (MRC, 2009). The topographical condition is characterized by low and flat features (Chea et al., 2016). The mean population density in the whole area is approximately 116 people/km^2, while the high density is found in the part of Vietnam, approximately 427 people/km^2 (General Statistics of Vietnam, 2016). The LMB was selected as the study area because of its significant role on supplying food, water, natural resources, accommodation, transportation and high ecological values for approximately 70 million residents (MRC website).

Fig. 1.1. Topographical map of the Mekong River basin (MRC website)

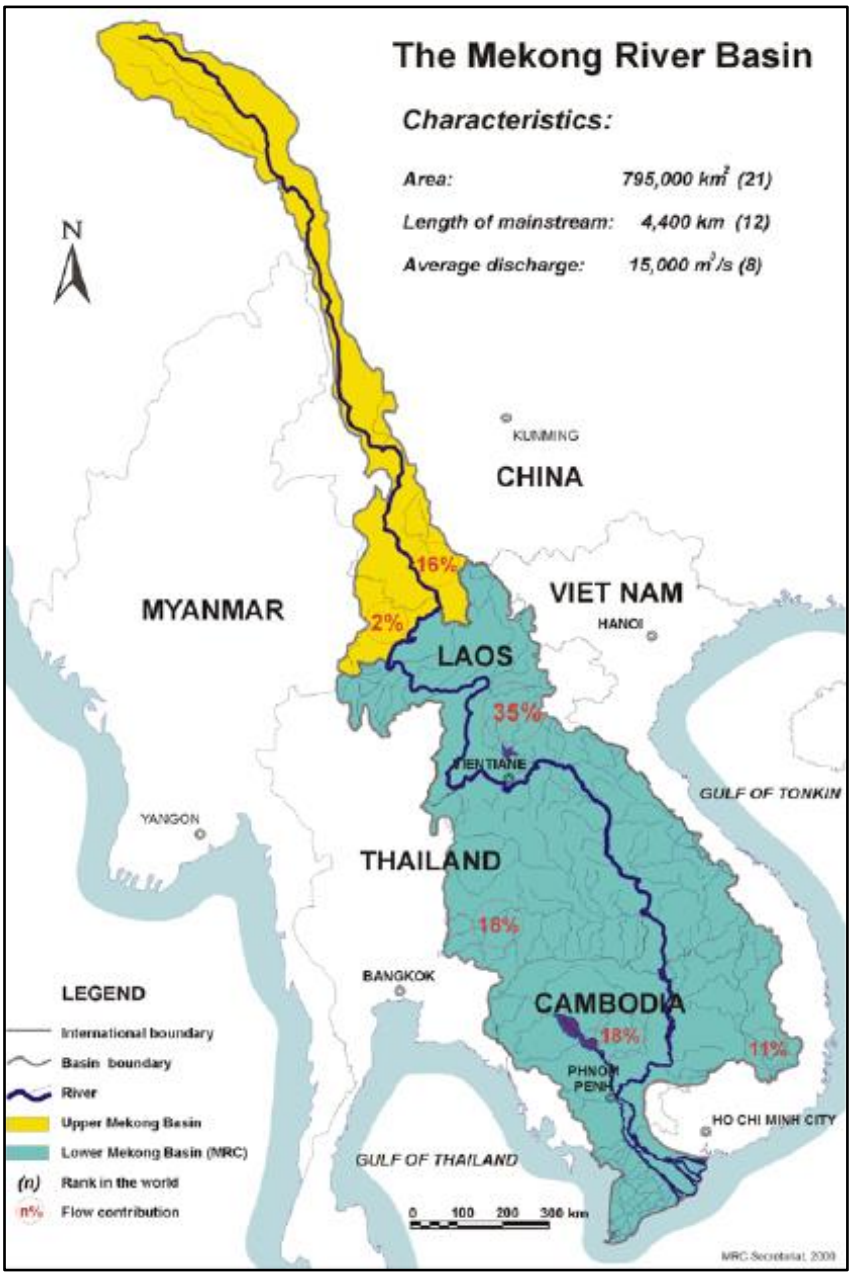

Fig. 1.2. The Upper Mekong Basin (in yellow) and the Lower Mekong Basin (in green) with flow contribution percentages (MRC, 2004)

1.3.2 Climate

The climate of the LMB is classified as tropical monsoon and dominated by two distinct monsoon seasons: the rainy southwest monsoon season from mid-May to early October; and the dry northeast monsoon season from October to March. The period of May - October presents approximately 85 - 90 % of precipitation with the mean annual precipitation of 1000 mm in the northeast Thailand to more than 3000 mm in the mountain regions of Laos (MRC website and Kite, 2001) (see Fig. 1.3 and Fig. 1.4).

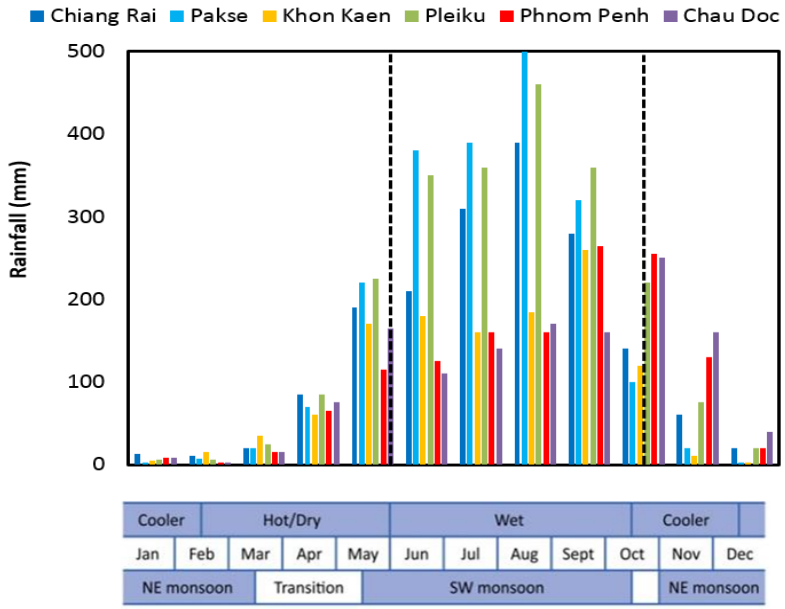

Figure 1.3. Temporary distribution of mean annual rainfall in some selected station of the LMB corresponding with colour dots in Fig. 1.4 (Data is extracted from the MRC website).

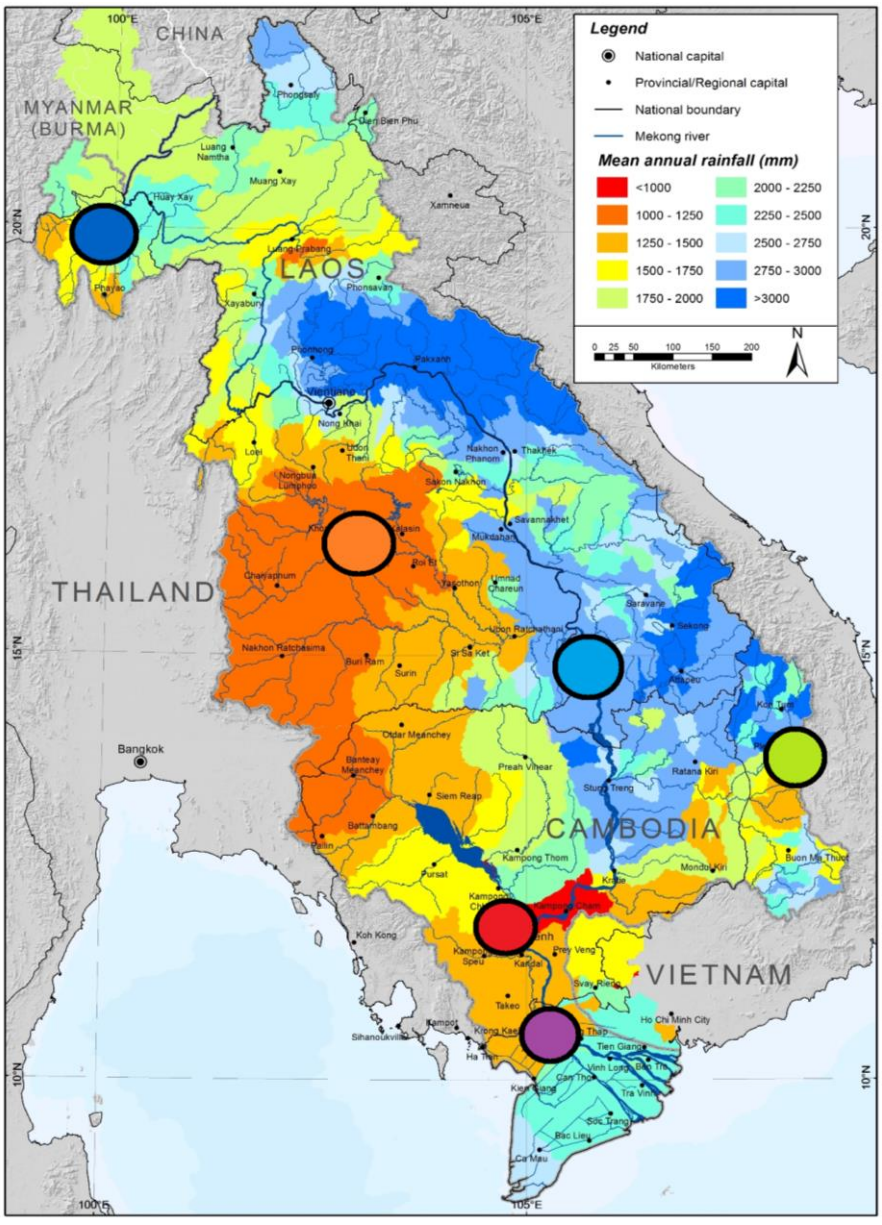

Fig. 1.4. Spatial distribution of mean annual rainfall in the LMB (MRC, 2005)

1.3.3 Hydrology

Hydrographs from the mainstream monitoring stations, Kratie and Can Tho (see Fig. 1.5) provide a good visual representation of the seasonal variation of the flow. The dry season occurs from November to April and the minimum flow appears in March - April, corresponding with the dry northeast monsoon period. The months of April - May belong to the first transition season. Annually, the flow rises in May and reaches the peak in September - November, corresponding with the rainy southwest monsoon period. After this time, the second transition phase occurs at the end of November.

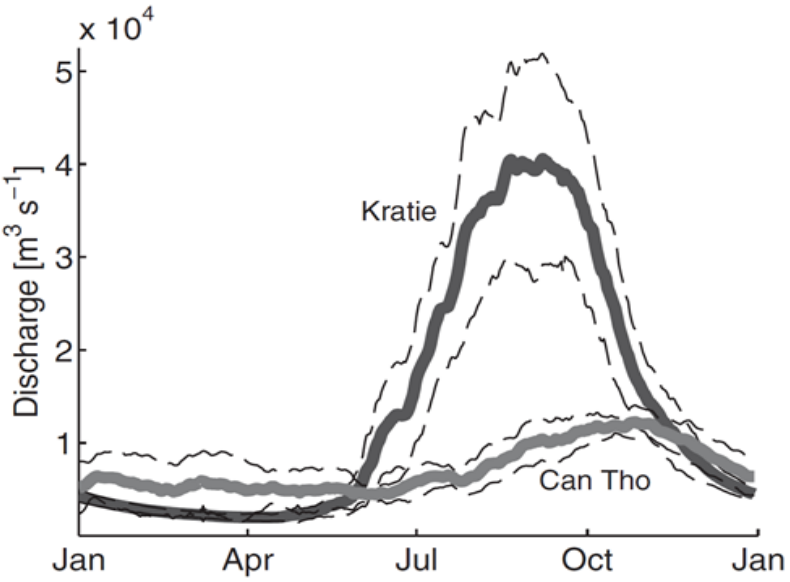

Fig. 1.5. Average historical discharge, ± one standard deviation, at Kratie, Cambodia and at Can Tho, Vietnam (Nowacki et al., 2015). The hydrological condition of Can Tho station experiences a peak discharge about 2 months later than in Kratie station.

In order to study the hydrological regime of the Mekong River, this region is divided into 6 reaches corresponding with 6 hydro-geographic zones, as below (see Fig. 1.6):

Zone 1: From the UMB to the border between China and Laos, the major water source is generated from snow melting on the Tibetan Plateau and plays an essential role in the hydrology of the lower mainstream.

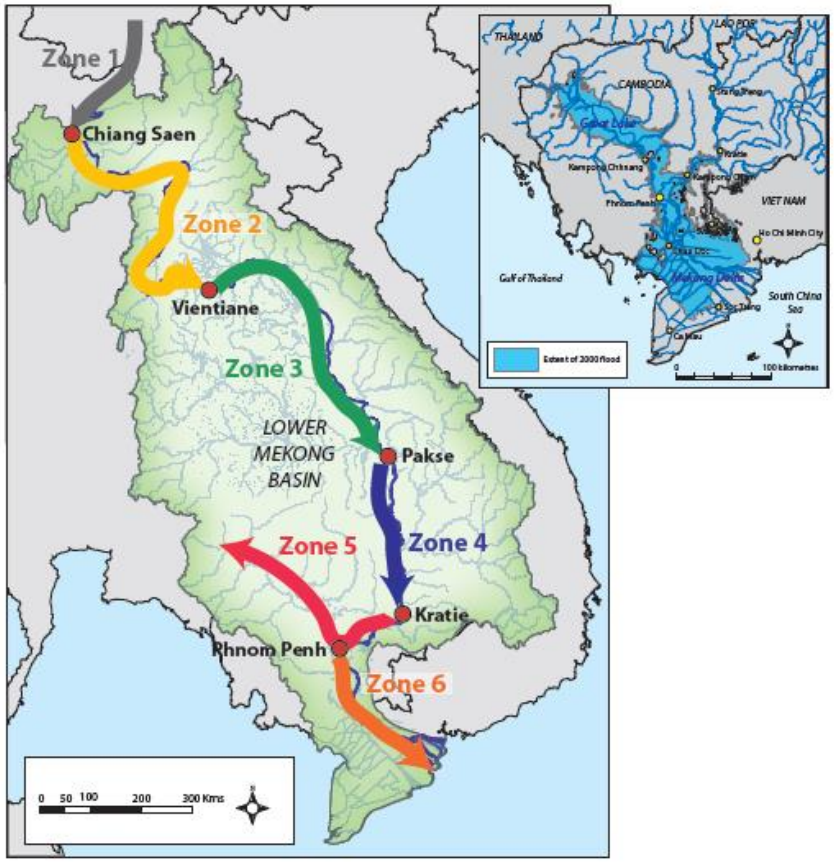

Fig. 1.6. Hydro-geographic zones in the Lower Mekong Basin 2004 (MRC, 2005)

Zone 2: From Chiang Saen to Vientiane, the topography of this reach is entirely mountainous and covered with natural forests. Few large-scale development activities occur in this reach, thus the hydrological response is the most natural in LMB. The hydrological condition starts to change rapidly at the downstream boundary of this reach.

Zone 3: From Vientiane to Pakse, this reach is contributed by large tributaries from Laos and river systems from Thailand. The tributaries in Laos are faced with an increasing water demand for agriculture activities and hydropower development. While the Mun and Chi rivers in Thailand are condensed

agricultural basins and it is considered as a significant reservoir for irrigation in dry season.

Zone 4: From Pakse to Kratie, the main hydrological contributions to the mainstream come from the Se Kong, Se San and Sre Pok catchments (the 3S catchment). These rivers make up the largest hydrological subcomponent of the LMB. However, its hydrology is alternated strongly by hydropower operations.

Zone 5: From Kratie to Phnom Penh, this reach consists of the Tonle Sap system, which is the largest freshwater storage in the Southeast Asia. It experiences an unique hydrological regime with seasonally bi-directional flow in the Tonle Sap (Oeurng et al., 2019).

Zone 6: From Phnom Penh to the seas, this part is very complex because the mainstream divides into tributaries before discharging to the East Sea of Vietnam and the Gulf of Thailand. It is controlled by a complicated artificial system of dykes and channels. The hydrodynamics are affected by the upstream flow and tidal regimes. Every year, 35 - 50 % of this zone area is inundated during the rainy season.

1.3.4 Tidal regime

Tidal mechanisms are key processes acting on water distribution in the deltas and sediment transport in the estuaries (Vinh, 2016). The Mekong Delta is affected by two tidal regimes: (1) The unsteady semi-diurnal tide from the East Sea of Vietnam with amplitude of 2.5 - 3.8 m. The highest tide occurs in December and January, the lowest tide appears in April; (2) The unsteady diurnal type from the Gulf of Thailand with amplitude of 0.5 - 1 m (Nhan, 2016).

During the low season, the tidal fluctuation can penetrate 228 km inland (Wolanski et al., 1996). During the flood season, the tidal effect is not as rigorous as during the low season. However, the flow is stagnant on high tide days, causing higher water level in the river and the intrafields (Tri, 2012).

1.4 Outline

Chapter 2 presents the behavior of sediment particles in the LMB by three representative environments: from the upstream fluvial condition to the lacustrine body and then to the estuaries. The characteristics are estimated simultaneously with hydrodynamic conditions by the combination of in situ measurements and laboratory analysis. The outcomes are particle size, settling velocity and their spatio-temporal evolution through flocculation. These data will be used for further studies on sediment transport along the LMB. This chapter also shows the occurrence of fluid mud layers, which contribute to the sedimentation process in the Mekong estuaries. The last section of this chapter devotes to the implications of the Mekong Delta based on fluid mud layers and mangroves.

Chapter 3 deals with the extension of an existing wetting - drying algorithm in two space dimensions and implementation into SLIM in a fully implicit way. This algorithm consists in applying a threshold value of fluid depth for a thin layer and a blending parameter in order to guarantee positive values of the water depth, while preserving local mass conservation and the well-balanced property at wet/dry interfaces. The technique is first validated against standard analytical test cases (Balzano 1, Balzano 3 and Thacker test cases) and then is subsequently applied in the Tonle Sap Lake, where the water level can vary about 10 m between the dry and the wet seasons. The outcomes of this work are the spatial and temporary flow distribution in the Tonle Sap, and its hydraulic relationship with the VMD.

The results of the TELEMAC - 2D are described in Chapter 4 to examine the influences of the multi-channel system on the distribution of flow and sediment dynamics in the VMD. Two scenarios are established to simulate the hydrodynamic and sediment transport alterations from the natural states to the current status of human intervention. In the light of this result, we revisit the literature and discuss the potential of numerical models in assessing the ongoing hydrological cycles in the context of human and natural modifications.

Chapter 5 summarizes the main findings of the thesis and their applications, followed by some perspectives for future research.

Chapter 2 Sediment properties in the Lower Mekong Basin

This chapter is based on the following publication:

Le, H. A., Gratiot, N., Santini, W., Ribolzi, O., Tran, D., Meriaux, X., Deleersnijder, E and Soares-Frazão, S. (2019). Suspended sediment properties in the Lower Mekong River, from fluvial to estuarine environments. *Estuarine, Coastal and Shelf Science*, 106522.

2.1 Introduction

Under human pressures and climate change, the Mekong River is faced with many serious issues linked with changes in sediment dynamics. One of the most evident transformations is the construction of large hydropower dams in the upstream reaches of the river and its tributaries, which are modifying the hydrological cycle, and reducing the sediment discharge into the floodplain and estuaries at an alarming level (Schmitt et al., 2017).

Sand mining, trapping by dams, and the resulting reduction of sediment flux are undoubtedly causing changes in the nature (and populations) of particles transported. Some expected consequences in geomorphology, floodplain fertility and pollutant dynamics are already presented (Kondolf et al., 2018), but need to be better studied. Previous studies conducted in the LMB indicated that the upper fluvial section was dominated by two particles size populations: silts, with a diameter of 10 - 20 μm; and sands, with a diameter of 63 - 200 μm, accounting for 78 % and 22 % of the total particle load, respectively (Peteuil et al., 2014). Downstream, in the estuary, flocculated fine particles

dominate. The observed floc size, reported in the literature, was 30 - 40 µm, constituting 60 - 80 % of the total sediment load in the high flow season. However, in the low flow season, the floc size increased to 50 - 200 µm, accounting for 70 - 80 % of the total volume (Wolanski et al., 1996 and Wolanski et al., 1998). This observed variability of sediment properties reflects a direct adjustment of physical properties along the streams, which operates at microscopic scales (flocculation, sedimentation and erosion), linked with hydrodynamic conditions and their seasonal variations. The different origins, together with different physicochemical and biological conditions between the sites, cause difficulties in interpreting the results.

Particle size, settling velocity and their spatio-temporal evolution through flocculation, are fundamental properties that need to be estimated to assess sediment transport and deposition processes in space and time (Manning et al., 2011a; Winterwerp, 2002). This is particularly true in the case of mud/sand mixtures, where complex interactions occur and need to be characterized for a realistic understanding of sediment dynamics (Manning et al., 2010). Conceptually, flocculation develops from primary particles into hierarchical structures, namely flocculi, microflocs and macroflocs. Primary particles mainly consist of fine particles with sizes of 1 - 6 µm, and can be organic or inorganic. They aggregate to form 1st order structures, so-called flocculi, with diameters of the order of 6 - 50 µm. They are usually hardly broken down into primary particles, even at the highest turbulent shear modulus experienced by particles in large rivers. Thus, it is generally considered that flocculi are a major component of sediment dynamics. Microflocs form the 2nd order of aggregation. They include primary particles and flocculi and have sizes of 50 - 200 µm. Finally, macroflocs are the largest particle structures. They are loose structures with a wide size distribution, ranging from hundreds to thousands of micrometers (Lee et al., 2012 and Fettweis et al., 2006). Flocs (micro and macro) are generally fragile structures, easily broken down when passing through high turbulent shear modulus (Manning et al., 2011a).

Flocculation at the microscopic scale, has some hydro-sedimentary and geomorphological impacts at scales of river reaches, estuaries and deltas, in particular because it promotes the formation of fluid mud layers. Fluid mud is defined as a mixture of high-concentrated fine sediments with water

(Bachmann et al., 2005). It is generated by liquefaction of cohesive sediment beds by waves or by an imbalance between settling and eddy diffusion near the bed, or by the convergence of sediment fluxes from upstream and downstream. In energetic environments, large particles such as sand are also found in fluid mud samples, but the portion is less than few percent (Mchannelly et al., 2007). Fluid mud masses may be advected over large distances horizontally without losing their coherent nature or internal chemical properties; and its horizontal convergence may often be a key mechanism of their accumulation (Mchannelly et al., 2007). Thus, fluid mud in thin layers is considered as an intermediate stage of deposition (before formation of consolidated bed layers) or bed erosion (under entrainment process by fluidization (Mchannelly et al., 2007). Its thickness varies from few centimeters to meters (Sottolichio et al., 2011; Azhikodan et al., 2018).

The occurrence of fluid mud is commonly observed in quiescent environments such as lakes and reservoirs (Mehta et al., 1991; Mchannelly et al., 2007) or in the Estuarine Turbidity Maximum zones (Uncle et al., 2006; Winterwerp et al., 2011; Azhikodan et al., 2018) occurring in estuaries, navigation channels, harbour basins or along muddy coasts (Bachmann et al., 2005; Schelske et al., 2006; Gratiot et al. 2007; Toorman et al. 2018). The turbidity maximum zone is often created by resuspension from the bed during parts of the tide and shows a significant drag reduction at high suspended sediment concentration (SSC) gradient (Dyer et al., 2002a and Dyer et al., 2002b). However, it has been poorly studied and reported in the literature dedicated to the LMB (Wolanski et al., 1998, Xue et al., 2010) and received some more interest recently (Gugliotta et al., 2019; Nittrouer et al., 2017; Gratiot et al., 2017).

This study combines in situ measurements and laboratory investigations to examine the physics of particles (especially flocculation properties, measured with new patented equipment developed by SCAF®) and to understand transport/deposition processes in the LMB. Sampling and analyses are performed in three contrasted environments: an upper fluvial reach in Laos (Fig. 2.1b), a lacustrine environment in Cambodia (Fig. 2.1c) and an estuarine environment in Vietnam (Fig. 2.1d). The same methodology was applied for these three contrasted environments (upstream river, lake and estuary). Results obtained allow for answering and discussing the following points:

- Are suspended sediment flocculated or not (percentages of cohesive versus non-cohesive particles transported in suspension)?
- If yes, are floc populations stable from upstream to downstream and/or highly dependent on hydrodynamic conditions (SSC, turbulence, salinity)?
- Are SS predominantly transported as washload (single path with no bed interactions), or does it experience successive phases of deposition and erosion?
- How much SSC increase can modify flocculation, sedimentation and how much this could contribute to the formation of fluid mud layers and, finally, modify the geomorphology of the LMB?

By answering the four questions above, this study proposes a better understanding of the physical properties of sediment and their transportation modes along the LMB. Because flocculation and fluid mud layers are playing an important role in the dynamic of the Mekong Delta and its fragile coastal ecosystems; such information will facilitate the implementation of integrated tools, such as ecological/geomorphological models, to go through a better management of this complex and large scale environment.

2.2 Specific study areas

Field investigations have been conducted at three locations of the LMB, assumed to be three representative of river morphological units, from the fluvial environment to the lacustrine and the estuarine environments (Fig. 2.1a).

2.2.1 Fluvial environment

The upper reach, located in Luang Prabang city, Laos (Fig. 2.1b) is selected as being a representative for a fluvial environment in the LMB. It is situated at altitude of approximately 300 m above sea level, covered with steep hillsides. The location is at the confluence of the Mekong and Nam Khan rivers, a tributary of the Mekong, which has been experiencing drastic land use changes, predominantly leading to erosion in the last decades (Ribolzi et al., 2017). At Luang Prabang, the Mekong River section is already wide, with

width of 600 - 700 m. However, when passing through gorges, the channel becomes swiftly narrow, approximately 100 m wide, and bounded by limestone pavement. The channel has a median depth of around 10 m, with maximum depth of approximately 30 m (Gupta et al., 2007).

The field survey was conducted for 8 days, from 26 June to 2 July 2017, at the beginning of the wet season. There were neither extreme floods nor low water situations, thus the hydrodynamic conditions were suitable for sampling and analysing a typical (median) suspended sediment distribution in the river. Twenty-seven samples were taken in the main Mekong River and its tributaries (Nam Ou, Nam Suang and Nam Khan tributaries). During the survey, hydro-sedimentary conditions were also characterized on two cross-sections with distances of approximately 20 km (Fig. 2.1a, see section 2.2.3). For each location, samples were collected in three vertical profiles (left bank – V1, middle bank – V2 and right bank – V3). In each vertical profile, 3 litres of water sample were taken at various depths (0.1 h, 0.4 h, 0.7 h and 0.9 h, h being total water depth).

2.2.2 Lacustrine environment

The Tonle Sap lake is selected to be one of our study areas because it has characteristics of a freshwater lake in a floodplain, that is situated in the centre of Cambodia (Fig. 2.1c). With a volume of 1.8 - 58.3 billion m^3, the Tonle Sap lake plays an essential role as the largest freshwater source in Southeast Asia (Kummu et al., 2014). It comprises a permanent waterbody, twelve tributaries, extensive floodplains and the Tonle Sap River, linking the lake to the Mekong River (Kummu et al., 2014). At the confluence, the river splits into the Bassac river (the Hau river) in the West and the Mekong River (the Tien river) in the East. The Tonle Sap system has strong and original hydrodynamic relationships with the Mekong mainstream (Kummu et al., 2008). During the wet season, flooding from the Mekong River causes a reverse flow direction, into the Tonle Sap Lake. The lake area then increases from 2500 km^2 to approximately 15,000 km^2, while the depth rises from 1 to 9 m. At the opposite, the slow release of floodwaters from the lake during the dry season is a very important water source to sustain the river discharge of the Mekong Delta (Hai et al., 2008). In this paper, we focus on the physics of particles. The

field survey was performed for 9 days from 13 October to 21 October 2018, during high flow season. The material used is freshly deposited sediment, collected near the Mekong River tributaries, after a flood season at the bottom layer.

2.2.3 Estuaries

The Mekong Delta is chosen for studying the sediment properties because of its complex topographical condition and its hydrological regime is rapidly changing in recent years under a number of anthropogenic stresses. The delta is situated at the most Southeast part of the LMB (Fig. 2.1d). It covers approximately 55,000 km^2 (Balica et al., 2014), extending from the Cambodia - Vietnam border to the Gulf of Thailand and the East Sea of Vietnam (Tran et al., 2018). Together with the Mekong River and the Bassac river, it separates into eight tributaries (Hung et al., 2014) before discharging into the East Sea (Wolanski et al., 1996 and Xing et al., 2017). At the interface between land and the sea, the estuary is strongly impacted by both flooding from upstream and the tidal flows, as well as wave forcing (Gugliotta et al., 2019).

Due to this region has the most complex condition in the LMB, three surveys with different seasonal conditions were conducted in the Song Hau Estuary (as part of the Lower Mekong Delta Coastal Zone - LMCDZ project), in December 2015, March and October 2016. During these surveys, three cross-sections (upstream - T1, middle - T2, downstream - T3), with distances of 10 and 15 km, respectively, were chosen to monitor and assess the impact of saline water intrusion on flocculation (Fig. 2.1d). At each location, samples were taken in three vertical profiles. In total, 104 samples with volume of 5 litres per sample were collected to investigate the spatio-temporal dynamics of suspended sediment for contrasted SSC and turbulent levels.

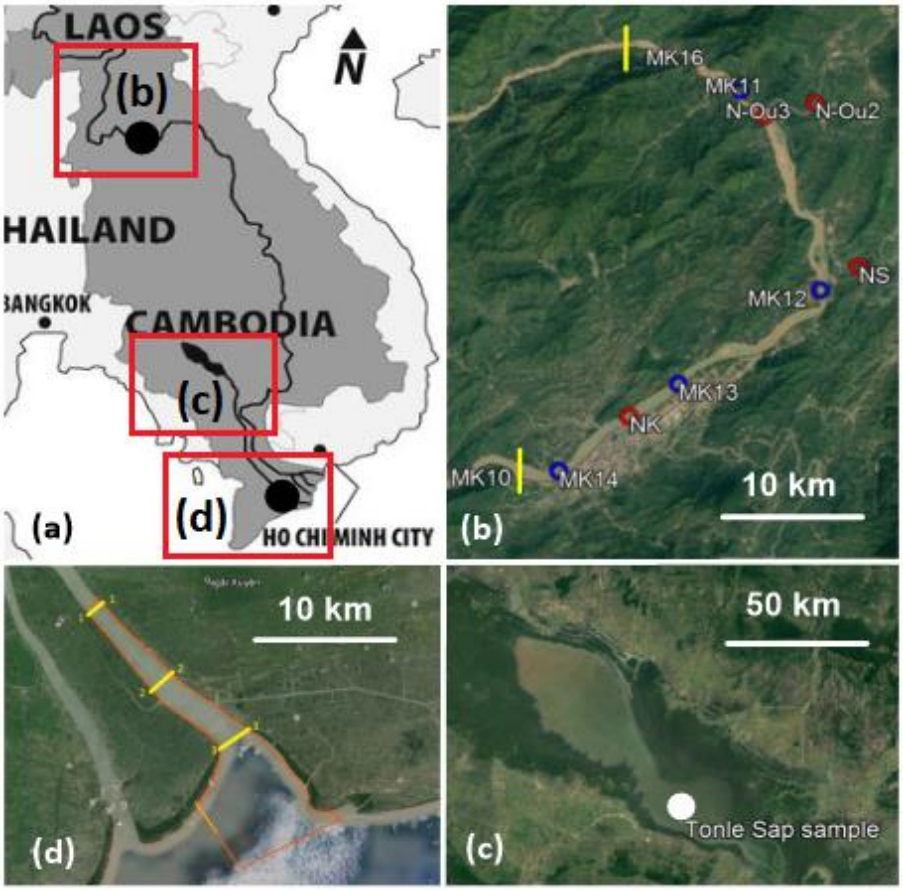

Fig. 2.1. Domains of interest [a. General map] (after Smardon et al., 2009). Sampling sites and locations in fluvial (Luang Prabang, Laos with blue dots reporting samples in main stream, red dots reporting samples in tributaries and yellow segments reporting cross-sections [b]), lacustrine environment (Tonle Sap floodplain, Cambodia with white dots showing the sampling location [c]), and estuarine environment (Song Hau estuary, Vietnam with yellow segments reporting cross-sections and red lines showing the local domain [d]).

2.3 Methods

The suspension regime of the sediments transported in a flow strongly depends on interactions between hydrodynamics, particle size, density and settling velocity. Thus, the understanding of particle size distribution (PSD) of suspended particulate matter is one of prerequisites to properly simulate

sediment dynamics (Fennessy et al., 1994). This study originally proposes a direct estimation of settling velocity and flocculation with the patented SCAF instrument (System for the Characterization of Aggregates and Flocs, Gratiot et al. 2015).

The five sections hereinafter describe the methodology adopted to measure the physical properties of suspended sediment and evaluate its transport dynamics. The instruments at our disposal are particularly relevant to estimate both particle size and settling velocity, but it was not possible to measure directly the density of flocs, which may be seen as a limitation.

2.3.1 A portable mixing tank device to reproduce natural inflow turbulent conditions

To measure PSD under turbulent conditions close to the ones experienced by natural rivers, 2 litres of water samples were introduced into a portable rectangular-base mixing jar tank (with diameter of 11.5 x 11.5 x 15 cm), and then mixed with an impeller for thirty minutes (Gratiot et al., 2017) for homogenous agitation in circulatory patterns. We assume that a pseudo equilibrium condition is reached for particles after that duration. During preliminary experiments, an Acoustic Doppler Velocity Profiler (Nortek Vectrino2) was immersed in the mixing tank filled with clear water, in order to measure the 3D turbulent field of velocity and deduce the mean turbulent energy dissipation rate G (s^{-1}). With a rotation speed of 100 rpm, G was about 44 s^{-1}, which corresponds to high shear rate conditions, such as observed near bottom in natural rivers and estuaries (Gratiot et al., 2017). For further details on the mixing tank device, the reader can refer to Gratiot et al. (2017, supplementary information).

2.3.2 PSD measurements and characterization of the particle-classes/ population/ group?

To characterize the different populations of particles, the terminology of Lee et al. (2012) is used. It is based on four classes, namely primary particles, flocculi, microflocs and macroflocs (as mentioned in the Introduction section). We utilize the LISST-Portable XR instrument to measure sediment particle sizes during mixing. The operational principle of the LISST-Portable XR is

based on laser light scattering (or laser diffraction). This instrument provides the logarithmical PSDs over 44-size bands in the ranges of particle size from 0.35 to 500 μm by using the Frauhofer approximation or the exact Lorenz-Mie solution. The volumic concentration unit is micro-litre/litre (μL/L), corresponding to sediment concentration of 30 - 1900 mg/L in the chamber of measurement. Each spectrum shows independent semi-log distributions of sub-populations, that were characterized by their mean particle size D_f, their standard deviation σ_{Df} and their relative volumetric concentration. The operating range of optical transmission recommended by LISST-Portable XR is 75 - 95 % because less than 75 %, significant contributions from multiple-scattering bias the size distribution results to lower sizes. This device has been utilized successfully in many contrasted environments, such as the Saigon - Dong Nai rivers, Vietnam (Nguyen et al., 2019), a hydropower plant in Malaysia (Azrulhisham et al., 2018), Northern French Alps (Antoine et al., 2015) and Philadelphia (Windt et al., 2017), among others.

The uncertainties of the LISST-Portable XR is due to sediments estimation, because it varies greatly due to hydraulic variability. Thus, the probabilistic approach that is based on Pearson system allows assessing the level of uncertainty. The Pearson parametric distribution approximation was computed based on the significant characteristic of Pearson system applying direct correlation between the first four statistical moments of SSC and PSD data obtained from the desilting basin.

For describing PSDs of primary particles, flocculi, microflocs and macroflocs, we apply a mathematical function to separate the signal into four log-normal distribution (Mikkelsen et al., 2006). Such post processing is also useful to prevent misinterpretation, resulting from air bubbles and other artefacts that can be observed in the raw particle size spectrum (Sequioa, 2016).

In this study, the PSD of each sample was measured in two steps, before and after two minutes of sonication, for a mechanical particle breakage under acoustic waves. Hence, it is possible to assess the proportion of sand and flocs because large-size particles built by smaller cohesive particles (silt or clay) are, at least partially, dispersed by sonication (Gratiot et al., 2017) while the sand particles are indivisible and then maintain a constant diameter after sonication.

2.3.3 Characterization of the settling and flocculation regimes

Depending on SSC, three settling regimes can be observed for natural sediment in aquatic environment (Van Leussen, 1994), namely (1) free settling, (2) flocculation and (3) hindered regimes. For the lowest SSC, flocculation is weak and particles are settling almost independently from each other (free settling regime). Particle settling velocity can then be broadly estimated by the Stokes' law or derived laws as the sum of individual particles settling down (Stokes, 1857; Winterwerp, 2002). The flocculation settling regime occurs with midrange of SSC (tens to hundreds of mg/L). The settling velocity of cohesive and mixed fine-grained sediments then becomes more complex because it is influenced by both particle interactions and individual properties (Manning et al., 2010), as well as turbulent shear (Winterwerp, 2002; Manning et al, 2011a). Flocculation is promoted, which results in larger particle sizes and higher settling velocities (Droppo et al., 2005). The hindered settling regime occurs at very high SSC (several grams per litre or more), and settling mostly occurs by mass, depending on the cohesion and suspension concentration (Camenen and Van Bang, 2011; Van and Van Bang, 2013).

To assess the settling velocity w_s (m/s) (and flocculation) for all these regimes in natural environment, we used the System for the Characterization of Aggregates and Flocs (SCAF), a patented instrument (Gratiot et al., 2015) that was successfully applied in some recent researches (Wendling et al., 2015, Gratiot et al., 2017, Legout et al., 2018, Nguyen et al., 2019). This instrument is a glass settling column with dimension of 20 cm high and 3.5 cm in diameter, equipped with 16 infrared (λ = 980 nm) emitters and 16 diametrically opposed photo-sensors measuring at a frequency of 210 Hz. SCAF instrument measures the light attenuation in the settling tube with depth and time during the deposition of particles (Gratiot et al., 2015). Sensors are located every 1 cm down the column with the lower sensor located at 1 cm above the bottom of the column. Measurements taken in the eight upper centimeters of the SCAF settling tube provided an estimate of flocs settling velocity under quiescent conditions, denoted $w_{s,q}$ (m/s) while measurements realized in the eight centimetres near the bottom of the settling tube provided an estimation of flocs settling velocity after flocculation by differential settling under settling dominated conditions, this latter velocity being reported

as $w_{s,\neq}$ (Wendling et al., 2015). In the case of non-cohesive particles, such as sand or silt, or clay particles with deflocculant, the settling velocity does not change during settling; $w_{s,q}$ and $w_{s,\neq}$ are similar and the flocculation index FI = $(w_{s,\neq} - w_{s,q})/ w_{s,q}$ is close to zero (Wendling et al., 2015). As SCAF instrument is based on by mass sedimentation of a fluid mud mixture in a settling tube, it is inherently affected by the shape, density and compositions of all particles presented in the sample.

2.3.4 Other hydrodynamic measurements

Complementary measurements were performed during field surveys. An Acoustic Doppler Current Profiler (ADCP), an Hydrolab probe (a multi-parameter probe measuring in-situ water quality parameters), SSC samplers and a EUTECH turbidimeter were used to characterize the water flow in the cross-sections, suspended solid concentration and physical parameters such as turbidity, temperature, pH, ORD, EC, salinity, etc. An YSI multi-parameter probe (Water Quality Sampling and Monitoring Meters and Instruments) was also used to check the average values of the measured physical parameters.

2.3.5 Characterization of the suspension regime

In order to characterize the suspension regime, the non-dimensional Rouse number (Rouse, 1937), which expresses the balance between the upward turbulence mixing (u_*) and the gravity forces (w_s) on the same particles in a river stream, was calculated for each flow condition encountered. The Rouse number is calculated as following:

$$R_o = \frac{w_s}{\beta \kappa u_*} \tag{2.1}$$

where the settling velocity w_s is inferred from the SCAF results (Fig. 2.5) or calculated by the Stokes' Law from the PSD measurements. κ is the von Kármán constant, taken equal to 0.41. The constant of proportionality β is the ratio of sediment to eddy diffusivity, describing the diffusion patterns of a fluid particle and a sediment particle. In water environment, it is often assumed that eddy viscosity is equal to eddy diffusivity, thus value β is typically hypothesised to be one (Rijn, 1984; Farrell and Sherman, 2013). u_* (m/s) is shear velocity. In the fluvial and estuarine environments, the shear

velocity u_* was derived from flow velocity by using the ADCP, with the assumption that the velocity profiles follow the logarithmic inner-law (so-called "Law of the Wall") (Sime et al., 2007; Santini et al., 2019, Eidam et al., 2017). In the lacustrine environment, u_* was computed from 2D hydrodynamic simulation results by the Second-generation Louvain-la-Neuve Ice-ocean Model (SLIM, https://www.slim-ocean.be/).

The application of Equation 2.1 to characterize the suspension regime is relevant, but we should underline that uncertainties can be high, as both w_s and u_* are hardly estimate in the field.

2.4 Results

2.4.1 Particle size distribution (PSD)

The PSD of all samples are gathered in a triangle sketch in Fig. 2.2. Before sonication, most of the particles are flocculi with an average contribution percentage of 46 %, 78 % and 78 %, for fluvial, lacustrine and estuarine environments, respectively (Fig. 2.2a). After sonication, the PSD displayed an increased number of primary particle class for all samples (51 %, 67 % and 32 %, respectively), while it witnessed the reduction in the percentage of flocculi and flocs (Fig. 2.2b). The Fig. 2.2 also shows a wider diversity of particle sizes in the Mekong estuary (blue circles and squares) than in the lacustrine and the fluvial environments (yellow and red circles, respectively). It illustrates that estuaries are complex and changing environments, which mix both fluvial and coastal water (see the sketch in Fig. 2.6 and the corresponding discussion section). In the case of the Mekong estuaries zone, sediment transport and deposition are strongly affected by fluvial inflow, tidal currents, but also resuspension of particles by wind-induced current, waves and coastal oceanic currents (Gugliotta et al., 2019; Marchesiello et al., 2019).

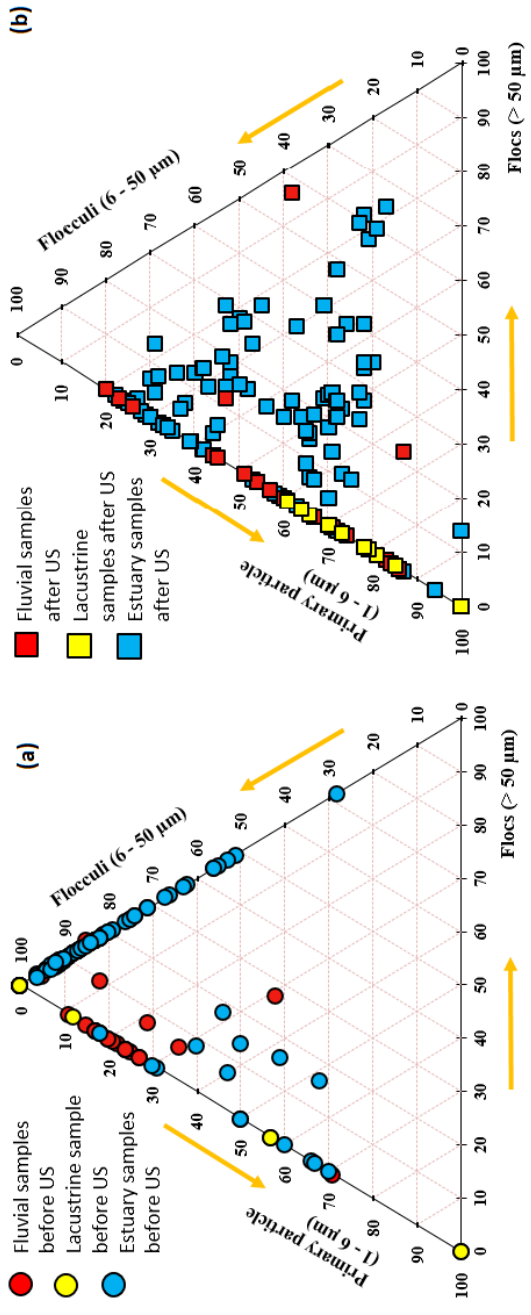

Fig. 2.2. Triangulars of PSD in upper parts and estuary analyzed (a) before and (b) after sonication

2.4.2 Suspended sediment versus hydrodynamic conditions

Fig. 2.3 aims at highlighting the role played by SSC on flocculation of particles. This figure shows both data collected in the field and in the laboratory, before and after sonication.

Particle size populations in the fluvial environment (Laos)

Fig. 2.3 (a) and Fig. 2.3 (b) present the PSD of particles populations sampled in the fluvial section. On average, the primary particles accounted for 37 % of all particle population (in volumetric concentration). The predominant population is flocculi, with a volume concentration of approximately 46 %. Microflocs and macroflocs were fewer and accounted for (only) 3 % and 14 % of the total volume, respectively. The macroflocs size reached a median diameter of 422 µm. Fig. 2.3 (b) shows the PSD plot after sonication. The sonication broke up particles so that the percentage of primary particles increased (+14 %) to 51 % and flocculi decreased slightly (-5 %) to 41 %. The percentage of microflocs remains stable and small (approximately 2 %), and the percentage of macroflocs decreases by more than two folds (to approximately 6 %). These coarsest particles were not all broken up by sonication, which indicates the presence of sand. The samples issued from the tributaries had generally similar PSDs than the ones in the mainstream. After sonication, PSD of these samples still exhibits high values, with a maximum diameter of 347 µm. It means that these water samples contain predominantly sand, which is in agreement with visual observations during field campaigns. A detailed examination of PSD before and after sonication confirmed that samples in fluvial environment consisted of both cohesive sediment and sand particles. These PSDs are in agreement with the results of Camenen et al. (2014).

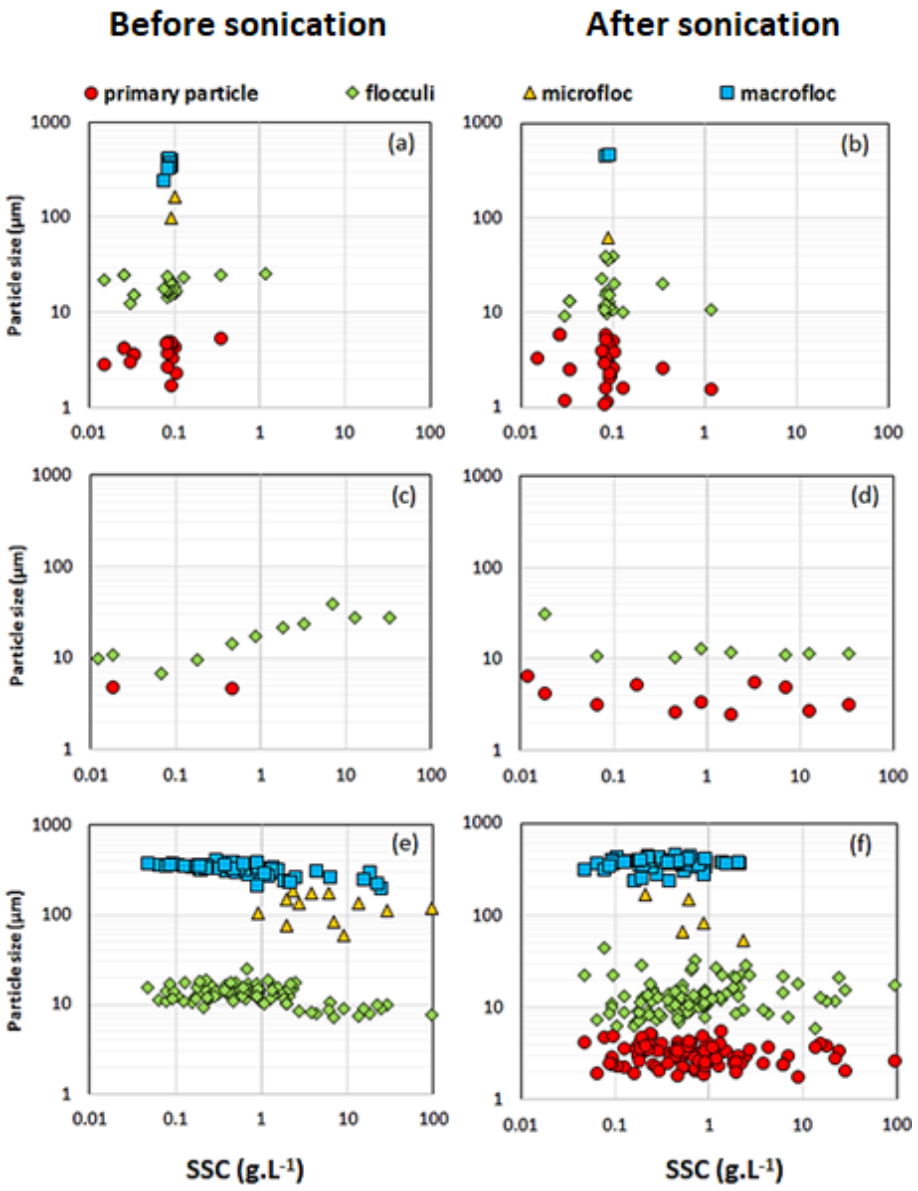

Fig. 2.3. Variation of particle classes with SSC in fluvial environment (a and b), lacustrine environment (c and d) and estuary (e and f) before (left graphs) and after sonication (right graphs)

Particle size populations in the lacustrine environment (Tonle Sap, Cambodia)

In the lacustrine environment, only two particle classes (primary particles and flocculi, without flocs and no sands) appear. Before sonication (see Fig. 2.3c), the percentage of primary particles and flocculi accounts for 22 % and 78 %, respectively. After sonication (see Fig. 2.3d), these percentages reverse with a predominance of primary particle (67 %) and a simultaneous decrease of flocculi (33 %). The particle size in the lacustrine environment were smaller (7 ± 3 µm) than in the fluvial part (18 ± 5 µm). Fig. 2.3c exhibits a clear rise (3 to 4 folds) of flocculi size with higher SSC, as a response of flocculation of primary particles (or colloids) on flocculi.

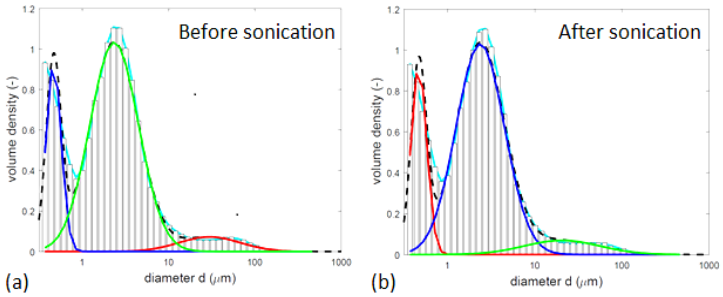

Fig 2.4. PSD of a sample in the Tonle Sap before (a) and after sonication (b). The first peaks in two graphs show the appearance of colloids with diameter of < 1 µm.

Interestingly, colloids were observed in some samples taken in the Tonle Sap, with diameters of < 1 µm (see Fig 2.4). After 12 hours of deposition in the mixing tank at rest, the particles still in suspension were both colloids with diameter of approximately 0.45 µm, which are consistence with a research conducted by Seah et al 2017, accounting for 21 %; primary particle (73 %) and few flocculi (6 %). After sonication, the structure of sediments presents the same pattern (21 % of colloid, 72 % of primary particles and 7 % of flocculi). This can be explained by a stable mixture of this sediment classes, which are hardly broken down into smaller particles even after sonication. Colloids play an important role and act as “catalyzers” of the interaction between sediment and substances in the water such as substance dissolved matter, substance from precipitation, absorbed ions and organic matters (Wendling et al., 2015).

Particle size populations in the estuarine environment (Song Hau river, Vietnam)

Fig 2.3 (e and f) display the PSD in the estuary versus SSC before and after sonication, respectively. Once again, flocculi is the dominant population of particles, with mean diameter of approximately 15 μm (in range of 8 - 20 μm), accounting for 80 % of total volume. Before sonication, only three classes of particle sizes exist in the estuarine samples, flocculi, microflocs and macroflocs. The prevailing fine silt population shows mean diameter of 7 - 12.5 ± 10 % μm, that constituted 83 - 94 % of total volume. Diameters of coarser population were in the range of 112 - 310 ± 10 % μm. After sonication, particle size reduced significantly. A group of primary particles (red circles), which were completely absent from the PSDs before sonication, appears in almost all samples, which undoubtedly demonstrates the cohesive nature of sediments in the estuary. Due to breakage into smaller particles under turbulence shear, diameters of fine particles (primary particles and flocculi) reduce to 1.8 - 4 ± 10 % μm and 6.3 - 12.2 ± 10 % μm, respectively while the size of coarse particle (microflocs) falls to 15 - 65 ± 10 % μm. A population of sand particles (with diameter > 200 μm), not broken-up with/after sonication, is also evidenced.

2.4.3 Settling velocity

Fig. 2.5(a) shows the variation of suspended sediment settling velocity with SSC, measured directly with SCAF instrument. For the three aquatic environments, settling velocity rises with SSC because of flocculation process. Even if there are only 5 SCAF samples in the fluvial environment, 9 samples in lacustrine environment, 19 samples in the estuary, the three curves exhibit similar trends, which support the existence of free settling, flocculation and hindered regimes, as previously depicted by Wendling et al. (2015).

The free settling regime is observed for the lowest SSC (tens of mg/L). Sediment settling velocity measured in the fluvial, lacustrine and estuarine environments are of the same order of magnitude, the mean settling velocities being approximately 0.02 - 0.08 mm/s in the fluvial section, 0.05 - 0.06 mm/s in the lake, and 0.01 - 0.02 mm/s in the estuary. The widest range of settling velocities observed in the fluvial environment is probably the fingerprinting

of a wide variety of compact soil aggregates, freshly eroded from the watershed, and not yet at equilibrium with the prevailing hydrodynamic conditions, as reported conceptually by Droppo et al. (2015). In this free settling regime, particles settle almost independently, the interaction between particles is poor, which is reflected by a moderate flocculation index (FI lower than 2) in all SCAF measurements (in Fig. 2.5, right panel). Flocculation predominates in the range of 0.4 - 4 g/L, thus the settling velocities of fluvial, lacustrine and estuarine sediments rise up to 0.2 mm/s, 0.1 - 2 mm/s and 0.03 - 0.8 mm/s, respectively.

In the lacustrine environment, a significant rise of settling velocity is found with higher SSC. The SCAF results show that the settling velocity of the lacustrine environment reaches the peak of 2.0 mm/s when SSC reach approximately 2.0 g/L.

In the estuary, the complex hydraulic regimes, including resuspension of freshly deposited sediments (Marchesiello et al., 2019) and the mixing between fresh water and saline water led to the formation of a zone of turbidity maximum and promote the formation of flocs (both microflocs and macroflocs) (Dyer et al., 2002a and Manning et al., 2007). As a consequence, the settling velocity also amplifies (Dyer et al., 2002b and Manning et al., 2011b). Beyond 4.0 g/L, hindered regime becomes predominant. It implies the decline of settling velocity in the lacustrine and estuarine environments, from 2.0 to 0.4 mm/s and from 0.8 to 0.1 mm/s, respectively.

The main difference of these three environments is that flocculation processes seem to appear at lower concentration in the fluvial environment (approximately 20 - 30 mg/L) than in the lake (approximately 1 - 2 g/L) or in the estuary (approximately 300 mg/L). We cannot exclude that the particles sampled in the fluvial environment are not real flocs, but correspond to soil aggregates that are not in equilibrium with their hydraulic environment (Droppo et al., 2005).

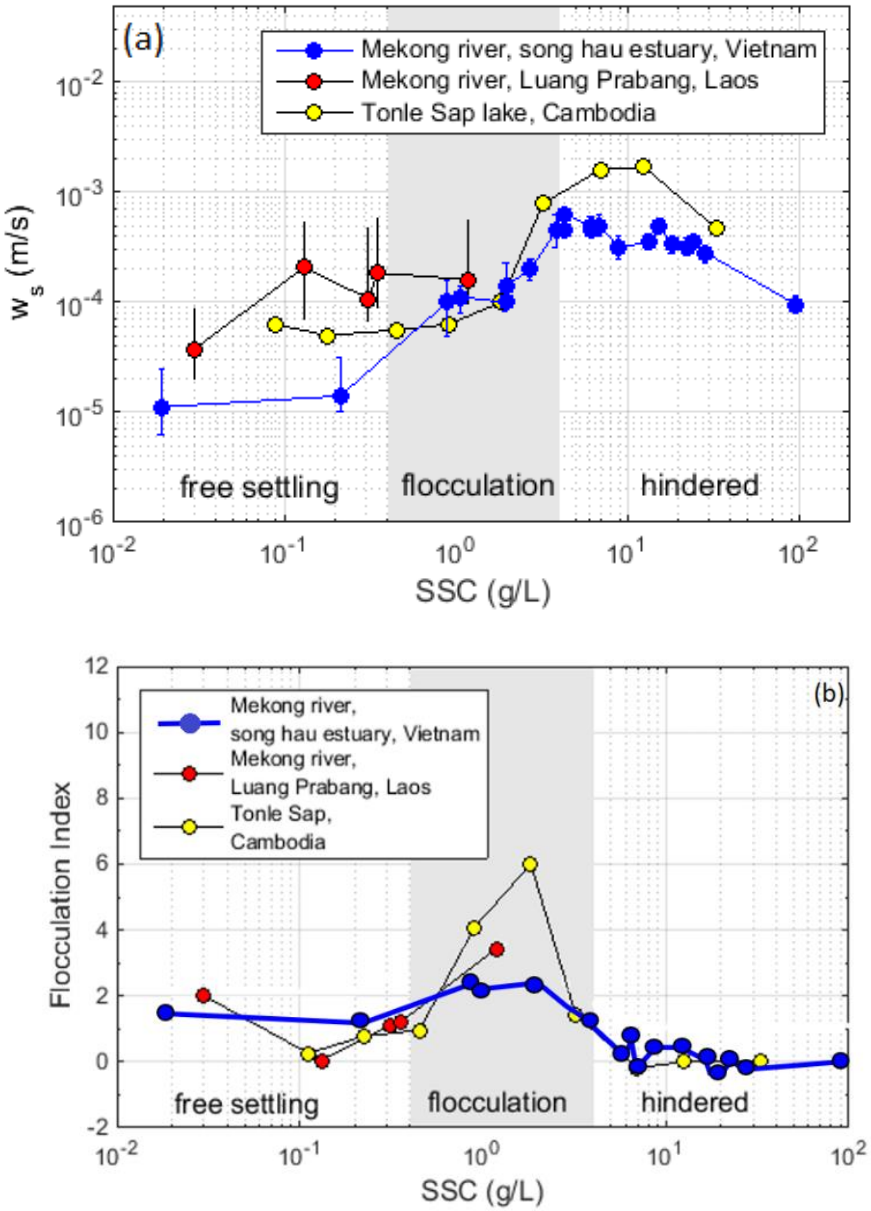

Fig. 2.5. Sediment properties in the Mekong Land to Ocean Continuum: (a) Variation of settling velocity with SSC measured directly with SCAF instrument and (b) Variation of the flocculation index with SSC.

The flocculation efficiency is higher for the estuarine environment (+ 60 % of increase of the settling velocity) and highest for lacustrine environment (+200 % of increase) than for the fluvial environment (+7 % of increase).

Concerning the Flocculation Index, sediment samples in the river and in the lake (red circles for fluvial environment and yellow circles in lacustrine environment, see Fig. 2.5b) exhibit a high dynamic, even in fresh water. The highest rate of flocculation is observed in the lacustrine environment, where the measured Flocculation Index increases from 0 to 6, when SSC increases from 0.1 to 3.0 g/L. Interestingly, after getting the Flocculation Index peak of 4 - 6, the efficiency of flocculation in the lacustrine environment fell to value of 0 - 1.75. It means that flocculation still occurs, but the volumetric concentration of particles is so high that the settling velocity cannot increase anymore. Settling velocity of small particles is hindered by the high SSC, whereas colloids are trapped on the surface of larger particles (Comba et al., 2009).

The estuarine sediments also experience three settling regimes with Flocculation Index in range of 0 - 3: (1) Free settling regime with constant Flocculation Index of 2, that is developed at low concentration of 300 mg/L; (2) Flocculation regime with FI < 3, where flocculation happens at SSC of 300 - 2700 mg/L; and (3) Hindered regime with Flocculation Index of approximately 1 because of the appearance of brackish water and high SSC of > 2.7 g/L. Flocs reach higher volumetric concentration for lower mass concentrations when flocculation is reinforced by differential settling (Gratiot et al., 2017).

2.5 Discussion

2.5.1 SS transport mechanisms along the Mekong

As mentioned in Section 2.2.4, the transport regime of suspended sediment along the LMB may be characterized through the non-dimensional Rouse number (R_o). For the upstream fluvial environment, the computed shear velocities were similar in the different sections monitored, u_* = 0.03 m/s for the MK10 and u_* = 0.04 m/s for MK16. The small difference between the two

cross-sections may be explained by the geometry of each cross-section, MK10 cross-section being wider than MK16 cross-section. The shear velocity in the Tonle Sap is 0.008 m/s by using SLIM simulation obtained by Le et al., 2020b; while a value of 0.010 m/s is obtained by using the Inner law. The R_o values in the estuary are estimated based on two representative particle sizes (15 µm for fine particles and 300 µm for sand) and the shear velocity is estimated with the recent work of Eidam et al. (2017).

The R_o values estimated for the fluvial, lacustrine and estuary environments are summarized in Table 2.1. In the fluvial environment, the R_o ranges between 0.002 and 0.009 at the two monitored river cross section (MK10 and MK16), which corresponds to the washload mode. Hence particles are presumably transported over long distances, without any interaction with the riverbed. Few sand particles are presents in the MK10 and MK16 cross section samples, with R_o values of 0.75 - 4.6. It means that the very fine sand particles are strongly sorted over the water depth, leading to a low suspension mode. As for the coarser sand fraction of the riverbed, the stream was not able to transport them in suspension.

Table 2.1. R_o value in two different conditions

Sample	**Mean diameter (µm)**	**u_* (m/s)**		**w_s (m/s)**		**Rouse value**	
		Law of Wall	Modelled results	SCAF	Stokes' Law	Min	Max
Fluvial (MK10)	19 ± 2	0.029	-	2.0E-05	1.2E-04	0.002	0.009
Fluvial (MK16)	18 ± 4	0.041	-	8.0E-05	1.2E-04	0.005	0.007
Tonle Sap	7 ± 2	0.014	0.008	5.0E-05	2.0E-05	0.005	0.015
Estuarine fine sediment	15 ± 2	-	0.01	3.0E-05	2.4E-04	0.007	0.058
Estuarine sand	300 ± 30	-	0.02	2.0E-02	9.5E-02	2.439	11.6

While R_o values of Tonle Sap samples vary from 0.005 - 0.015, corresponding to flow modes ranging from washload to strong suspension load (Vanoni et al., 1946 and Udo et al., 2011). It is assumed that sediments are deposited near bed during one part of the year and eroded under wind-induced currents during

another part of the year. According to Kummu (2008a), the net budget of sediment is almost in equilibrium between deposition and erosion.

In the estuary, the value of the R_o for the fine sediments ranges between 0.007 - 0.058, which corresponds to strong suspension mode; while the values for sand vary from 2.4 to approximately 12, which corresponds to the bedload mode and sedimentation dominated regime (Gugliotta et al., 2019). This finding coincides with a recent study by Marchesiello et al. (2019) that the Mekong sediments consist of various compositions (fine sediments and sands) and under effects of complex forces. Thus, coastal muds are exposed to wave-induced resuspension and wind-induced transport, while sands are concentrated near the estuaries.

2.5.2 Predominance of flocculi in the Lower Mekong Basin and consequences for sediment transport

As quantified in this paper, flocculi is the dominant particles population in all three environments monitored at regional scale (46 % in the fluvial environment, 78 % in the lake and 78 % in the estuary). The existence of sand was noticed, but can mostly be found near the bed with few percent of volume.

In the LMB as in many other large hydrosystems under tropical climates, we may anticipate that particles' populations (and its consequences) fluctuate seasonally and year after year. As designed, this study cannot catch this variation, however, we believe that it describes a general pattern that could be of interest when establishing some monitoring strategies in similar large tropical hydrosystems in Southeast Asia, and probably elsewhere. At large scale, Rouse analysis presented in Table 2.1 showed that particles are mainly transported with a strong suspension regime, evenly as washload by river flow. By these modes, they are transported abundantly along the main river and tributaries, partially over the floodplains during the flood season (Kondolf et al., 2014, Manh et al., 2014, Manh et al., 2015) and then, are deposited along shore and on the whole subaqueous delta, before having cycles of resuspension/deposition, principally under waves forcing (Marchesiello et al., 2019). Our measurements in the fluvial section show that few sands are transported in the water column because their transport is completely governed by the stream power. During high flow with enhanced stream

powers working with other sediment sources (riverbanks and floodplains), the finest sands are lifted into upper layer.

This methodology can explain two distinct transport modes of two particles populations in the Mekong estuary: washload is well mixed throughout the water column and sand are transported prevailing near the bottom. It leads to distinct geomorphological forms, with the presence of alternated tidal flats and sand bars as observed in many river mouths (Ta et al., 2002; Gupta et al., 2002; Anthony, 2015).

2.5.3 Occurrence of fluid mud layers in the Mekong estuary

According to measured data during our three surveys in the estuary, a fluid mud layer was sometimes presented near bottom, with SSC values abruptly increasing beyond 0.4 g/L, corresponding to the transition to the flocculation regime (Fig. 2.5; Gratiot et al., 2017). Fig. 2.6 sketches the sediment transport from the river to the estuary in low flow season (a) and high flow season (b) with locations of vertical profile sampling. In this figure, the blue profile represents a schematic profile measured in low flow season and the purple one represents a profile measured in high flow season. Fig. 2.7 reports all SSC value observed near bottom ($z = 0.9h$ - SSC_{nb}) for the vertical profiles realized in the estuary in December 2015 (50 profiles), March 2016 (44 profiles) and October 2016 (47 profiles). Each vertical profile is represented by a single point in Fig. 2.7. The three curves show the sorted distribution of all SSC_{nb} values for the three seasons. The curves show that the percentage of profiles which exhibits high SSC values, compatible with fluid mud layer occurrence, is very high during low flow season (66 % of profiles in Dec 2015 and 95 % profiles in March 2016) and is much smaller during high flow season (9 % profiles in October 2016).

By multiplying SSC_{nb} values with the corresponding settling velocity w_s reported in Fig. 2.5, we can estimate the settling flux capacity of fluid mud layers $\phi = SSC_{nb} \times w_s$ and thus assess their potential contribution to sedimentation (Fig. 2.7(b)). The cumulated sorted series demonstrate the strong linearity between sediment concentration and settling flux (i.e. potential of sedimentation). Fig. 2.7(c) shows that the 10 % of the most concentrated fluid mud layers contributes to 60 % of the sedimentation during

low flow season (blue curves) and more than 98 % during high flow season (purple curve).

As a preliminary conclusion, our study confirms the existence of fluid mud layers and quantifies broadly their frequency of occurrence in the estuary. Fluid mud layers are observed within distances of approximately 30 km from the coastlines in both high flow and low flow seasons. However according to Wolanski et al. (1998), the location of fluid mud layer in the Mekong Estuary varies spatially with river discharges and tides. In the high flow season, most of sediment deposits in shallow coastal waters, approximately 10 - 20 km from the coast (Wolanski et al., 1998 and Marchesiello et al., 2019). In low flow season, fine sediment is well mixed with saline water penetrating about 40 km inland, carrying sediment up-river to a turbidity maximum zone. Further upstream, at Can Tho, approximately 120 km from the coast, no turbidity maximum is found in the freshwater region of the estuary. Thus, the positions of fluid mud layers and turbidity maximum, which are promoted by SSC concentration in the range 0.4 - 4 g/L, can hardly be observed for distances higher than 120 km inland. This situation could change in the future, under the cumulated effect of subsidence and sea level rise.

According to Spearman and Manning (2008), the mass balance between accretion and erosion of cohesive sediment during tidal cycles in estuarial location can occur when threshold shear stresses for both deposition and erosion operate simultaneously.

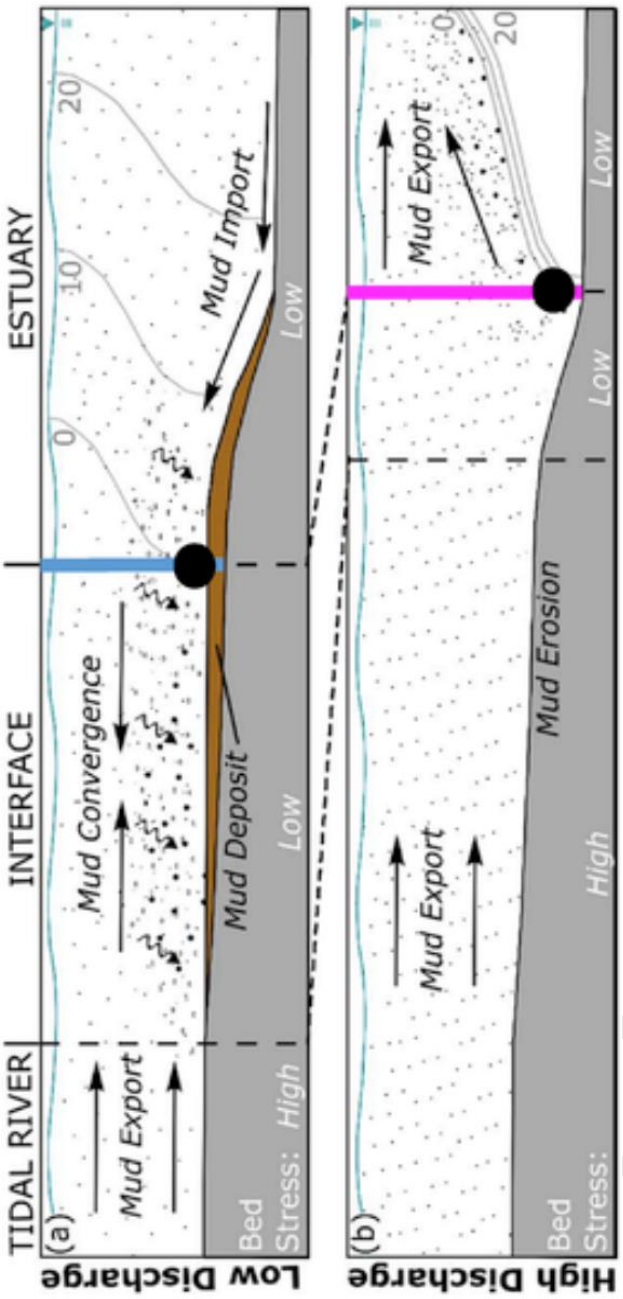

Fig 2.6. Conceptual summary of salinity stratification (grey lines), SSC (dot concentration), relative near-bed shear stress, suspended particle aggregation (dot size), net sediment advection (black arrows), and mud deposition/erosion within the tidal river, tidal river – estuary interface, and estuary during (a) low and (b) high discharge seasons. Relative weight of transport arrows varies with season and regime. Not drawn to scale (after McLachlan et al., 2017). The blue line shows the vertical profile in low flow season and the purple line shows one in high flow season with SSC. The black dot shows the sampling height (near bottom, at 0.9 h).

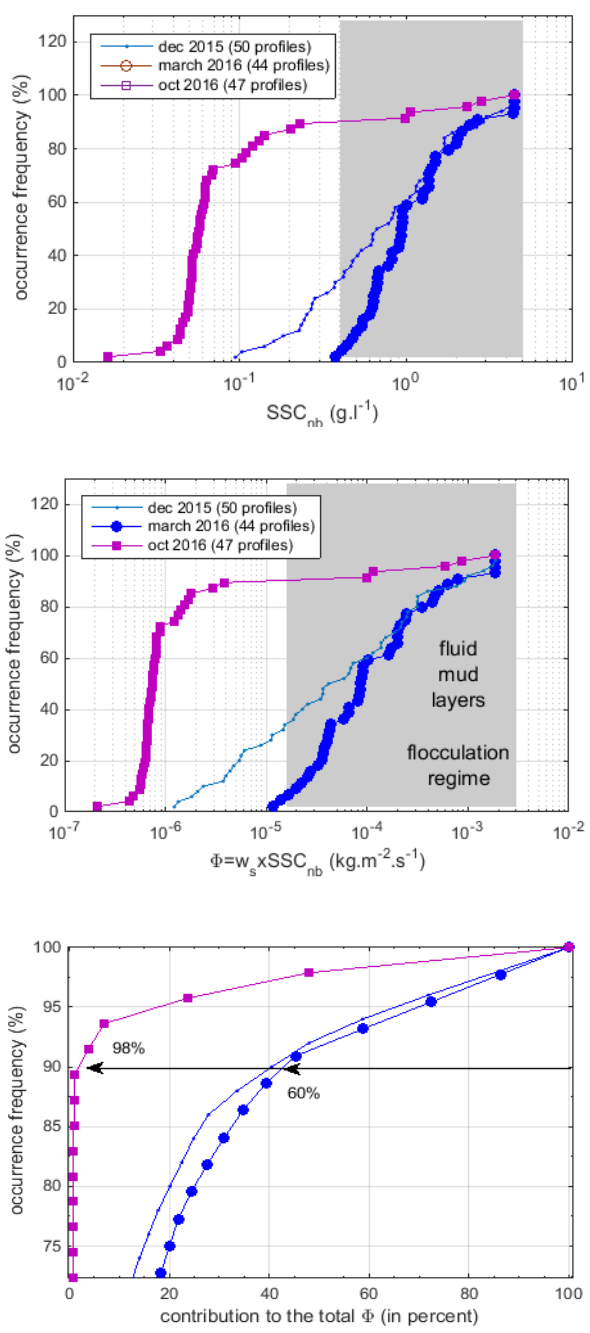

Fig 2.7. Data corresponds to SSC measured near bottom (SSCnb). Data are sorted from lowest to highest SSC (a), corresponding settling flux (b) and contribution to the total (c). The blue line shows the vertical profile in December 2015; the blue line with dots shows one in March 2016 and the purple line shows one in October 2016 with SSC near bed.

2.5.4 Implication for Mekong Delta management

In the Mekong Delta, the flocculation process plays an essential role in the formation of fluid mud layers by enhancing the downward flux of sediment when freshwater mixes with seawater and sediments become trapped at the convergence point. Sediments leaving the Mekong Delta appear to go through cycles of trapping and resuspension in the estuary, before being partially advected seaward on the subaqueous delta and along shelf, as fluid mud along the bottom salinity front. The fluid muds have far-reaching effects on the coasts by reducing boundary shear stresses, attenuating of waves over a soft muddy bottom, affecting water-column /seabed exchanges, and serving as the agent of outward growth of the subaqueous delta (Marchesiello et al., 2019). In addition, fluid mud layers can lead to rise in fluid viscosity and density, and the reduction of bottom shear stresses can affect the tidal wave propagation (Gabioux et al., 2005). Thus, without flocculation, the particles would be carried directly offshore (Kineke et al., 1996). The appearance of fluid mud layer under flocculation regime provides a mechanism for rapid and strong sedimentation in the estuaries and lead to local siltation and mud accretion. Once deposited in the bed, fluid mud layers contribute to bedform development and stability (Schindler et al., 2015). We should underline that bedform consolidation and stability is hardly predictable. It depends on both physical and biological near bed processes (Parson et al., 2016) that evolve continuously for sediment mixtures containing cohesive mud and biologically active substances such as microorganisms, bacteria and microphytobenthos who form biofilms (Malarkey et al., 2015).

How can we anticipate the impact of human activities on sediment dynamics, floculation and fluid mud layer formation at the regional scale? As reported in the recent publications of Schmitt et al. (2017) and Ha et al. (2018), human pressure, through sediment trapping and sand mining, already leads to a significant decrease of SSC in the estuaries. Our study points out that SSC is a determining factor affecting, first flocculation, and secondly, the formation of fluid mud layers in the Mekong estuary. There is a critical threshold of around SSC = 0.4 g/L, that can be seen as a tipping point for sediment processes. If the occurrence of SSC beyond that point decreases, the deposition rate will strongly reduce (no linear effects), while the erosion rate

will probably increase because of a decrease of sediment quantity, and because of the reduction of drag coefficient in the regions of fluid muds (Dyer et al., 2002a), which enhances boundary shear stresses nearshore, coinciding with erosional areas in the Mekong estuaries (Kineke et al., 1996). As fluid mud layers in the Mekong estuaries are a key factor to promote flocculation and "boost" natural sedimentation, we do believe that some regular monitoring programs should be realized. In terms of coastal management, a simple measure that should be seriously considered is mangrove reforestation. Because of cohesiveness, sediment particles transported out into mangrove forests during tidal inundation flocculate and form larger flocs. Thus, mangroves are not just passive colonisers of mud banks but they are active in trapping suspended sediment, with positive feedback on shore protection (Furukawa et al., 1997; Anthony and Gratiot, 2012; Gratiot and Anthony, 2016). According to Minderhoud et al., 2019, the sedimentation rate in the Mekong coastal mangrove forests is 36 - 67 mm/year, while this rate of other floodplain areas is 6 mm/year. This mechanism was recently characterized through a deep geomorphological study conducted along the muddy coast of the Guianas. In this environment, which is comparable to the Mekong shore, Brunier et al. (2019) observed and quantified some exceptional rates of muddy shoreline retreat following mangrove removal for field rice production. Apart from this mechanism, mangroves play a role as a buffer between sea and land to prevent river sediment from re-entrainment to the ocean at ebb tide (Furukawa and Wolanski, 1996).

2.6 Conclusion

Field surveys and laboratory analysis were performed at the regional scale in the fluvial, lacustrine and estuarine environments of the Lower Mekong River to provide a physically-based assessment of sediment transport regimes, flocculation, and fluid mud layer dynamics. The independent evaluation of particle size and settling velocity provides a good assessment of particles behaviour and allows characterizing the R_o number and corresponding regimes in a robust way. Suspended sediments in fluvial and lacustrine environments are predominantly flocculi (97 % and 100 % of total volume, respectively) and primary particles, the modes are transported as washload or

with a regime of strong suspension. Some of these particles (primary particles and flocculi) probably experience phases of deposition and resuspension, mostly in the adjacent floodplain, during their routing through the Mekong River, but we observed comparable sub distributions for fluvial, lacustrine and even estuarine environments. This finding indicates that the primary particles and flocculi populations very probably reach the estuary without any important physical transformations (i.e. with similar PSD). In the estuary, the complex mixing between fluvial and coastal waters and sediments offers optimal conditions of salinity, that leads to a higher diversity of particles, with significant proportions of microflocs and macroflocs (25 % of total volume), in the sand size range (diameter > 300 µm).

The original estimation of flocculation indexes with SCAF instrument allows defining clearly the flocculation regime. This later is the most efficient for SSC in the range of 0.4 – 4 g/L. In fluvial, lacustrine and estuarine environments, flocculation regime develops for the same range of SSC, beyond approximately 0.4 g/L. Flocculation then becomes a key process, but its impacts on particles populations differs with the different environments. In the Tonle Sap Lake, flocculation promotes the aggregation of colloids and primary particles on flocculi. In the estuarine environment, flocculation leads to the formation of a new population of particles, the micro-flocs. In the fluvial environment, the data were too scarce to draw a clear conclusion, as freshly eroded aggregates could not be yet in equilibrium with river hydro-sedimentary conditions.

As a consequence of these microscopic changes at scales of particles, our study confirms the regular occurrence of fluid mud layers (55 - 60% of occurrence) near the bottom in the Mekong Delta with distance of less than 120 km from the coastline, concentrated in 30 km in both high - and low - flow seasons. Fluid mud layers, which are intrinsically linked with flocculation processes, are early steps of landforms evolutions and participate to the geomorphology of the Mekong Delta. In the light of this study and considering the degree of vulnerability of the delta to ongoing hydro-sedimentary changes, we may provide two recommendations: Firstly, the continental sediment flux needs to be restored (or at least maintained) and human driven subsidence needs to be controlled. Under those conditions, fluid

mud layers should remain a driver of river and coastal geomorphology, as it has been the case over the last millennia. Secondly, the perception of mangrove should be reconsidered as reforestation is probably the optimal manner, in both technical and environmental aspects, for ensuring sediment trapping and preserving fluid mud layers and mudflat, with positive feedbacks on mangrove colonization. In other words, mangroves cannot compensate regional disequilibrium in sediment balance, but they can facilitate the transformation of diluted suspended sediment into fluid mud layers.

Taking into account the degree of uncertainty of field and laboratory measurements with natural fresh sediments, and the degree of variability of sediment properties in such large and human-impacted systems, there is a clear interest to adopt a monitoring strategy that would extend the study in time and space.

Chapter 3 The Wetting – Drying algorithm implemented in SLIM and application to the Tonle Sap

This chapter is based on the following publication:

Le, H. A., Lambrechts, J., Ortleb, S., Gratiot, N., Deleersnijder, E. and Soares-Frazão, S. (2020). An implicit wetting–drying algorithm for the discontinuous Galerkin method: application to the Tonle Sap, Mekong River Basin. *Environmental Fluid Mechanics*, 1-29.

3.1 Introduction

Floodplains have indisputable roles in river basins over the world (Burt, 1996) by providing livelihood for riparian residents (Craig et al., 2004), biodiversity of river ecosystems (Ward et al., 1999) as well as reducing flood risks for the downstream areas (Wheather and Evan, 2009). However, floodplains are subject to river floods or flow regulation inducing possible long periods of inundation with wetting and drying phases (Baldwin and Mitchell, 2000). These phenomena impact both the physical and biological aspects of the domain (Warner et al., 2013), especially during extreme events such as floods (Vater et al., 2015), affecting the natural functions of floodplains. Thus, an accurate representation of wetting - drying processes in a floodplain, and adjacent continental water bodies, is a crucial issue for hydrodynamic models. Dealing with very shallow flows, temporary submergences, a wide spectrum of time scales and complex morphologies, high spatial and temporal

resolutions often require (Medeiros and Hagen, 2013) large computational time. Even with the development of powerful and parallel computers (e.g. D'alpaos and Defina, 2007), the question of computational time remains an open challenge for geoscience modelers addressing large domains and long-lasting floods.

Wetting - drying is an issue that has received considerable attention since decades (Kärnä et al., 2011). In early developments, the prevailing strategy of most hydraulic modelers was to adopt mesh deformation at the wet/dry front. However, this approach was quite difficult in the context of complex bathymetries and flow configurations (D'alpaos and Defina, 2007; Gourgue et al., 2009, Kärnä et al., 2011; Vater et al., 2015) because the nodal coordinates vary at each time step and parameterization is required for moving the boundaries according to the flow variables. Recent research focuses on developing wetting - drying algorithms for fixed meshes. All schemes must satisfy both local and global mass conservation together with momentum conservation (Dresback et al., 2002). According to (Medeiros and Hagen, 2013), four categories of wetting - drying algorithms can be considered:

(1) Element removal algorithm: elements are considered as being dry or wet, and dry elements are removed from the computational domain. The drawback of this procedure is that mass and momentum conservation may be broken, causing the numerical simulation to be unstable (Kärnä et al., 2011).

(2) Thin layer: a threshold depth is imposed in the whole computational domain, ensuring positive water depths. If the water depth falls below this threshold in a given element, this element is considered dry and the corresponding velocity is set to zero. This threshold depth, however, corresponds to a substantial water volume in the dry areas (Casulli, 2009), leading to possible mass conservation issues. However, the strongest advantage of this approach is that it is easily applicable in two- or three dimensions (Gourgue et al., 2009). The drawback of this algorithm is a rapid transfer of elements from dry to wet states near the wetting front that increases the stiffness of the problem, restricting the time step in explicit temporal discretisation and worsening the conditioning of the non-linear system in implicit temporal discretisation. The algorithm also requires a higher spatial mesh resolution, resulting therefore in increased computational time.

(3) Depth extrapolation algorithms: a new depth in the dry cells is extrapolated from the surrounding wet cells. The modified depth is then used to compute the velocity. The concerned cells are thus integrated into the wet domain. However, this artificial wetting of dry elements causes artificial leakage between adjacent cells (Bradford and Sander, 2002). Mass conservation is affected and, hence, needs to be enforced by corrective schemes (Begnudelli and Sander, 2006).

(4) Negative depth algorithms or so-called artificial porosity approach: the model can run with negative depths, the subsurface flow being controlled by porosity terms. The advantage of this method is that it is no longer required to separate wet and dry cells (Gourgue et al., 2009) and a smooth transition between wet and dry cells is ensured (Kärnä et al., 2011). However, the method has several disadvantages. As the artificial porosity is applied not only to negative depths but also to a certain height above the actual sea bottom or riverbed (Martin et al., 2018), it results in unphysical properties in the fictitious porous layers. In addition, a lack of mass conservation is observed (Gourgue et al., 2009) because of artificial mass transfers from dry to wet areas (Heniche et al., 2000).

Even though semi-implicit schemes exist (Kärnä et al., 2011), most of the current methods resort to explicit time-marching schemes, which are constrained by the Courant-Friedrichs-Lewy (CFL) condition (Casulli and Stelling, 1998; Candy, 2017). Explicit time integration requires high temporal resolutions making such schemes rather expensive in terms of computational cost. Therefore, they are not suitable for large-scale and complex domains and for long time simulations.

The present work is an attempt to overcome the weaknesses mentioned above by implementing the implicit algorithm developed by Vater et al. (2015) in SLIM (Second-generation Louvain-la-Neuve Ice-ocean Model, www.slim-ocean.be), a discontinuous Galerkin finite element model. The model is applied to conduct a study with the central aim of investigating the flow configurations in Lake Tonle Sap, an integral part of the Mekong River system. It is first tested against several cases with analytical solutions before being applied in a natural domain to identify the hydraulic connection between the Tonle Sap lake and the Mekong Delta.

3.2 The Wetting – Drying scheme

3.2.1 SLIM, a discontinuous Galerkin finite element model

SLIM is a hydrodynamic model based on a discontinuous Galerkin finite element method over unstructured grids that has been developed at the Université catholique de Louvain, Belgium for more than ten years. SLIM includes different options, ranging from one- to three-dimensional modules: the one-dimensional version is a section-averaged model for river networks; the two-dimensional depth averaged version is generally applied to shallow, complex domains; the three-dimensional version is a baroclinic model for coastal flows that solves the 3D hydrostatic equations under the Boussinesq approximation. The model has been applied to various domains, such as Lake Tanganyika, Africa (Gougue et al., 2007), the Great Barrier Reef, Australia (Lambrechts et al., 2010), the Scheldt estuary, Belgium and Netherlands (Gourgue et al., 2013), the Mahakam Delta, Indonesia (De Brye et al., 2011; Pham Van et al., 2016), the Columbia River, USA (Vallaeys et al., 2018), and various lakes of Titan, Saturn's moon (Vincent et al., 2016). Flow field, sediment transport, water renewal timescale and ecological issues were tackled.

3.2.2 The Wetting – Drying algorithm

Governing equations

The shallow-water equations are derived by integrating over the water column the Navier-Stokes equations, assuming that the pressure is hydrostatic and the fluid density is constant. Water flows are generally well represented by those equations if the water column is well mixed and the vertical dimension is much smaller than the typical horizontal scale. The conservative shallow water equations read:

$$\frac{\partial H}{\partial t} + \boldsymbol{\nabla}.(H\boldsymbol{u}) = 0 \tag{3.1}$$

$$\frac{\partial H\boldsymbol{u}}{\partial t} + \boldsymbol{\nabla}.\frac{H\boldsymbol{u}Hu}{H} + g\boldsymbol{\nabla}\frac{|H|H}{2} + \frac{n^2 g}{H^{\frac{7}{3}}}|H\boldsymbol{u}|H\boldsymbol{u} + fe_z \times |H\boldsymbol{u}| - \boldsymbol{\nabla}.(H\vartheta\nabla\boldsymbol{u}) = gH\nabla h \tag{3.2}$$

where t is time and ∇ is the horizontal del operator; H is the actual water depth, and $\mathbf{u} = (u,v)$ is the horizontal velocity vector averaged over the water column; H and u are the state variables that depend on time and position; η is the free surface elevation $\eta = H - h$, where h is the water depth measured from a reference level; f is the Coriolis parameter; e_z is a vertical unit vector pointing upward; g is the gravitational acceleration ($g = 9.81$ m/s^2); υ is the horizontal eddy viscosity. The latter is parameterized by (Smagorinsky, 1963). The bed shear stress is evaluated with the help of the Chezy - Manning - Strickler formulation with n being the Manning coefficient. For solving the shallow-water equations, explicit time marching schemes must meet the CFL condition to ensure numerical stability, leading to small values of the time step size. Implicit time marching allows for much longer time steps, which is appropriate for meshes with variable resolution and long simulations (Casulli and Stelling, 1998; Candy, 2017), and corresponds to the choice made for the present simulations. To maintain this implicit time stepping efficient even at wet/dry fronts, appropriate algorithms have to be developed. An extension of the 1D algorithm (Vater et al., 2015) is presented hereinafter.

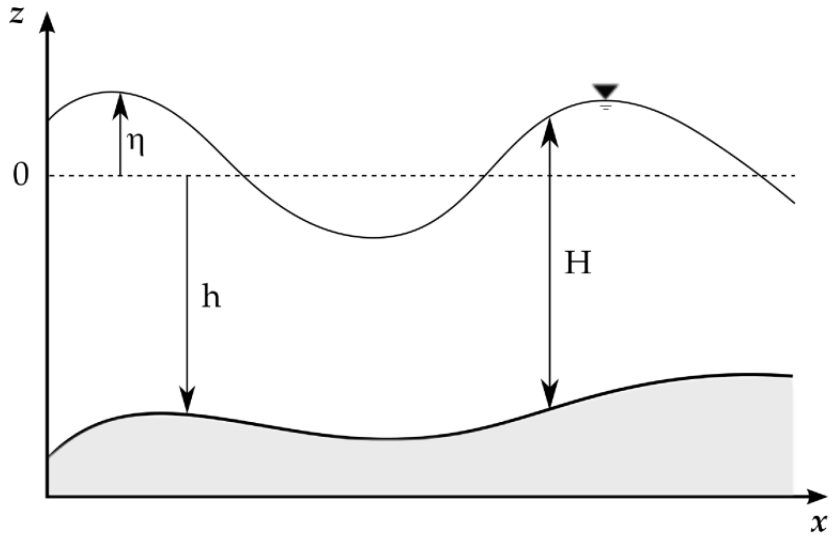

Fig. 3.1. Water column geometry, where η and h denote the free surface elevation (positive upwards) and the reference depth, respectively. The actual depth of the water column is $H = h + \eta$ (Pham Van et al., 2016)

Wetting - drying algorithm

The algorithm for an explicit temporal discretisation is detailed in Vater et al. (2015). Here we focus on its extension to an implicit time scheme. Three main problems occur when the water depth becomes zero (H = 0): (1) the occurrence of artificial gradients in the surface elevation that can influence the momentum equation and result in an unbalanced scheme; (2) the occurrence of negative depths; (3) ill-conditioned computation of the velocity $u = (Hu)/H$.

When one node is dry on an element, the discontinuous Galerkin discretization does not represent the physical situation accurately near the wet/dry interface: two distinct situations can be identified (see Fig. 3.2a and Fig 3.2b). In situation (a), the artificial gradient of surface elevation would remove water from an already dry node. To prevent this, the gravitational force should be ignored on the element. In situation (b), the surface elevation gradient is different from zero and the water flows from higher elevation nodes to the dry node. The gravitational force has to be preserved. To distinguish between those two situations, the method proposed by Vater et al. (2015) compares the maximum value of the surface elevation with the minimum bathymetry on the element: $s = \max(\eta) + \min(h)$. When the value of s is smaller than a given threshold ε, the gravity is cancelled on the element. This procedure guarantees that the mean water depth H over each element will be positive at the end of one time step. An additional slope-limiting algorithm is applied locally on each element to guarantee a positive depth at the nodes. To be usable in an implicit temporal scheme, this on/off switch has to be regularized. In order to do so, we multiply the gravity fluxes between the nodes of a partially dry element by a blending parameter α, defined according to Eq. (3.3). When the value of s is less than a threshold value ε, the blending parameter α is 0 (see Fig. 3.2a). When the value of s is larger than 5ε, the blending parameter α is equal to unity (see Fig 3.2b). In other situations, α is interpolated from 0 to 1. This yields

$$\alpha = min\left(1, max\left(0, \frac{s-\varepsilon}{4\varepsilon}\right)\right) \tag{3.3}$$

In addition, the water depth is limited to ε_2 in the bottom drag and wind stress parametrization to avoid unrealistic forcing. We use $\varepsilon_2 = \varepsilon$ in the three test cases below.

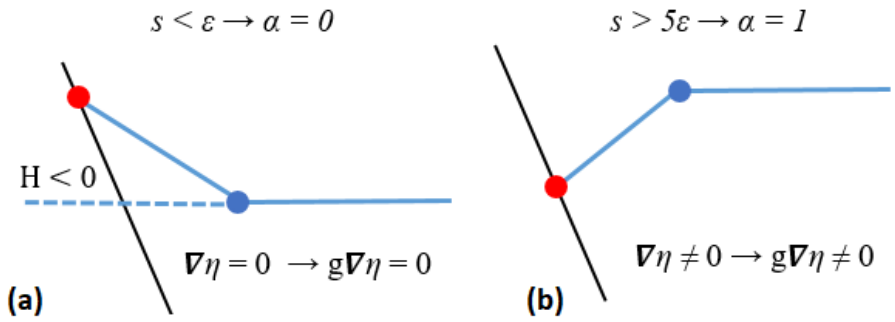

Fig. 3.2. Evolution of free surface when using a blending parameter: (a) *s* is smaller than the tolerance value and (b) *s* is higher than the tolerance value; bottom (black line), water surface (blue line), water surface in dry cell (dashed line) and cell nodes (dots).

3.2.3 Validation of the algorithm

In this section, the performance of the proposed algorithm is assessed on the basis of several test cases. Below, all the values of the variables are expressed in the International System of Units, i.e. m (meter), s (seconds) etc. The discrete initial conditions and the bottom topography are derived from the analytical ones by interpolation at the nodal (cell interface) points.

The Balzano 1 test case

Three idealized one-dimensional test cases developed by Balzano (1998) are widely used to evaluate the accuracy of various wetting - drying methods (Yuan and Falciner, 2008) because they exhibit problematic conditions in a simple setup (Candy, 2017). Originally, the computational domains of these three Balzano test cases are one-dimensional basins with a length of 13800 m. However, as the purpose of this paper is to test the implementation of the new wetting - drying algorithm in the two-dimensional version of SLIM, these domains are modified by adding a width of 7200 m. It is then verified that the solutions of the two-dimensional simulations performed by means of SLIM on unstructured meshes correspond to the one-dimensional solutions of the original Balzano test cases. In all Balzano test cases, the Coriolis force, the surface stress and the horizontal viscosity are not taken into account. The simulation time step is 1 s. The only difference between the three test cases is the bathymetry. The first Balzano test case aims at simulating a wave run up

on a basin with a uniform bed slope (see Fig. 2.3). The undisturbed water depth is $h = x/2760$, where x is the coordinate in the main direction of the basin.

The threshold thickness ε is a key issue in the wetting - drying algorithm. Mass conservation should be satisfied and the computational cost needs to be affordable. As the Balzano test case 1 is a simple one, it is possible to run it with different values of ε and to investigate the sensitivity of the results to these values. The width and length of the domain are kept identical for all simulations while the slope is modified with the depth varying from 3 to 50 m corresponding to variations of ε in a range of 0.001 - 1 m. Fig. 3.4 shows the relation between ε and the reference depth. It is clear that the value of ε should be increased as the depth increases. The blue dots indicate the runs where the simulation can work with ratio of ε/depth exceeding 0.2 %. If the ratio is smaller than 0.2 %, the non-linear Newton - Raphson solver does not converge. Therefore, the threshold value ε is selected to be 0.01 m for all test cases.

In the first Balzano test case, a sinusoidal water level variation is imposed at the open boundary (x = 13800 m) with a period of 12 h and an amplitude of 2 m. Our model results are in agreement with previous publications such as (Gourgue et al., 2009; Kärnä et al., 2011; Balzano, 1998). According to the summary by Yuan and Falciner (2008), some schemes cause unintended problems, for examples wiggles in the free surface profile during the wetting phase and in the drying phase, and pronounced underestimation (negative water thickness) or overestimation (positive water thickness) in the retention volume. By applying the proposed algorithm in SLIM, with the threshold value ε, the water thickness remains always positive and limited in dry areas (see Fig. 3.5), the retention volume is never underestimated, and the overestimation is controlled.

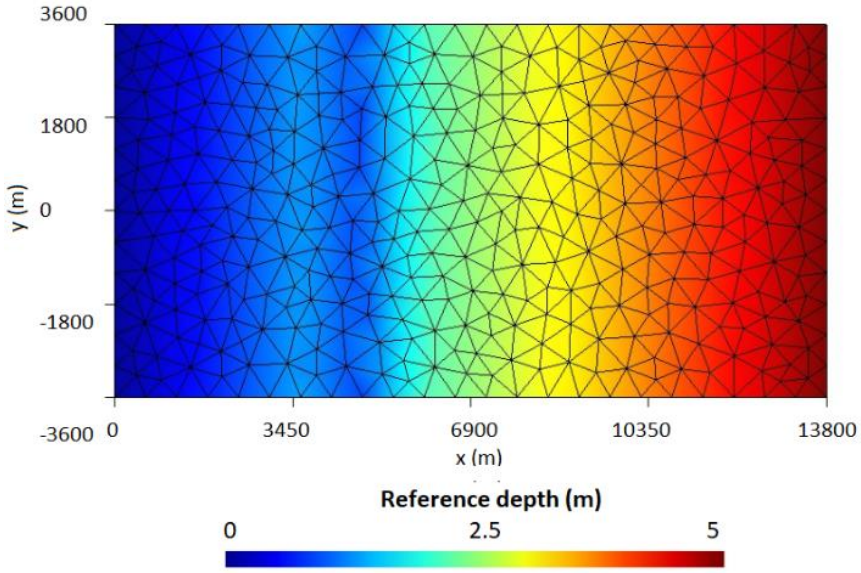

Fig. 3.3. Mesh with 500 m edge size and 716 triangular elements used for the Balzano 1 testcase

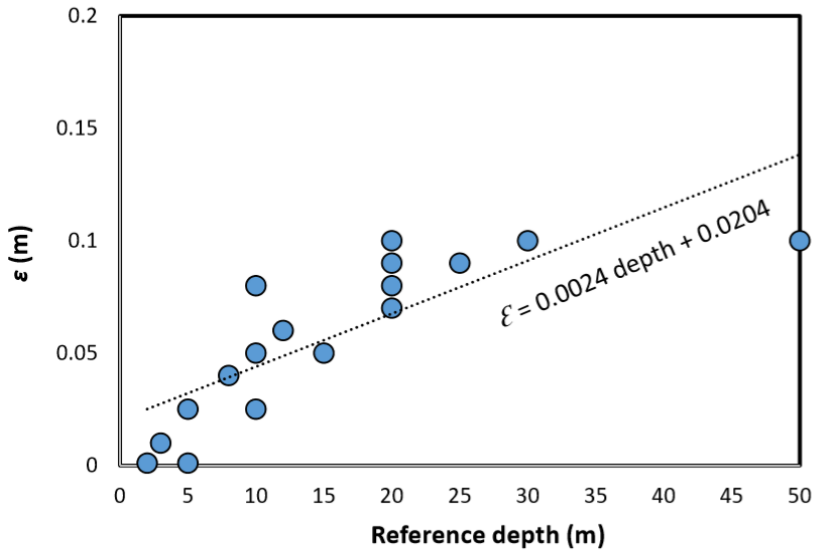

Fig. 3.4. The relation between the minimum value of ε and the reference water depth for the mesh illustrated in Fig. 3.3

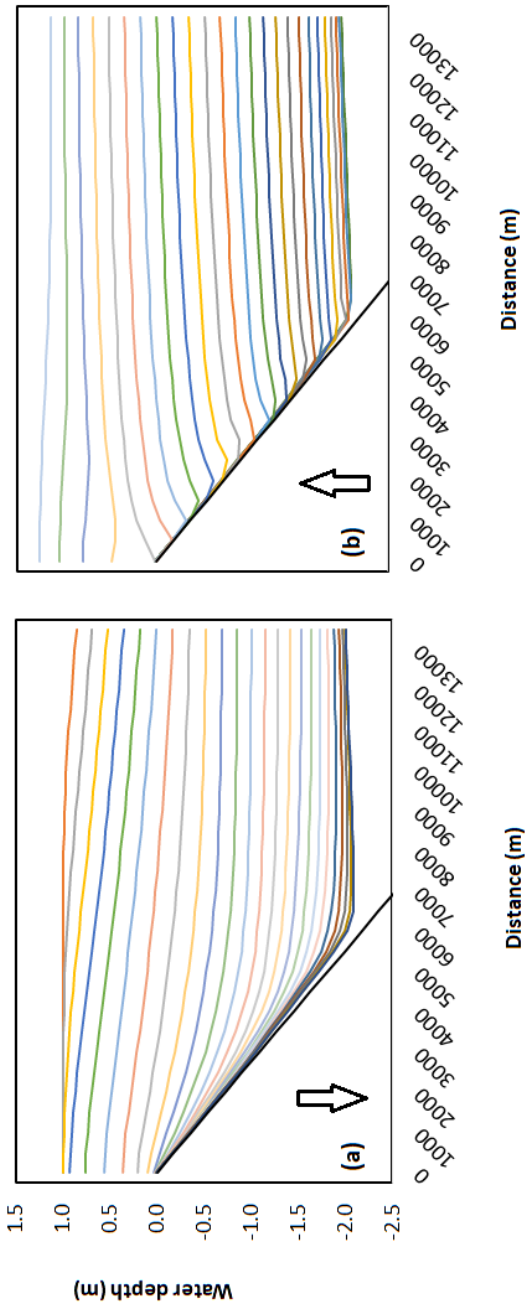

Fig. 3.5. First Balzano test case: vertical section through the domain of interest, showing the bottom (black line) and the water surface evolution every 600 s (colour lines), during the drying (a) and the wetting (b) phases with downward arrow and upward arrow, respectively

The Balzano 3 test case

The same simulation as the Balzano 1 test case is repeated, but with a modified bathymetry. The new bathymetry contains a small reservoir that can retain water in the drying phase (see Fig. 3.6). The analytical expression of the bathymetry is as follows:

$h = x/2760$ if $x \leq 3600$ m and $x \geq 6000$ m

$h = 30/23$ if $3600 \text{ m} < x < 4800$ m

$h = x/1380 - 50/23$ if $4800 \text{ m} < x < 6000$ m

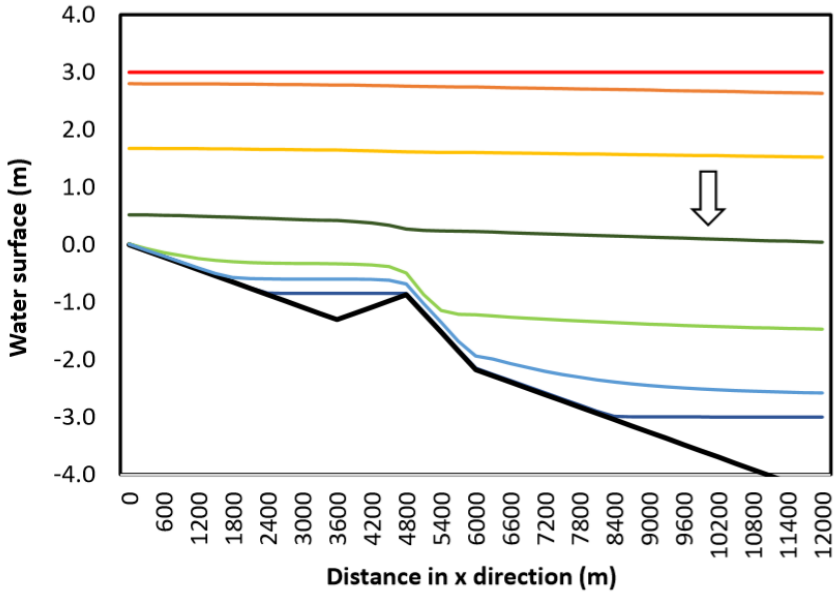

Fig. 3.6. Third Balzano test case: vertical section through the domain of interest, showing the bathymetry (black line) and the water surface evolution at the initial condition (red line) and equilibrium (blue line) by downward arrow

The mesh comprises 706 triangular elements of uniform size with edges of about 600 m. A sinusoidal water level variation is imposed at the open boundary with an amplitude of 3 m initially. The free surface elevation at the open boundary decreases from 3 to -3 m at the open boundary after 12 h of simulation. Then, water level is kept constant for an indefinitely long time in order to test whether water is leaking through the dry area, out of the small

intermediate basin. Indeed, with some wetting - drying methods, some water can flow from the reservoir to the rest of the basin, even when the mean surface level inside the reservoir is below the local peak of the bathymetry. Here, after 36 h of simulation, the expected water level is maintained in the reservoir. The physics does not seem to be altered at the limits between wet and dry areas. The simulation ends after 48 h and confirms that no negative water thickness appears in the whole domain.

The Thacker test case

This last test case has also been used by Balzano (1998) to compare the best methods of his review, and also e.g. by Gourgue et al. (2009); Kärnä et al. (2011); Nielsen and Apelt (2003), Vater et al. (2015). It reveals if a method is strictly mass conservative. The domain is a circular closed basin with a radius R = 430.62 km, so that no water can enter or leave the domain; the bed is a paraboloid of revolution. At the initial time, the free surface is also a paraboloid of revolution. The free surface moves with periodical oscillations and wetting - drying occurs in the vicinity of the outer boundary of the domain. In the absence of the Coriolis force, surface stresses and dissipation (neither viscosity nor bottom stress), the analytical solution for the non-linear shallow water equations is known (Thacker, 1981). Here, the mesh is generated with a size gradually increasing from 10 km near the boundary to 30 km at the center. The total number of triangles is 14114. The simulation time is 72 hours (256,200 s), corresponding to 6 periods, allowing for a good assessment of the water surface evolution in the basin. Water depth in the center of the basin at rest is h_0 = 10 m and initial surface water elevation is η_0 = 2 m. The unperturbed water depth and the free surface elevation are as follow:

$$h = h_0 \frac{R^2 - r^2}{R^2} \tag{3.4}$$

$$\eta = h_0 \left(\frac{\sqrt{1-A^2}}{1 - A\cos\varpi t} - 1 - \frac{r^2}{R^2} \left(\frac{1 - A^2}{(1 - A\cos\varpi t)^2} - 1 \right) \right) \tag{3.5}$$

with

$$\varpi^2 = \frac{8gh_0}{R^2} \tag{3.6}$$

$$A = \frac{(h_0+\eta_0)^2-h_0^2}{(h_0+\eta_0)^2+h_0^2} \tag{3.7}$$

where r is the radial coordinate ($r = 0$ at the center of the domain).

The threshold thickness ε is fixed to 0.01 m and the simulation time step is 1 s. The analytical expressions of the bathymetry and the solution of the non-dissipative problem are given by Eq. (3.4) - (3.7). However, the proposed wetting - drying method, by using an implicit time integration, introduces numerical dissipation. This results in the slight damping of the wave depicted in Fig. 3.8 showing the time evolution of the water level at the centre of the basin: overall, there is a fairly good agreement between the numerical solution and the analytical solution. The evolution of the free surface elevation at the center of the domain during 72 hours is shown in Fig. 3.7. The mass conservation is assessed for 3 simulations with 3 different time steps. The results confirm 100 % of mass conservation for time step of 1 s. Less than 0.001 % of mass is lost after 72-hour simulation with time steps of 10 s and 100 s.

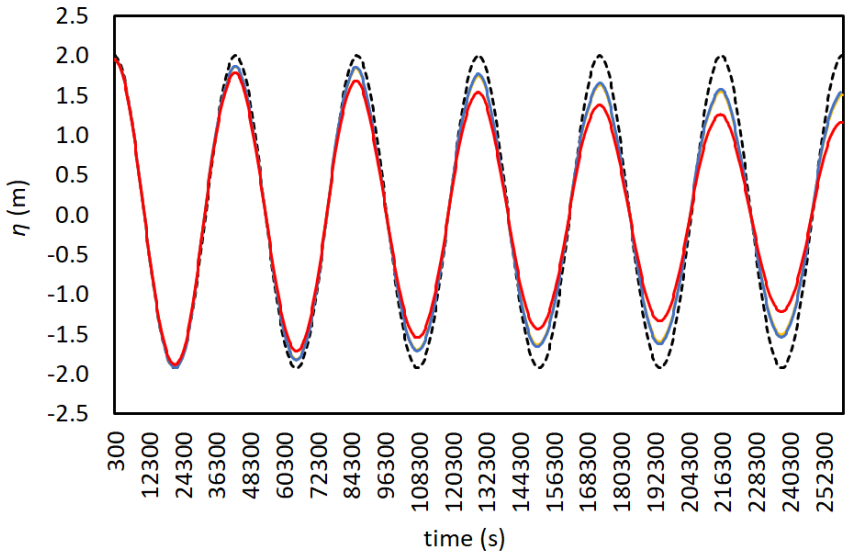

Fig. 3.7. Thacker test case: Evolution of water surface elevation in the domain center with different time steps: dash black line is the exact solution of Thacker, assuming zero dissipation; blue line (dt = 1 s), orange line (dt = 10 s) and red line (dt = 100 s)

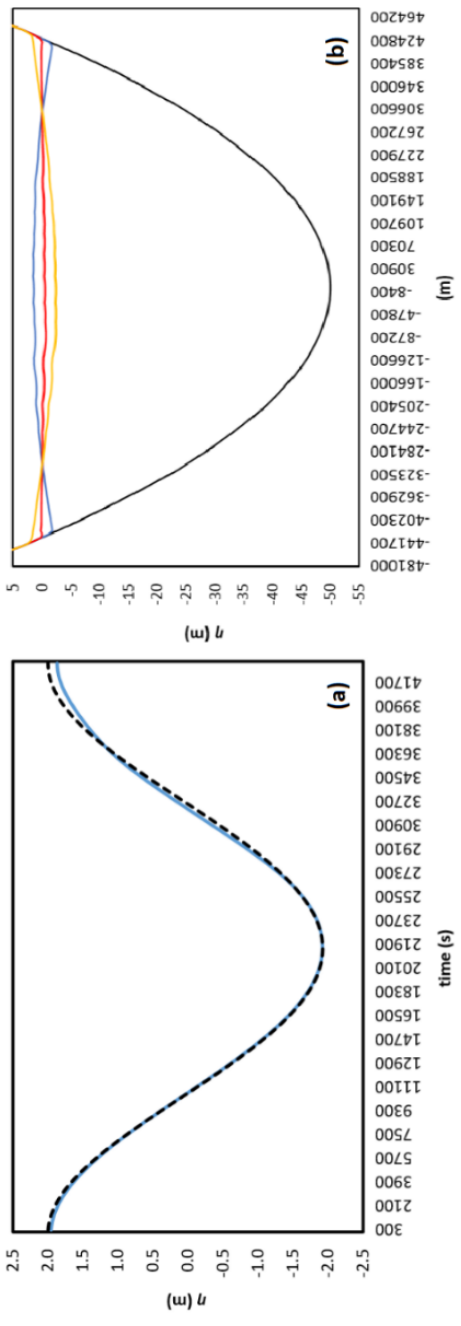

Fig 3.8. Thacker test case: (a) Comparison of water surface elevation in the domain center: with the dashed line representing the analytical solution and the continuous blue line representing the numerical solution; (b) Vertical section showing the sea bed (black line) and position of simulated water surface at initial time (blue line), after 3 hours (red line) and after 6 hours (orange line)

3.3 Application to the Tonle Sap

The proposed wetting - drying algorithm has been assessed by several analytical test cases, showing that the scheme is well-balanced, mass conservative and stable for rapid transitions of the wet/dry interface with different time steps of 1 s, 10 s and 100 s. Hopefully, the proposed technique is a robust method, which is able to handle realistic and complex water bodies. It is seen below that it can simulate the inundation process and subsequent drying in the Tonle Sap lake, Cambodia floodplain.

3.3.1 Domain description

The Tonle Sap is located in the Cambodian floodplain which contributes largely to the Mekong River dynamics (Kummu et al., 2014). It comprises a permanent lake, 12 tributaries, extensive floodplains and the Tonle Sap River linking the lake to the Mekong River. The permanent lake extends over of a large territory towards the Northwest of Cambodia, with dimensions of 75 km x 32 km, and comprises a small part in the Southeast of the domain with dimensions of 35 km x 28 km (Ji et al., 2018; Campbell et al., 2009). The lake and its floodplains form the largest freshwater source in Southeast Asia (Kummu et al., 2014). The Tonle Sap River with a length of approximately 120 km (Siev et al., 2016) is situated at the Southeast end of the Tonle Sap lake and joins the Mekong River at Chaktomuk confluence. At the confluence, the river splits into the Bassac River in the West and the Mekong River in the East.

The hydrology of the Tonle Sap is driven by the monsoonal flood regime of the whole Mekong River Basin (Penny, 2006; Berg et al., 2007). As a result, the Tonle Sap has a unique hydrological regime. In the flooding season (from June to October), when the water level of the Mekong River is higher than in the Tonle Sap lake, reserve flows takes place from the Mekong River into the lake. In addition, discharges from the 12 tributaries and overland flow provide additional water sources for the lake. Therefore, the water level in the lake increases from 1.44 m to 9.09 m above the sea level (Kummu et al., 2014). At the beginning of the dry season (November), the water level in the Tonle Sap lake reaches a peak value and its level becomes higher than the level in the

Mekong River. Thus, the flow changes direction and water discharges from the Tonle Sap lake towards the Mekong River. Hydrologically, the lake functions as a regulatory reservoir for the VMD (Campbell et al., 2009; Thanh et al., 2017), storing approximately 50 % of total Mekong inflow and releasing 90 % of outflow to the Mekong River (Royal Haskoning, 2010), providing a freshwater inflow to the downstream region in dry season (Hai et al., 2008). With this phenomenon, the flooded area varies from 7,190 to 12,720 km^2 (Kummu et al., 2014) and causes the occurrence of dry areas after water recedes. This specific hydrological behavior is vital for all the riparian communities (Kummu et al., 2014).

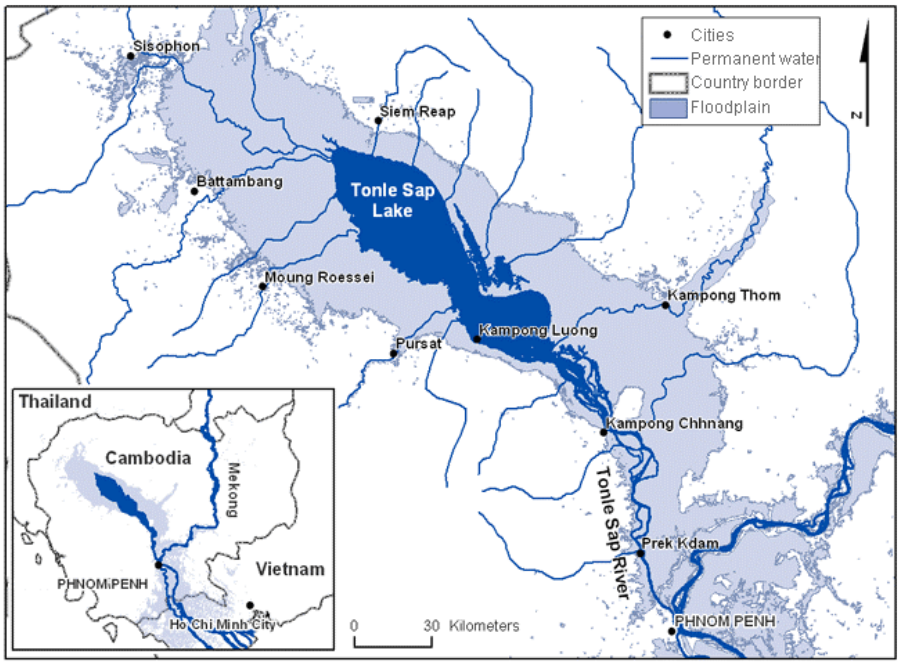

Fig. 3.9. Map of the Tonle Sap system and its sub-catchments (WUP-JICA, 2004)

The new wetting - drying algorithm integrated in SLIM is used to simulate the complex flow regime of the Tonle Sap. The computational domain extends over the floodplains and is limited to the south at Phnom Phenh, at the confluence with the Mekong River at Chaktomuk. The model uses a spherical coordinate system and the multi-scale mesh is generated by the algorithm developed by (Remacle and Lambrechts, 2018; Lambrechts et al., 2010). The

mesh consists of 187,906 triangular elements with 94,544 nodes. The finer mesh elements are used to represent the 12 tributaries and the Tonle Sap River while the coarser mesh elements are used for the floodplains and the permanent lake. The mesh resolution varies from 200 m to 2000 m in order to take into account the wide range of physical processes occurring in the simulation domain. The application of this multi-scale mesh allows to simulate both small-scale and large-scale processes within a single model without nesting (Vallaeys et al., 2018). Our model does not take into account the interaction between groundwater and surface water.

Table 3.1 Sub-catchments of Tonle Sap (Lu et al., 2014)

No.	**Sub-catchment**	**Area (km^2)**
1	Chinit	8236
2	Sen	16359
3	Staung	4357
4	Chikreng	2714
5	Siem Riep	3619
6	Sreng	9986
7	Sisophone	4310
8	Mongkol Borey	10656
9	Sangker	6052
10	Dauntri	3695
11	Pursat	5965
12	Boribo	7153
	Lake (average)	2887
Sum		85,989

3.3.2 Model set-up

The bathymetry of the simulation domain was constructed from two data sets. First, the topographical data were obtained from the Mekong River Commission (MRC, 2003) under the form of a Digital Elevation Model (DEM) with a 50 x 50 m grid resolution. Then, local cross-section measurements done by the MRC provide a description of the bed elevation in the lake and the river. The bathymetry of the lake is very irregular with variations from - 50 to 0 m. By this domain, value 0 is the origin of the vertical axis at the bottom of the lake. The negative values of the vertical axis mean the bathymetry in the upward direction (Fig. 3.10).

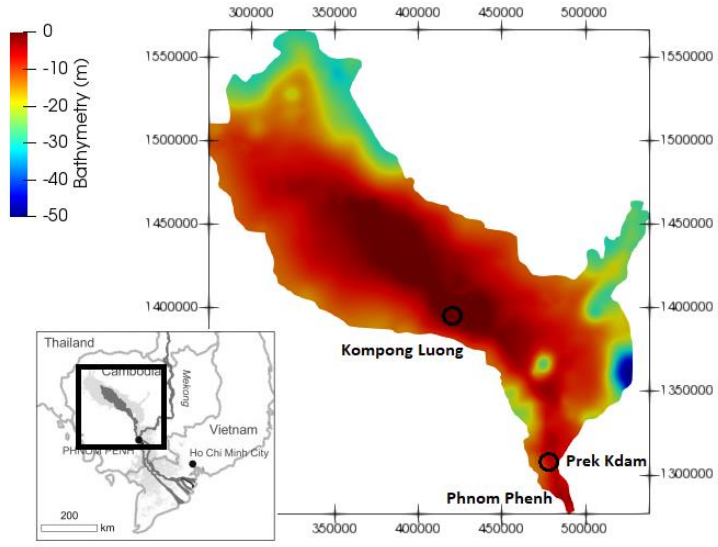

Fig. 3.10. Location and bathymetry of the domain with Kompong Luong station and Prek Kdam station. By this domain, value of 0 is the origin of the vertical axis at the bottom of the lake. The negative values of the vertical axis mean the bathymetry in the upward direction.

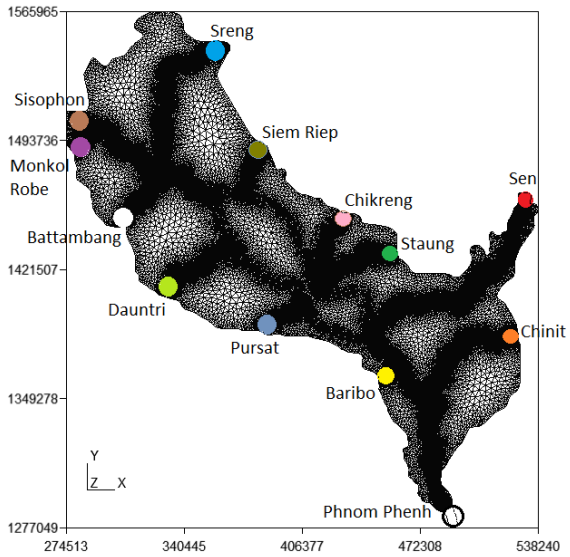

Fig. 3.11. Computational mesh. The color dots show the 12 stations corresponding to the tributaries as water inputs and the white dot represents the downstream boundary of the model at Phnom Phenh station

The daily discharge from the 12 tributaries and the daily water level at Phnom Phenh (downstream boundary) are imposed at the boundaries of the computational domain (Fig. 3.11). These data (Fig. 3.12) were obtained from the Mekong River Commission. No-slip and impermeability conditions are set along the close boundaries. The downstream open boundary condition consists of the water level variation measured at Phnom Phenh. Daily water level measurements at Kompong Luong station, located in the lower part of the lake; and at Prek Kdam, located in the Tonle Sap River, are presented in Fig. 3.13; they are used here below for model validation. These data are collected from the monitoring network of the Mekong River Commission since 1994 to present. The numerical simulations are performed to determine (1) the spatial and temporary fluctuations of the Tonle Sap flow as well as the changes in water level and inundated area of the Tonle Sap system; and (2) the hydraulic relation between the Tonle Sap and the Mekong River. To cope with the large bathymetry gradient in this real topography, the water velocity on partially dry elements is clipped to 1 m/s. The threshold for drag parameter ε_2 is set to be 0.5 m.

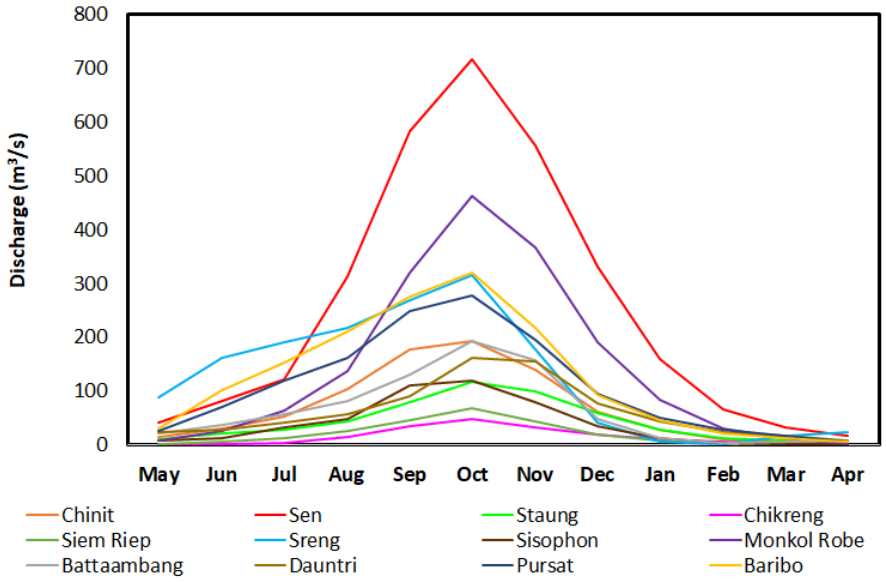

Fig. 3.12. Average monthly discharge at the 12 stations indicated in Fig. 3.11

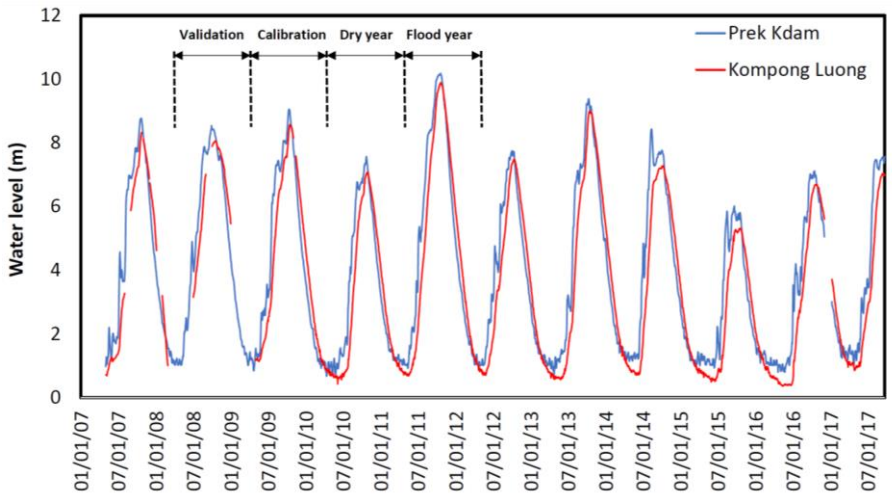

Fig. 3.13. Water level at Kompong Luong (red line) and Prek Kdam (blue line) from 12 hydrological years 2006 – 2017

Model calibration and validation

Hydrodynamic modeling of a natural domain requires a careful selection of parameters (e.g the Manning coefficient) to simulate the physical conditions as closely as possible to real conditions. In addition, the parameters of the implicit wetting drying algorithm are calibrated to maintain numerical stability and a reasonable simulation time. Model calibration and validation are performed by comparing the water level observed at Kompong Luong and Prek Kdam stations and the simulated ones (see Fig. 3.10). Then using the calibration model, the filling and emptying processes of the lake is analysed for two extreme situations: a dry and a wet year. The calibration period is selected from 1/5/2008 to 30/4/2009 and the validation period is from 1/5/2009 to 30/4/2010 because these periods are representative for normal hydrological conditions (see Fig. 3.13). The simulated data will be compared to observed water levels at these two stations. The Manning coefficient is used for parameterizing the bottom friction. From the calibration simulations with different Manning coefficients (n = 0.032 s/m$^{1/3}$, 0.035 s/m$^{1/3}$ and 0.038 s/m$^{1/3}$, see Table 3.2), the optimal one was found to be n = 0.035 s/m$^{1/3}$ in the whole domain, which is in a good agreement with previous studies (Manh et al.,

2014). The threshold value of water depth ε for the wetting - drying algorithm is selected by the method applied in the Balzano test case 1 and considering the computation cost, it is fixed to be 0.1 m. The quantitative assessment of the results for each tested value of the parameters is achieved using the Nash-Sutcliffe coefficient (NSE):

$$NSE = 1 - \frac{\sum_{i=1}^{n}(H_{obs,i} - H_{simu,i})^2}{\sum_{i=1}^{n}(H_{obs,i} - \overline{H_{obs}})^2} \tag{3.8}$$

where $\overline{H_{obs}}$ is the mean value of observed water depths, $H_{obs,i}$ is the observed water depth at time t = i Δt and $H_{simu,i}$ is the numerically simulated water depth at time t = i Δt, n being the total number of time steps. The mean absolute error (MAE) is applied to measure the absolute differences between simulated results and observed data as follows:

$$MAE = \frac{\sum_{i=1}^{n}|H_{obs,i} - H_{simu,i}|}{n} \tag{3.9}$$

In addition, the Root Mean Square Error (RMSE) is also used to evaluate the quadratic average difference between computed results and observed data.

$$RMSE = \sqrt{\frac{\sum_{i=1}^{n}(H_{obs,i} - H_{simu,i})^2}{n}} \tag{3.10}$$

The summary of model validation is shown in the Table 3.2 and Fig. 3.14 and Fig. 3.15. They present good agreements with observed data thus the validated parameters will be applied for testing different scenarios in severe conditions, for the flooding year 2011 and dry year 2010 as described below.

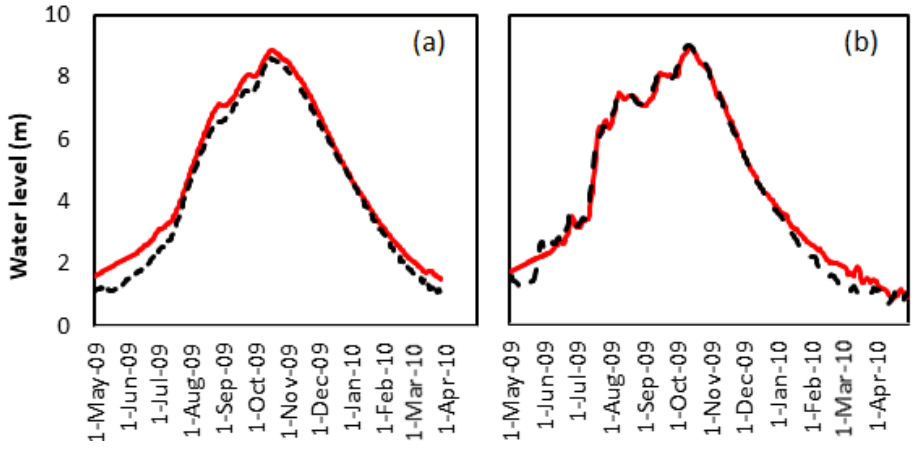

Fig. 3.14. Calibration of water level in Kompong Luong station (a) and Prek Kdam station (b) from 1/5/2009 to 30/4/2010. The red continuous line corresponds to the simulated results and the dashed black line corresponds to in situ measurements.

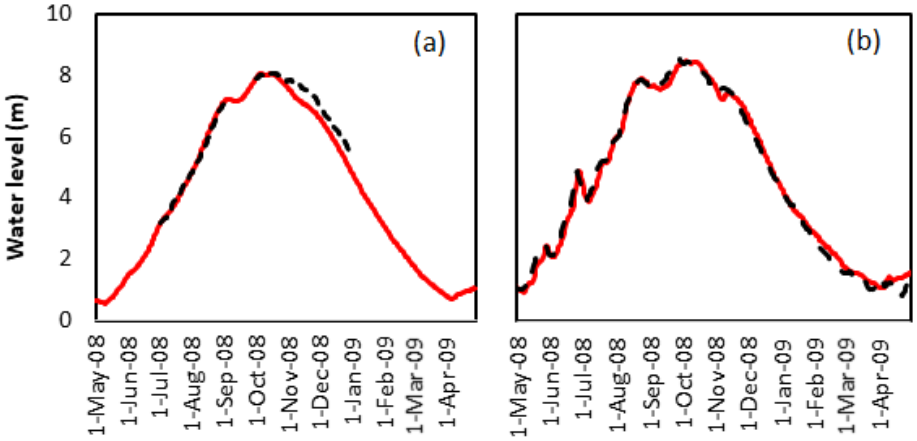

Fig. 3.15. Validation of water level in Kompong Luong station (a) and Prek Kdam station (b) from 1/5/2008 to 30/4/2009. The red continuous line corresponds to the simulated results and the dashed black line corresponds to in situ measurements.

Table 3.2. Model validation

	Kompong Luong		Prek Kdam	
	Calibration	Validation	Calibration	Validation
n = 0.032 s/m$^{1/3}$				
RMSE (m)	0.70	0.90	0.36	0.23
MAE (m)	0.53	0.79	0.27	0.18
NSE (%)	92.56	63.78	98.31	99.23
n = 0.035 s/m$^{1/3}$				
RMSE (m)	0.61	0.30	0.41	0.22
MAE (m)	0.29	0.23	0.34	0.23
NSE (%)	94.63	95.97	97.70	99.36
n = 0.038 s/m$^{1/3}$				
RMSE (m)	0.66	0.85	0.21	0.21
MAE (m)	0.26	0.73	0.56	0.73
NSE (%)	93.44	67.71	98.03	99.36

3.3.3 Results

Flood pattern 2011

The hydrological year 2011 (May 2011 until April 2012) is selected because this year is regarded as historically extreme for both the spatial extent area and the water depth of this seasonal inundation across the Cambodia floodplain and the VMD (Manh et al., 2014) (see Fig. 3.13) during 88 years of observation (MRC, 2015). Simulation results are illustrated in Fig. 3.16, where the extent of the inundated area as well as the representative depth-averaged velocities are illustrated for each month. The wetting - drying process can be clearly identified: panels (a) and (b) are a transition period of dry - wet seasons; panels (c), (d), (e), and (f) are months of the wet season; panels (g), (h), (i), (j) and (k) are months of the dry season. The blue colour shows wet areas and gray colour shows dry areas. The arrows illustrate representative current magnitudes and directions. The white line is the limit of the wet areas. So, a flooding and dewatering pattern can be observed, as a result of water depth fluctuations with respect to the real topography. The inundation area is calculated by using SLIM postprocessing software, ParaView 5.6.0 (https://www.paraview.org/). Fig. 3.16 (a) represents the results for May 2011. It may be noted that this month is the end of the dry season and the beginning of the flood season, so there are relatively large dry

areas, which are located almost over the whole domain. Only the permanent lake is flooded with a mean water level of 1.06 m and a wet area of 2216 km^2. The southern part of the domain has the lowest bed elevation, thus the water flows from this point in the northwestern direction to the lake and starts filling up the domain. Flows from the northern tributaries also begin reaching the lake. Thus, the wet area extends gradually. Fig. 3.16 (b) shows the situation of June 2011. This month is the beginning of the wet season. The lake has inflow and outflow, however the prevailing direction is flow towards the lake. Together with flows from tributaries, the flow from the Mekong River makes water level rise sharply to 1.65 m and the wet areas expand on both sides of the lake. Vectors representing current flow clearly show the dominance of water discharge from the Mekong River to the lake. In Fig. 3.16 (c) for July 2011, the water level rises up to nearly 3.27 m, with an inundated area of approximately 6783 km^2 and the input water of the lake is strongly sourced from the Mekong River and its tributaries. Fig. 3.16 (d) and Fig. 3.16 (e) correspond to August and September 2011, which are in the middle of the wet season. Therefore, the water depth is very high with values of approximately 8.03 m. The prevailing flow direction is from the Mekong River towards the lake and the dry areas are getting smaller. October is the end of wet season, as shown in Fig. 3.16 (f); the water level reaches its peak at 9.66 m and the maximum inundated area is approximately 14,580 km^2. Approximately 90 % of the floodplain area is covered by water at the peak level. The dry areas are only located in the north, east and mountain of the whole domain. At the end of this month, when the water level in the lake is higher than in the river, the flow starts changing its direction, toward the Mekong River. The current is the strongest at Prek Kdam. November - April is the dry season and thus the panels show outflow from the lake, see Fig 3.16 (g) - Fig 3.16 (l), the water levels and surface areas reduce gradually to the minimum levels of 1.33 m and 3142 km^2, respectively, exactly in April 2012. Based on the topographical condition, the northern part of the lake is getting dry first while the southeast part is always wet and flow in this area is strongest.

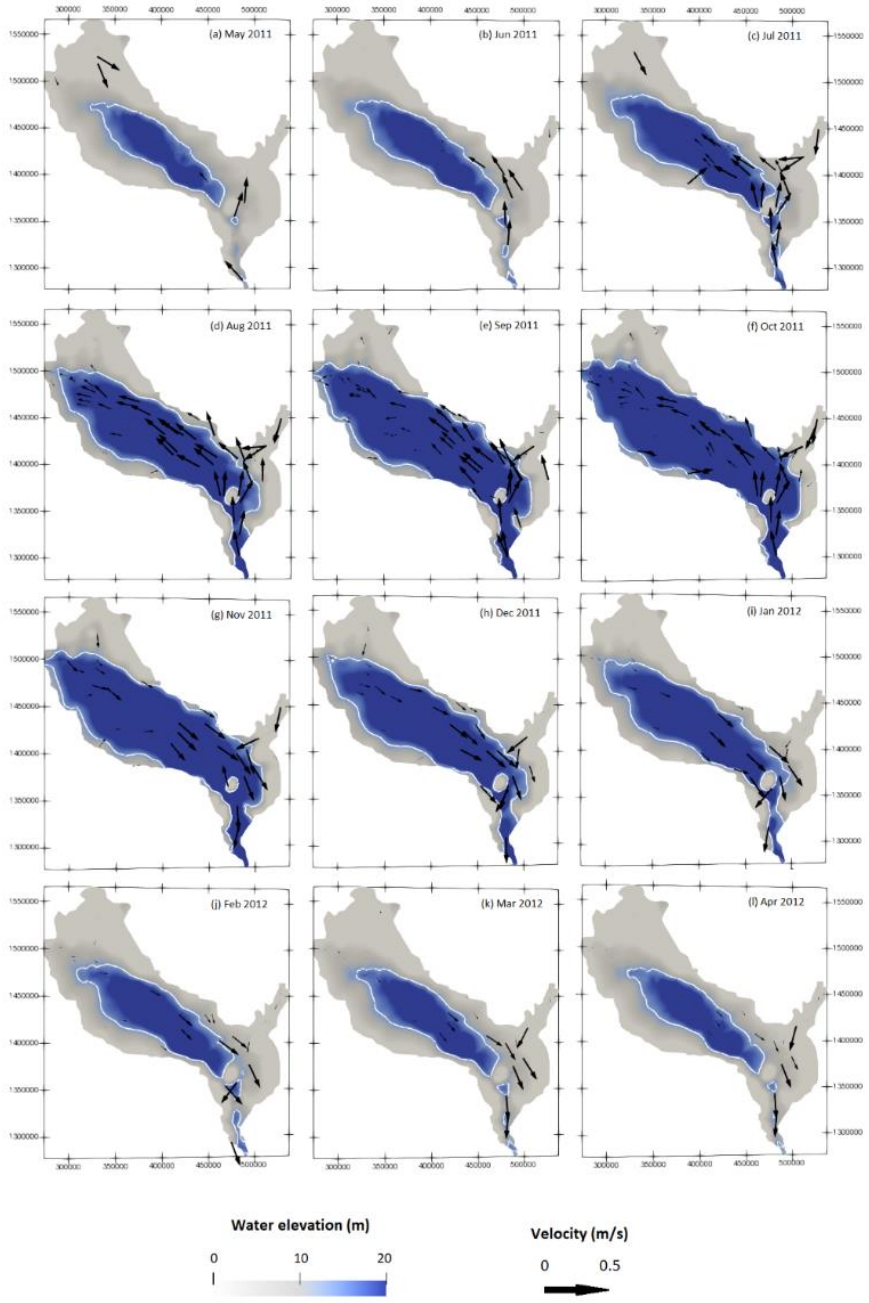

Fig. 3.16. Surface water area and flow patterns simulated for the extreme flood year 2011

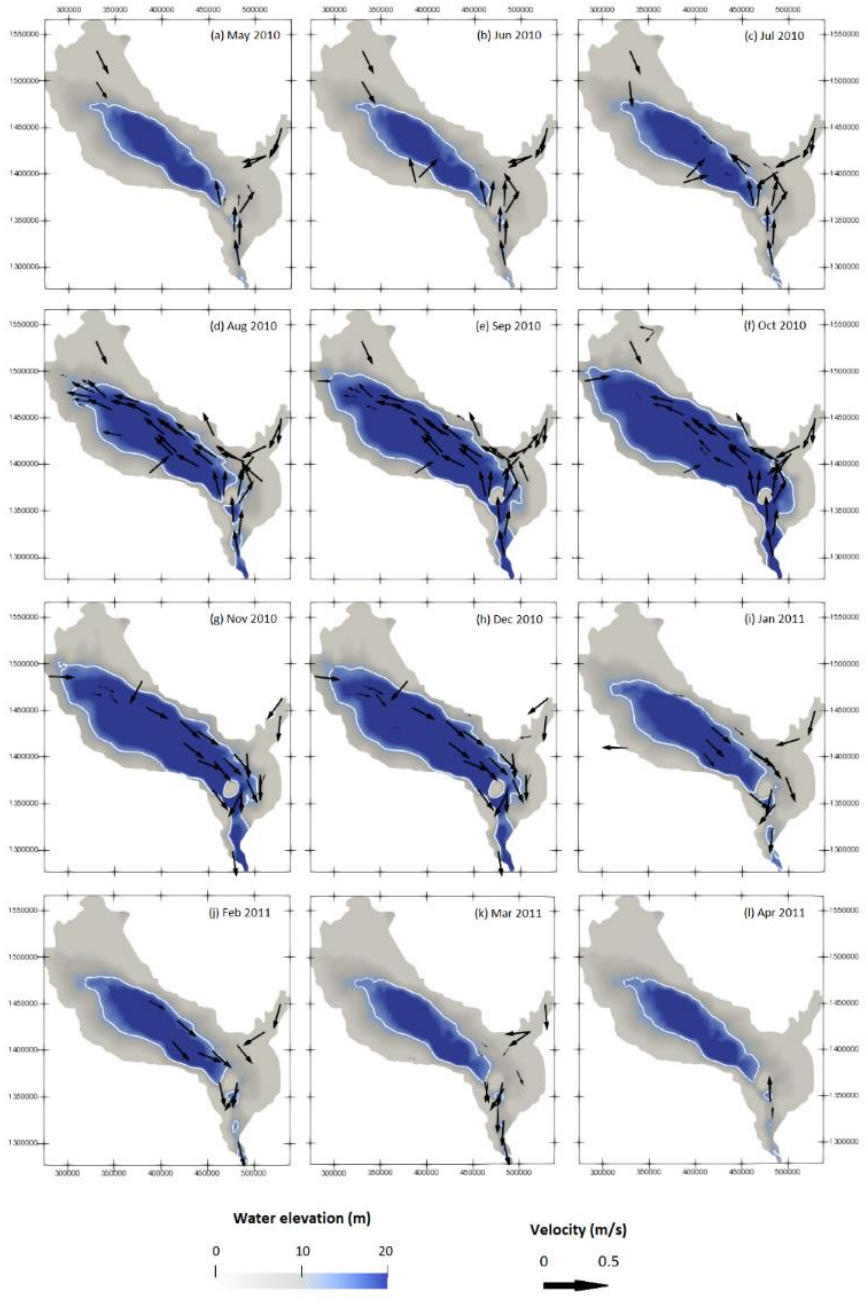

Fig. 3.17. Surface water area and flow patterns in dry year 2010

Dry pattern 2010

According to the observed data from (MRC, 2015 and Manh et al., 2014) and Fig. 3.13, the year 2010 (May 2010 to April 2011) is the driest year in the observation period. This simulation is implemented to reproduce the surface area and flow panels in comparison with the flood year. Similarly to year 2011, the period of May - October is the wet season, and the period of November - April is the dry season. From May to July 2011 (see Fig 3.17(a), Fig 3.17(b) and Fig 3.17(c), the main water sources of the lake originate from the Mekong River and the Tonle Sap's tributaries. Thus, water level in the lake varies gradually from 0.95 m to 1.47 m, the wet area increases to 3564 km^2 at the end of July 2011. From August to October 2011, the lake receives water from two sources, mainly from the Mekong River and a partly from its tributaries. Strung Sen is a major tributary of the Tonle Sap in both area and discharge (see Table 3.1 and Fig. 3.12). Thus, it plays an essential role supplying water for the Tonle Sap. After this period, the water level goes up to 7.13 m, corresponding to an area of 12,648 km^2. The period of November - April corresponds to the dry season, thus the water level and surface area reduce sharply to the minimum values of 1.21 m and 2592 km^2. The variations of water level, surface area and water volume between 2010 and 2011 are presented in Table 3.3.

3.3.4 Discussion

Variation of Tonle Sap in a year

According to the observed hydrographs of the Mekong River and of the 12 tributaries of the Tonle Sap, and to the diagrams of water level evolution in the lake, four distinct phases can be identified in the flood regime of the lake: (1) the rising phase (May - August), when the water level rises fast and water occupies larger areas; (2) the wet phase (September - November), when the water level grows slowly and the changes of inundated area are no more significant; (3) the receding phase (December - February), after the peak water level records, when the water levels significantly decreases as well as the flooded area; and (4) the dry phase (March - April), when the water level and flooded area reduce again to minimal values. During the simulation of the flooding year (2011), the inundated area has increased by 12364 km^2 from

2216 km^2 (mean value) to a maximum value of 14580 km^2, corresponding to a variation of the water level between 1.06 m and 9.66 m. As a result, a large area is exposed to transitions from dry to wet condition and vice versa. Similar features are observed during the dry year (2010), as the inundated area has increased by 10804 km^2 from 1841 km^2 to a maximum value of 12645 km^2, corresponding to a variation of water level between 0.95 m and 7.14 m. This result confirms the close relation between the flood-pulse features of the Tonle Sap Lake and flooding - dewatering phenomena, which are under the direct impact of the flow from the Mekong mainstream (Kummu et al., 2008; ADB, 2009b; Ji et al., 2018).

Variation of Tonle Sap between flood and dry years

Regardless of the type of flow conditions (flooding year or dry year), the hydraulics of the Tonle Sap presents key features related to the flow driven by the Mekong River. According to simulated results, during both considered years, significant monthly variations are observed from the beginning of the wet season and reach a peak in October, then the observed values reduce until the end of the dry season (see Fig. 3.18 and Table 3.3). However, the amplitude of the phenomena differs: in October, the highest water level and surface area of year 2010 (dry year) are 74 % of the same values recorded in year 2011 (flooding year), while the maximum water volume in 2010 corresponds to less than 58 % of that in 2011.

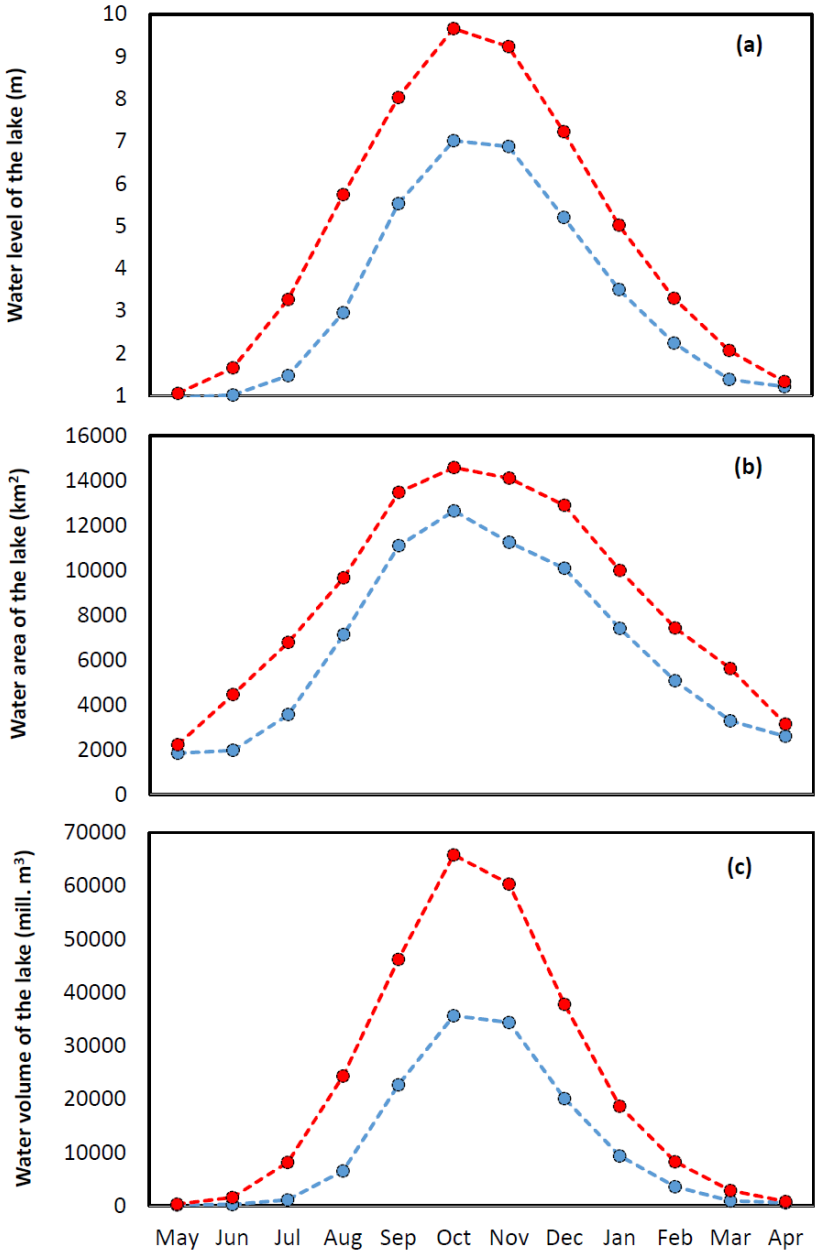

Fig. 3.18. Variation of water level (a), surface area (b), water volume, (c) between flooding year (red) and dry year (blue) in the Tonle Sap lake

Table 3.3 Variation of lake characteristics between 2010 and 2011

	Dry year 2010	**Flood year 2011**	**Difference**
Min level (m)	0.95 *(11 May 2010)*	1.06 *(12 May 2011)*	0.10
Max level (m)	7.14 *(01 Nov 2010)*	9.66 *(22 Nov 2011)*	2.47
Level variation (m)	6.19	8.60	2.65
Min area (km^2)	1,841	2,261	420
Max area (km^2)	12,645	14,580	1,935
Area variation (m^2)	10,804	12,364	1,560
Min volume (mill. m^3)	1.02	1.56	0.54
Max volume (mill. m^3)	40,674	69,916	29,242
Volume variation (mill. m^3)	40,673	69,914	29,241

Flow contribution

The monthly discharge at Prek Kdam is calculated from SLIM results and compared with the measured discharge at Phnom Phenh; and with the total discharge from 12 tributaries of the Tonle Sap (Fig. 3.19). The monthly discharge at Prek Kdam shows two groups of values. The negative values mean inflow from the Mekong River towards the lake, that occurs during the wet season. The maximum monthly value is approximately 7100 m^3/s. The positive values start from November to April, meaning that the flow is outward. The maximum monthly value is about 5000 m^3/s, approximately 2100 m^3/s lower than in flood season. It can be explained by the contribution of flow from tributaries. The minimum monthly flow appears in April with value of approximately 750 m^3/s. At this time flow from the Tonle Sap is the main water source supplying the Mekong Delta. The discharge from Phnom Phenh and the total discharge from the 12 tributaries show the time lag with maximum value in September and October, respectively. As the amplitude of the discharge at Phnom Phenh is 10 - 20 times higher than the one of the tributaries, it confirms the flow pulse of the Tonle Sap is dominated directly by the flow regime from the Mekong River under the cyclic episodes of flooding and drying. This outcome is consistent with (WUP-JICA, 2004; Ji et al., 2018).

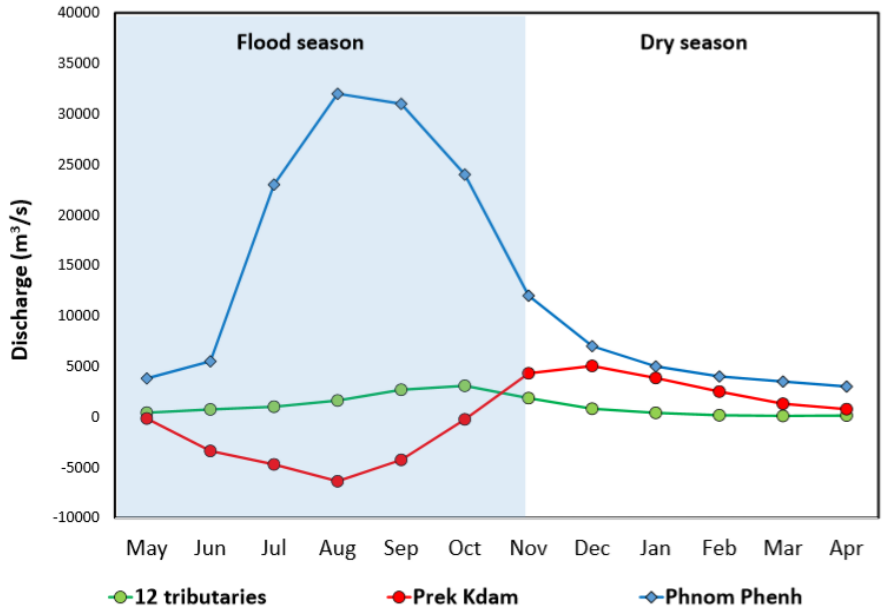

Fig. 3.19. Mean monthly discharge at Phnom Phenh (blue - measured) and total discharge from 12 tributaries of the Tonle Sap (green - summary) in comparison with discharge at Prek Kdam (red - simulated) for the period 2008 - 2012

Comparison with previous studies

To confirm the accuracy of the present wetting - drying algorithm, our results are compared with those achieved by previous studies. These results show the consistency with previous works done by Kummu et al. (2014) on water balance analysis, conducted for a period of 1997 - 2005 (Table 3.4). The differences can be explained by three reasons: (1) two studies were conducted for two different periods; (2) the results from Kummu et al. (2014) were calculated based on a water balance model, considering overland flow, precipitation and evaporation, while SLIM results focused on surface water dynamics; and (3) the values of surface area and water volume are calculated by SLIM postprocessing and the rating curves of the Tonle Sap characteristics were conducted based on measured data in 2002 (WUP-JICA, 2004).

The hydraulic simulation conducted by Fujii et al. (2003) shows a maximum water volume of 77.5 km^3. The maximum discharges inward and outward the

lake are 7900 m^3/s and 8200 m^3/s, respectively. These differences between two results can be attributed to the fact that Fujii et al. (2003) performed their simulations based on data from 2002, that is a particular year with high flooding and two peaks in the whole Mekong basin. Moreover, the data used by his study were not affected by the operation of the hydropower cascade in China that began in 2008 (Ji et al., 2018).

Table 3.4 Comparison with previous studies

Parameter	**Water balance calculation (Kummu et al., 2014)**	**Hydro dynamic simulation (Fujii et al., 2003)**	**Measured data (MRC, 2015)**	**Satellite image analysis (Ji et al., 2018)**	**SLIM modeled results**
Min water level (m)	1.19	-	-	-	0.95
Max water level (m)	10.36	-	-	-	9.66
Min surface area (km^2)	2,061	-	-	2,445	1,841
Max surface area (km^2)	15,280	-	-	16,508	14,580
Min water volume (km^3)	1.3	-	-	-	1.02
Max water volume (km^3)	76.1	77.5	-	-	69.9
Max inflow discharge (m^3/s)		7,900	7,032	-	7,662
Max outflow discharge (m^3/s)		8,200	8,176	-	8,160

MRC (2015) stated that the maximum inflow and outflow discharge from the Mekong River to the lake observed in period of 2008 - 2010 were 7032 m^3/s and 8176 m^3/s. These values are similar to the SLIM results.

By remote sensing technique, Ji et al. (2018) has utilized MODIS data from 2000 to 2014 to assess the variations of Tonle Sap wet area. The minimum area is 2445 km^2, appearing in 2005 and the maximum area is 16508 km^2, appearing in 2011. The maximum values are approximately 20 % higher than our simulated results. This difference can be acceptable because inflows to the lake consist not only from the Mekong mainstream and tributaries but also

from overland flow, precipitation and groundwater recharge in both wet and dry seasons (May et al., 2011).

The Moderate Resolution Imaging Spectroradiometer (MODIS) on NASA's Terra satellite also captured the images of flooding area in the Tonle Sap system on August 24, 2011 (see Fig. 3.20a) and August 26, 2010 (see Fig. 3.20b) (Brackenridge, 2011). These images used a combination of visible and infrared light to better distinguish between water and land. The significant changes are apparent between August 2010 and August 2011, which are in agreement with our simulated results. In 2011, the water level was higher in and around Tonle Sap, and large areas of water covered the ground north, east, and south of Phnom Phenh.

The biggest differences between the SLIM results and other previous studies are the minimum values of water level, water area and water volume. However, considering the measured data (see Fig. 3.13), the minimum water level observed in this period is 0.87 m, approximately 8 % lower than SLIM results, different values of the water area and water volume can be found in other works.

The role of Tonle Sap system in the Mekong Basin

During flooding phases, the water volume of Tonle Sap lake increases by about 69,560 km^3, from 0.356 km^3 to 69,916 km^3. A large amount of water from the Mekong River comes into the Tonle Sap lake. It means that the lake works as a floodwater storage for the Mekong system, particular for the Mekong Delta. During the dry season, a high discharge from the Tonle Sap lake flows to the Mekong Delta. This value is estimated up to 5000 m^3/s, approximately with the one measured in Phnom Phenh. It confirms that the Tonle Sap lake is a major water supplying source for the Mekong Delta in the dry season.

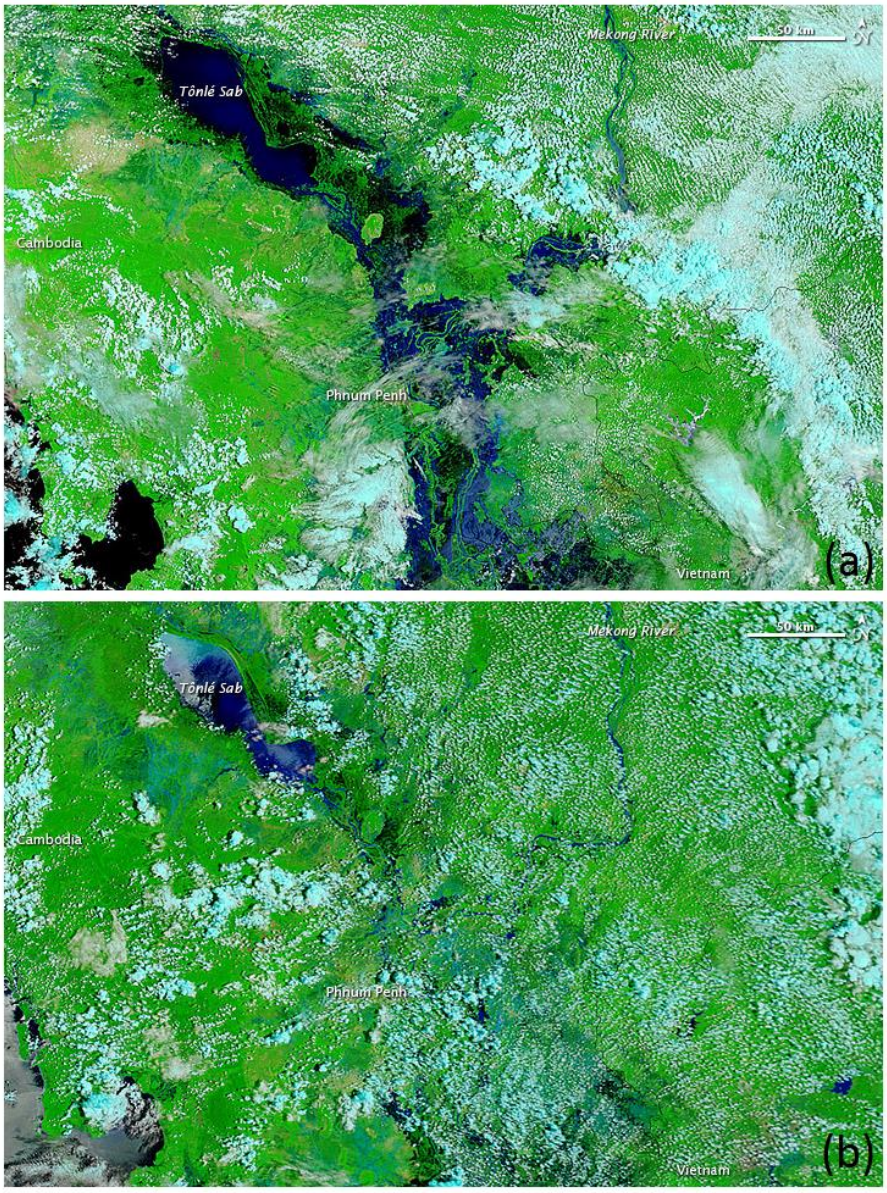

Fig. 3.20. Flooding areas in the Tonle Sap in the mid-rainy season 2011 (a) and the mid-rainy season 2010 (b). Vegetation is shown by green colour, clouds are in pale blue-green. Water ranges in color from navy to silver-blue. The silver tones of the water result from sunlight reflecting off the water surface. Retrieved from https://earthobservatory.nasa.gov/images/51746/flooding-along-the-mekong-river

3.4 Conclusion

The wetting - drying algorithm successfully implemented in SLIM reproduces well watering and dewatering processes in both theoretical test cases and in a realistic domain. The method is based on a threshold value and a blending parameter. At each time step, the total water depth in each cell is compared to a user-defined threshold value. If the total water depth is lower than that value then that cell is considered dry. It shows both local mass conservation and rapid transition of a wet/dry interface.

The simulation results confirm that wetting - drying processes play an essential role in simulating the flow regime and water depth fluctuations of the Tonle Sap lake as well as the whole system. The simulation results also reveal the spatial and temporary distribution of the surface water areas and currents in the floodplain, which are controlled by imposed discharge from 12 tributaries as well as the water level in the downstream boundary at Phnom Phenh. Seasonal variations in the inundated area of the Tonle Sap lake are dominantly influenced by the flow regime in the Mekong River. The modelled results can also provide discharge and water level data at locations, lacking monitoring of hydrological data. The model is confirmed to be a powerful tool to understand the flow dynamics of the Tonle Sap system as well as its hydrological roles in the Mekong Delta in both wet and dry seasons.

All the wetting - drying algorithms require parameters. In the algorithm implemented in SLIM, we apply 3 parameters, ε_1, ε_2, ε_3 for a threshold value of fluid depth for a thin layer, advection, bottom drag and wind stress, respectively. SLIM is a research tool with advanced features, that is still in development. Thus, we hope to improve our algorithm in SLIM in order to convert these parameters into dimensionless ones that would be valid and facile for a large range of applications.

Chapter 4 Simulation of the hydrodynamics and sediment transport in the Vietnamese Mekong Delta

This chapter is based on the following manuscript:

Le, H.A., Nguyen, T., Gratiot, N., Deleersnijder, E. and Soares-Frazão, S. (2019). Impacts of the multi-channel network on the flow dynamics and sediment transport in the Vietnamese Mekong Delta (in preparation).

4.1 Introduction

River deltas have been of fundamental importance to civilization for thousands of years (Wright et al., 1978 and Bianchi, 2016) because of their fertile flat lands, abundant fresh water for living and agricultural practices, fish sources and suitability for transport (Garschagen et al., 2012). Major ancient civilizations grew along rivers, with their first inhabitants learning how to live with natural flooding cycles in the deltas (Simmons et al., 2007). Nowadays, approximately 2.7 billion people occupy river deltas (Best et al., 2018). Thus, human intervention has major influences on the growth and evolution of these regions, through engineering controls of the flow paths and sediment dynamics across the whole deltas (Syvitski et al., 2009). In addition, higher demands on living standards and food sources cause stressful pressures on river deltas over the world (Molden et al., 2013), and even more seriously in emerging countries, which need to find a balance between economic and environmental considerations. The governments of many countries promote economic development plans based on their river resources (Barbier, 1987).

As a consequence, thousands of large-scale hydropower dams have been built in upstream parts, while high density irrigation channel systems have been constructed downstream in deltas. They are also receiving praiseworthy successes on economy and residential livelihoods. However, the natural state of deltas (and their biodiversity), is being destroyed dramatically by human on-going ambitions (Best et al., 2018). Unsurprisingly, this holds true for the Mekong Delta.

The Mekong River begins its course on the Tibetan Plateau of China, flows through Myanmar, Laos, Thailand, Cambodia and Vietnam (Wolanski et al., 1996) before draining into the East Sea of Vietnam. The Mekong Delta covers an area of 55,000 km^2 in Cambodia (26 %) and Vietnam (74 %) (Dung et al., 2013, Balica et al., 2014). This delta is at the core of various economic sectors, encompassing agriculture, fishery and forestry of these countries (Västilä et al., 2010). The part in Cambodia shows much differences from the one in Vietnam. The delta in Cambodia has witnessed little anthropogenic influences and can be considered almost natural with only a few control structures, whereas the Vietnamese part is under large regulations by a huge system of navigation and irrigation channels, sluice gates, pumps and extensive dyke systems. These systems have deliberately altered/regulated the natural hydrodynamics and sediment transport conditions in the Vietnamese part of the delta (Hung et al., 2012 and Eslami et al., 2019). However, up to date, the hydrodynamics and sediment transport conditions in the Vietnamese Mekong Delta (VMD) are still incompletely documented. Historical studies generally focused on small regions of the delta (Hung et al., 2012, Hanington et al., 2017). Only recently researches have paid more attention to the whole domain by extensive monitoring networks (Dang et al., 2016, Gugliotta et al., 2017), satellite observations (Balica et al. 2013 and Yamazaki et al. 2014) and by applying 1D (Hoa et al., 2008, Katoush et al., 2017, Duong et al., 2018 and Dang et al., 2018a), semi/quasi 2D (Triet et al. 2017), or 1D - 2D coupled models (Le et al. 2007, Eslami et al., 2019, Thanh et al., 2020). Other works are concentrated in the impacts of the dyke systems on the hydrodynamics (Fujihara et al., 2015, Duc Tran et al., 2018, Aires et al. 2020). Even so, only few works have assessed comprehensively the impacts of the dyke and multi-channel system on the flow dynamics and sediment transport processes at a

large scale. In addition, overland flow and water exchange between irrigation compartments also induce vital effects on the delta conditions (Manh et al., 2014) that cannot be solved by 1D models. The present study utilizes a two-dimension numerical model, TELEMAC-2D coupled with SISYPHE, to reevaluate the flux of water and sediment in a pseudo-realistic way to examine the effects of the multi-channel network on spatial and temporal distribution of flow and sediment dynamics in this large scale domain. Two scenarios are established to evaluate the alterations by development activities on the deltaic natural conditions. The simulations enable us to analyze changes in historical flood and sediment dynamic patterns in 2011 across the VMD, due to its complex network of tributaries and channels. The numerical strategies below are considered in this work:

- Simulating the spatial and temporal distributions of the inundation processes and sediment dynamics in the VMD;
- Reevaluating impacts of the multi-channel network on flow dynamics and sediment transport in the VMD.

4.2 Domain description

The Mekong Delta was formed by the deposition of sediments from the Mekong River over thousands of years (Tri et al., 2012, Anthony et al., 2015 and Zoccarato et al., 2018) resulting in a total area of 55,000 km^2 (Dung et al., 2013, Balica et al., 2014), the third largest delta in the world (Anthony et al., 2015). The VMD is located in the most Southern part of the Mekong Delta. It covers an area of approximately 40,000 km^2 (Thanh et al., 2019), accounting for 12 % of the Vietnam territory area, homelands of 18 million people (Renaud and Kuenzer, 2012, Garschagen et al., 2012). While approximately 95 % of water resources of the VMD (World Bank, 2019) come from upstream countries (from China to Myanmar, Thailand, Laos and Cambodia), it plays an indisputable role in the Vietnamese economy and local residential livelihoods. Three-quarters of this region is used for agricultural production (Kakonen, 2008). The VMD produces 56 % of rice, 50 % of fishery and 70 % of fruit yield of Vietnam (General Statistics of Vietnam, 2016) and they also play a significant role in agricultural exports. The delta is often divided into

four sub-basins: the Long Xuyen Quadrangle (LXQ) basin, the Plains of Reeds (PoR) basin, the area between the Tien and Hau Rivers and the Ca Mau Peninsula area (Fig. 4.1b) based on their characteristics and functions.

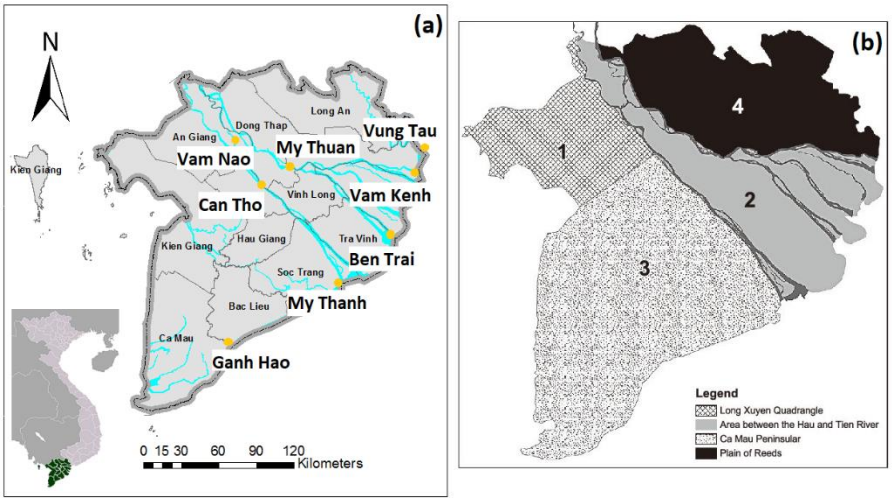

Fig 4.1. (a) Hydrological stations (orange dots) applied for model calibration and validation and (b) Sub-areas in the VMD

This delta is one of the lowest-lying area in the world (Eslami et al., 2019) with the mean topography elevation varying 0 - 4 m a.s.l. (Hoanh et al., 2014), except the upstream part of the delta and the higher area in the Northwest, where the terrain reaches elevations up to 12 m. The elevation of the central part ranges from 1.0 to 1.5 m whereas coastal areas have lower elevation of 0.3 - 0.7 m (Tri et al., 2012). The delta's hydraulic regimes are governed by two major tributaries - the Tien River (the Mekong River) and the Hau River (the Bassac River) (Duong et al., 2018a), which drain into the East Sea of Vietnam through eight estuaries (Fig. 4.1a).

A distinct feature of the VMD is the intensive management of the multi-channel and dyke systems, which aim at regulating flood, preventing saltwater intrusion and optimizing human activities, such as agriculture and transportation (Tran Anh et al., 2018). With the encouragement of the State and local governments, the agricultural production has been incentivized intensively over the last decades, leading to a mass development of man-made infrastructures (Dang et al., 2016). At present, these structures comprise 7000

km of main channels, 4000 km of secondary on-farm channel systems, 193 spillways, 409 reservoirs, 528 junctions, 29 sluices and 749 compartments (Van et al., 2012). These numbers are still increasing (Hung et al., 2012). The system is concentrated in the flood-prone areas to efficiently drain out floodwater from the LXQ basin and the PoR basin to the Gulf of Thailand (the West Sea of Vietnam) and to the Vam Co River before debouching to the East Sea of Vietnam (Thanh et al., 2020). The channel system in the VMD, which was first constructed in 1824 (Hung et al., 2012), is fully interconnected, without separation between irrigation and drainage ones (Renaud and Kuenzer, 2012). The main channels take water directly from the Tien River and the Hau River with 70 - 100 m in width and 3 - 5 m in depth. Compartments between dykes are connected to the main channels by a network of secondary channels with 30 - 50 m in width and 2 - 3 m in depth. Large parts of the VMD are controlled by sluice gates and pumps, which are managed by local authorities (Hung et al., 2012). It is important to notice that the numerical model may help in a better understanding of water and sediment fluxes in order to improve its management but would never capture the real complexity of the network and its local controls.

Together with the channel network, the first dyke was constructed in 1930 (Hoanh et al., 2014). The dyke systems have been expanded since 1975 (Dang et al., 2018), when the demand of food and nutrients was increasing sharply after the Vietnam reunification (Hoanh et al., 2014). After several flood events, especially the devastating flood of 2000, the dyke system was reinforced in order to maintain agricultural cultivation even during flood seasons. The dyke systems comprise low and high ring dykes. The low dyke with an average crest level of about 2.0 - 2.5 m a.s.l. (Thanh et al., 2019), aim to protect paddy fields against the early flood peak arriving from mid-July to mid-August, ensuring that farmers can cultivate two rice crops per year by keeping floodwater in the paddy fields after the summer crop (Triet et al., 2017). The high dykes were designed with the average crest level of about 4.0 - 4.5 m a.s.l. (Hung et al., 2012), approximately 0.5 m above the flood peak of the year 2000, located mainly along the Tien River and the Hau River (Thanh et al., 2020). These high dykes aim at protecting rice fields during the whole year thus they can facilitate the cultivation of three crops per year in An Giang and Dong Thap provinces (Fig. 4.1a, Fig. 4.2 and Fig. 4.3).

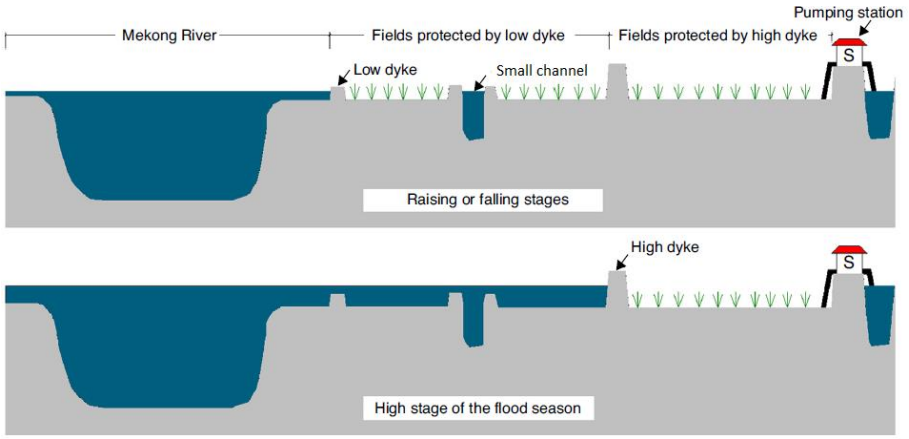

Fig. 4.2. Sketch of river and floodplain cross-sections highlighting the effect of flood prevention infrastructure in the floodplains (Dang et al., 2018b; Arias et al., 2019)

Located in the North Pacific monsoon climatic region (Tamura et al., 2010), the climate of the VMD has two separate seasons per year. The wet season normally lasts from June to November, whereas the dry season from December to May (Eslami et al., 2019). The precipitation in the wet season contributes to approximately 85 % of the annual rainfall (MRC, 2005), and leads to flooding of large areas in the delta (MRC, 2005). In addition, the region is under effects of the tropical cyclones (Darby et al., 2016), causing difficulties in predicting flood behaviors and inundation (Best et al., 2018). This flooding dynamics however also contributes to the area's highly fertile alluviums and fish productivity (Eastham et al. 2008, Hapuarachchi et al. 2008).

The total annual water volume of the VMD is about 500 billion m^3 (84.4 % from the upstream and 15.6 % from the regional rainfall). The flow is very abundant during the flood season, particularly during September - October, where the flow rate can reach up to 25,000 m^3/s in Can Tho and My Thuan (Duy Vinh et al., 2016). The flow during the dry season is rather low, with a mean discharge lower than 6,000 m^3/s. (Tri et al., 2012).

Fig. 4.3. ENVISAT image presents the Mekong Delta in Cambodia and Vietnam. Light brown color in the North shows less intensive agricultural areas in Cambodia. The dark brown in the South shows non-rice production area in the VMD. Green color shows intensive agricultural areas in Vietnam with numerous channel systems and compartments. Retrieved from the European Space Agency (ESA) website.

The VMD estuaries and coasts experience semidiurnal tides from the East Sea of Vietnam with amplitudes of 1 - 3.5 m and diurnal tides from the West Sea of Vietnam with amplitudes of 0.8 - 1 m (Le et al., 2007). The tides also influence the hydraulic condition in the VMD estuaries (Nguyen et al., 2006), especially the tidal regime of the East Sea plays an important role and becomes a predominant factor controlling the hydrodynamics of the VMD coastal area because of its stronger amplitudes and semi-diurnal cycles (Thanh et al., 2020).

According to Nhan (2005), the VMD is potentially exposed to higher risks of relative sea level rise, which combines both rising sea levels of 2.8 - 3.3 mm/year (Takagi et al., 2016 and Minderhoud et al., 2019) and land subsidence of 20 - 30 mm/year (Minderhoud et al., 2019). Besides serious floods in the wet season, high tides combined with deep canals, low hydraulic slope and bed gradients can cause extensive saltwater intrusion in the low flow season (especially in March and April) (MRC, 2005).

4.3 Model set-up

4.3.1 TELEMAC 2D

The TELEMAC-MASCARET system (http://www.telemacsystem.com), which was introduced by the National Hydraulics and Environmental Laboratory - a part of the R&D group of the Electricité de France (EDF), is an open numerical modelling system to study environmental processes in free surface transient flows. The primary purpose of TELEMAC is to simulate the flow dynamics in a waterbody via the solution of the Shallow Water Equations (Vu et al., 2015). TELEMAC-2D solves the continuity equation and momentum equations simultaneously using a finite-element technique:

$$\frac{\partial h}{\partial t} + \vec{u}.\vec{\nabla}h + h.div(\overrightarrow{u}) = S_h \tag{4.1}$$

$$\frac{\partial u}{\partial t} + \vec{u}.\vec{\nabla}u = -g.\frac{\partial Z}{\partial x} + S_x + \frac{1}{h}div\left(h\vartheta_t\vec{\nabla}u\right) \tag{4.2}$$

$$\frac{\partial v}{\partial t} + \vec{u}.\vec{\nabla}v = -g.\frac{\partial Z}{\partial y} + S_y + \frac{1}{h}div(h\vartheta_t\vec{\nabla}v) \tag{4.3}$$

where h is the depth of water (m); u, v are velocity components (m/s); g is the gravitational acceleration (m/s^2); z is the free surface elevation (m); t is time (s); x, y are horizontal space coordinates (m); S_h is the source or sink of fluid (m/s) and S_x, S_y are source or sink terms in dynamic equation (m/s^2), ϑ_t is momentum diffusion coefficient and ∇ is the gradient operator.

TELEMAC-2D simulates hydrodynamic variables such as flow depth (h) and depth-integrated velocity components (u, v) along X and Y directions at every node of an unstructured triangular mesh. To simulate sediment transport in a

waterbody, SISYPHE, is internally coupled with TELEMAC-2D. SYSIPHE is a finite element morphodynamic module of the TELEMAC-MASCARET modelling system. The sediment composition is represented by a finite number of classes, each characterized by its mean diameter, density and settling velocity. In SISYPHE, the depth-averaged form of the transport/diffusion equation is solved.

$$\frac{\partial hC}{\partial t} + \frac{\partial h\overline{uC}}{\partial x} + \frac{\partial h\overline{vC}}{\partial x} = \frac{\partial}{\partial x}\left(h\epsilon_s \frac{\partial C}{\partial x}\right) + \frac{\partial}{\partial y}\left(h\epsilon_s \frac{\partial C}{\partial y}\right) + E - D \tag{4.4}$$

Where C is sediment concentration, ϵ_s is the sediment diffusivity coefficient. E - D is the net erosion minus deposition flux of sediment. The erosion E and deposition D fluxes, defined by Eq. (4.5) and (4.6), need to be specified at the bed, in order to determine the exchange of mass between the water column and the sediment bed.

$$E = -\left(\gamma_t \frac{\partial C}{\partial t}\right)_{z=0} \tag{4.5}$$

$$\mathrm{D} = -\left(w_s C\right)_{z=0} \tag{4.6}$$

The erosion and deposition rates need to be specified as a function of the hydrodynamic bed shear stress τ_b and bed properties. The following classical Krone - Partheniades laws are applied (Partheniades, 1962):

$$\begin{cases} E = M\left[\left(\frac{u_*}{u_{*e}}\right)^2 - 1\right] & if\ \tau_b = \rho u_*^2 > \tau_{ce} = \rho_w u_{*e}^2 \\ E = 0 \end{cases} \tag{4.7}$$

where M is the erosion parameter (kg/m²/s), u_{*e} is the critical erosion shear velocity (m/s), τ_{ce} is the critical shear stress for erosion (N/m²) and ρ_w is the density of water (kg/m³).

The deposition rate is represented by the deposition law:

$$\begin{cases} D = w_s C\left[1 - \left(\frac{u_*}{u_{*d}}\right)^2\right] & if\ u_{*d} < u_{*d} \\ D = 0 \end{cases} \tag{4.8}$$

where w_s is the settling velocity (m/s), u_{*d} is the critical deposition velocity (m/s). The critical shear stress for deposition is determined equal to $\tau_{cd} = \rho_w u_{*d}^2$ (N/m²).

4.3.2 Data utilization

All data used as inputs for the model were obtained from official sources, summarized in Table 4.1. Fig. 4.1(a) shows the location of hydrological stations used for model validation. Hourly data allows capturing the tidal influence and investigating the phase coherence between different gauging stations. The latter helps to understand the dependency of tidal propagation on the different water levels.

Table 4.1. Data sources

Data type	Frequency	Data source
River network and channel cross-sections	surveyed from 1995 to 2000 with updated between 2005 and 2010	HoChiMinh city University of Technology, Vietnam Southern Institute for Water Resources Research, Vietnam MRC
Hydraulic infrastructure operations	Hydraulic infrastructure embedded in the model are based on official regulations for 2010 - 2011	
Hydrological data	Can Tho and My Thuan (hourly Q and H in 2010 and 2011; and daily SSC from 2009 to 2011)	Lower Mekong Coastal Delta Zone project
	Tan Chau and Chau Doc (hourly Q and H) in 2010 and 2011 Vung Tau, Ben Trai, Ganh Hao, Vam Kenh (hourly H) in 2010 and 2011	National Center for Meteo-Hydrological forecasting, Vietnam Vietnam – German University
Offshore wind	The hourly wind data at 10 m	NCEP NOAA
Offshore Tidal constituents	Amplitude and phase of tidal constituents	TPXO 8.0

4.3.3 Computational mesh

Fig. 4.4 shows the domain and bathymetry of the VMD with reference to the Hondau datum (the Vietnamese official benchmark system, identical to mean sea level). In the upper part of the domain, the model is bounded to Tan Chau (the Tien River) and Chau Doc (the Hau River). In the estuarine area, the river distributaries drain into the sea and the model boundary is expanded approximately 70 - 80 km offshore. The model is first set up to represent the pseudo-realistic conditions of the VMD (Scenario 1). In such a full domain, we select two main rivers (the Tien River and the Hau River), eight estuaries,

the primary and secondary channels. The tertiary and quaternary channels are neglected, because this system connects with the two main rivers and drains directly into the seas. Roads and dykes are presented by high elevations in the bathymetry (see Fig. 4.4 and Fig. 4.5).

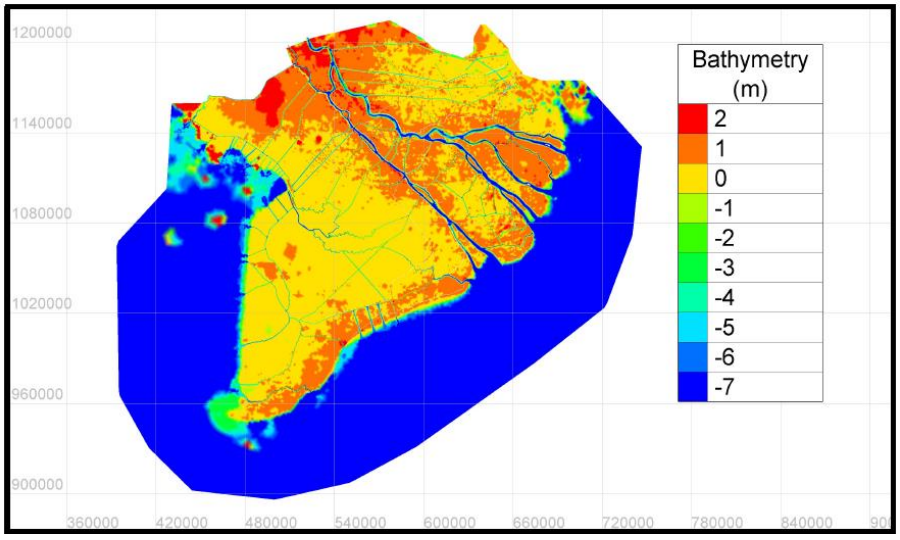

Fig 4.4. Bathymetry of the VMD

The numerical simulations are based on an unstructured mesh (see Fig. 4.5), where triangular cells are used to optimize the simulation. The triangular elements with small sizes of 80 – 100 m are applied in the channels; a larger size of 300 m is for the main rivers; a size of 300 - 2000 m is for the floodplain and the largest size of 4000 m are for offshore settings. The total number of triangular elements is 524,097 with 268,010 nodes.

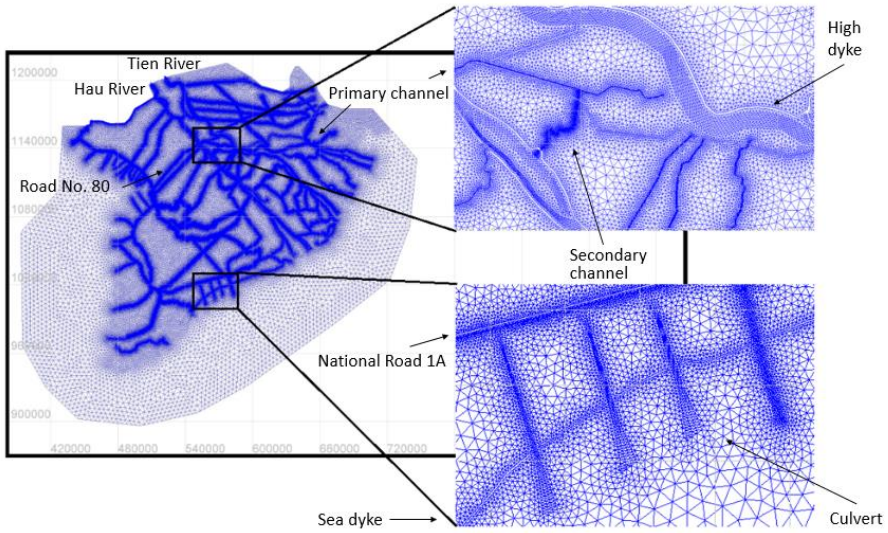

Fig 4.5. Computation mesh for Scenario 1 with main rivers, multi-channels, roads and culverts

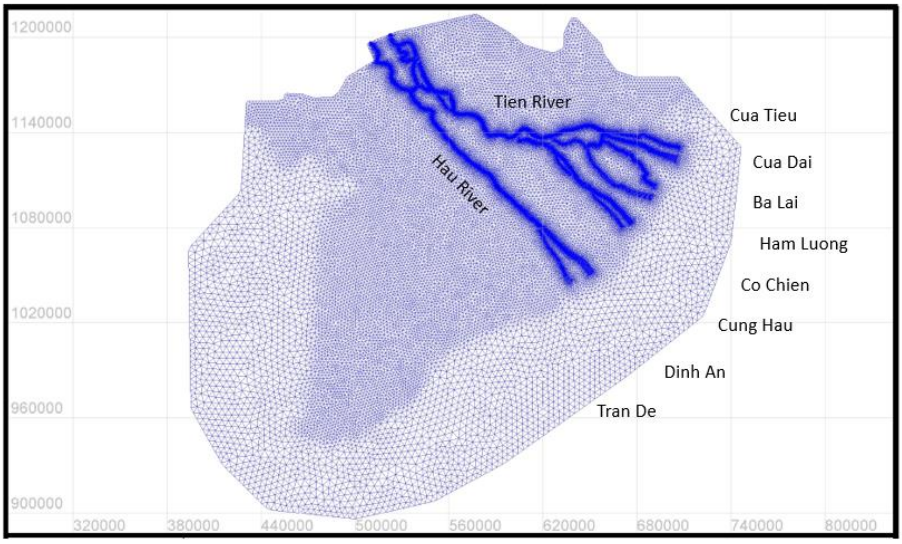

Fig 4.6. Computation mesh for Scenario 2 with Tien and Hau Rivers

In order to assess the impacts of the multi-channels on the flow dynamics and sediment transport in the VMD, a simplified computation mesh (see Fig. 4.6) is generated with the two main rivers (the Tien River and the Hau River) and eight estuaries, without the channel network (Scenario 2). The computational area is similar to that of Scenario 1. The mesh configuration of this scenario is made of 113,559 elements and 56,665 nodes. This second scenario can be seen as representative of the delta situation prevailing before the construction of the dykes and channels, and comparisons of the results will thus allow assessing the impacts of these infrastructures.

4.3.4 Parameters and simulation set-up

Boundaries

Boundary conditions, given for each of the boundary points, includes hourly discharge data at Tan Chau (the Tien River) and Chau Doc (the Hau River) for the upstream boundaries.

The tidal data base of TPXO (https://www.tpxo.net/global) is applied as a real sea water level dataset in both the West and East Seas for the downstream boundaries. Otherwise, a coefficient to calibrate sea level and a coefficient to calibrate tidal range are also adjusted to transfer the information between a large scale model and the boundaries of a local model (Pérez-Ortiz et al., 2013).

Parameters of hydrodynamic simulation

In the coastal area, the bed roughness can vary greatly under flood conditions and generally interact with large scale morphodynamic processes and tidal propagation (Raune et al., 2009). Thus, the friction law used in this model is defined by the Nikuradse roughness length scale (Nikuradse, 1950) because this roughness parameter is sensitive with tidal cycles (Knight et al., 1981) and well represented the tidal propagation (Le Hir et al., 2000) in the coastal area.

The simulation uses a constant viscosity coefficient throughout the domain. The overall viscosity coefficient (molecular + turbulent viscosity) is provided in the simulation with a default value of 10^{-6} m^2/s (corresponding to the molecular viscosity of water).

Wind is variable in time and space; and the hourly wind data at 10 m by NCEP NOAA (https://www.ncep.noaa.gov/) is applied in the simulation. According to the introduction by the Institute of Oceanographic Sciences, the United Kingdom, the coefficient of wind influence is selected as 0.565×10^{-6} because most of the wind velocity is < 5 m/s (TELEMAC - 2D User Manual). The atmospheric pressure is taken into account by using a default value of 10^5 Pa. The threshold depth of wind is applied to avoid unphysical wind velocities with a constant value of 3 m.

The Coriolis effects are neglected in the simulation. The initial water elevation is supplied by a constant elevation of 0 m. The simulation time-step set up in this simulation is 20 s.

Parameters of sediment transport simulation

The relevant hydrodynamic variables can be jointly imposed in the SISYPHE module. The time step of internal coupling SISYPHE is equal to the time step of TELEMAC-2D.

According to Le et al., 2020a, sediment properties in the VMD are described using 4 size classes, namely primary particle, floccculi, microfloc and macrofloc. The choice of 4 size classes for simulation by SISYPHE is a simplified representation of the actual particle size distribution in the VMD. For each class, the settling velocities are determined according to the grain size and fraction. The first three grain sizes represent fine particle sizes and the largest grain size represents non-cohesive sand particles. This sub-populations choice is in line with Bravard et al. (2014), who mentioned that the river carries mostly silt and clay, however, sand also plays a major role in downstream sediment transfer during floods.

4.4 Calibration and validation

4.4.1 Hydrodynamics

Due to the purpose of this study concentrates in the historical flood year 2011, the periods of 10 - 19 September and 25 September - 4 October 2011 are

selected for the model calibration and validation because they are representative for the peak flood season in the VMD.

Table 4.2. Nikuradse roughness for subdomains and the study area

No.	Subdomain	Nikuradse roughness	No.	Subdomain	Nikuradse roughness
1	Tien river	0.1	**4**	Co Chien estuary	0.01
2	Hau river	0.12	**5**	Ham Luong estuary	0.01
3	Vam Nao conjunction	0.1	**6**	The remaining area	0.1

The model was calibrated by adjusting the Nikuradse roughness length scale in six main areas (Table 4.2); and the tidal coefficient parameter to calibrate sea level of -0.4 m and coefficient to calibrate tidal range of 1.2.

The resulting water levels were evaluated at eight measurement stations (the locations are presented in Fig. 4.1a, the model validation results are presented in Fig. 4.7, Fig 4.8 and Table 4.3), which are key stations with the highest data accuracy in the Mekong Delta. The match between simulated and observed water levels was evaluated by the Nash-Sutcliffe efficiency coefficient (NSE) (Nash and Sutcliffe, 1970), Mean Absolute Error (MAE) and Root Mean Square Error (RMSE).

$$NSE = 1 - \frac{\sum_{i=1}^{n}(H_{obs,i} - H_{simu,i})^2}{\sum_{i=1}^{n}(H_{obs,i} - \overline{H_{obs}})^2} \quad (4.9)$$

where $\overline{H_{obs}}$ is the mean value of observed water depths, $H_{obs,i}$ is the observed water depth at time t = i Δt and $H_{simu,i}$ is the numerically simulated water depth at time t = i Δt, n being the total number of time steps.

The mean absolute error (MAE) is applied to measure the absolute differences between simulated results and observations:

$$MAE = \frac{\sum_{i=1}^{n}|H_{obs,i} - H_{simu,i}|}{n} \quad (4.10)$$

The Root Mean Square Error (RMSE) is also used to evaluate the quadratic average difference between computed results and observed data.

$$RMSE = \sqrt{\frac{\sum_{i=1}^{n}(H_{obs,i} - H_{simu,i})^2}{n}} \quad (4.11)$$

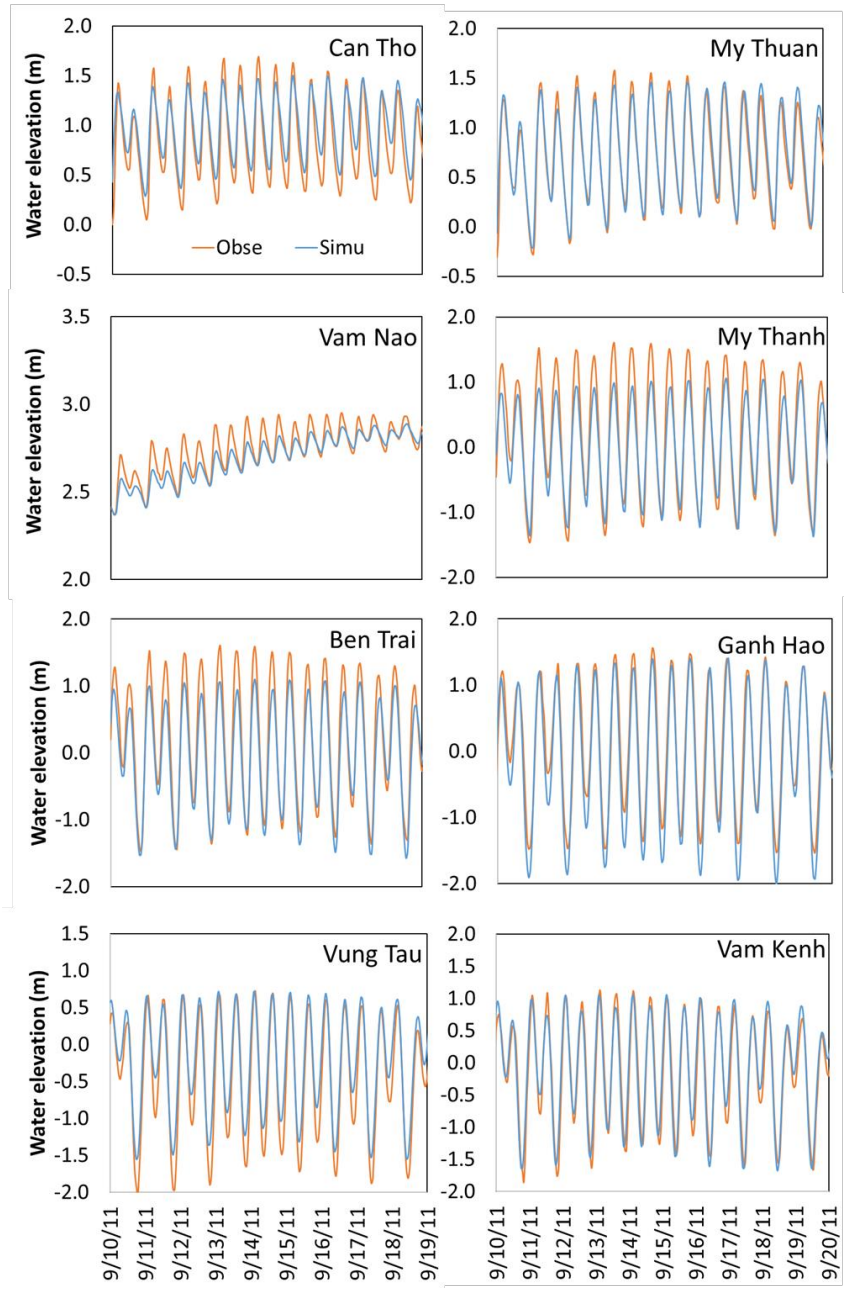

Fig. 4.7. Model calibration. The red lines present the measured data and the blue lines present the simulated one.

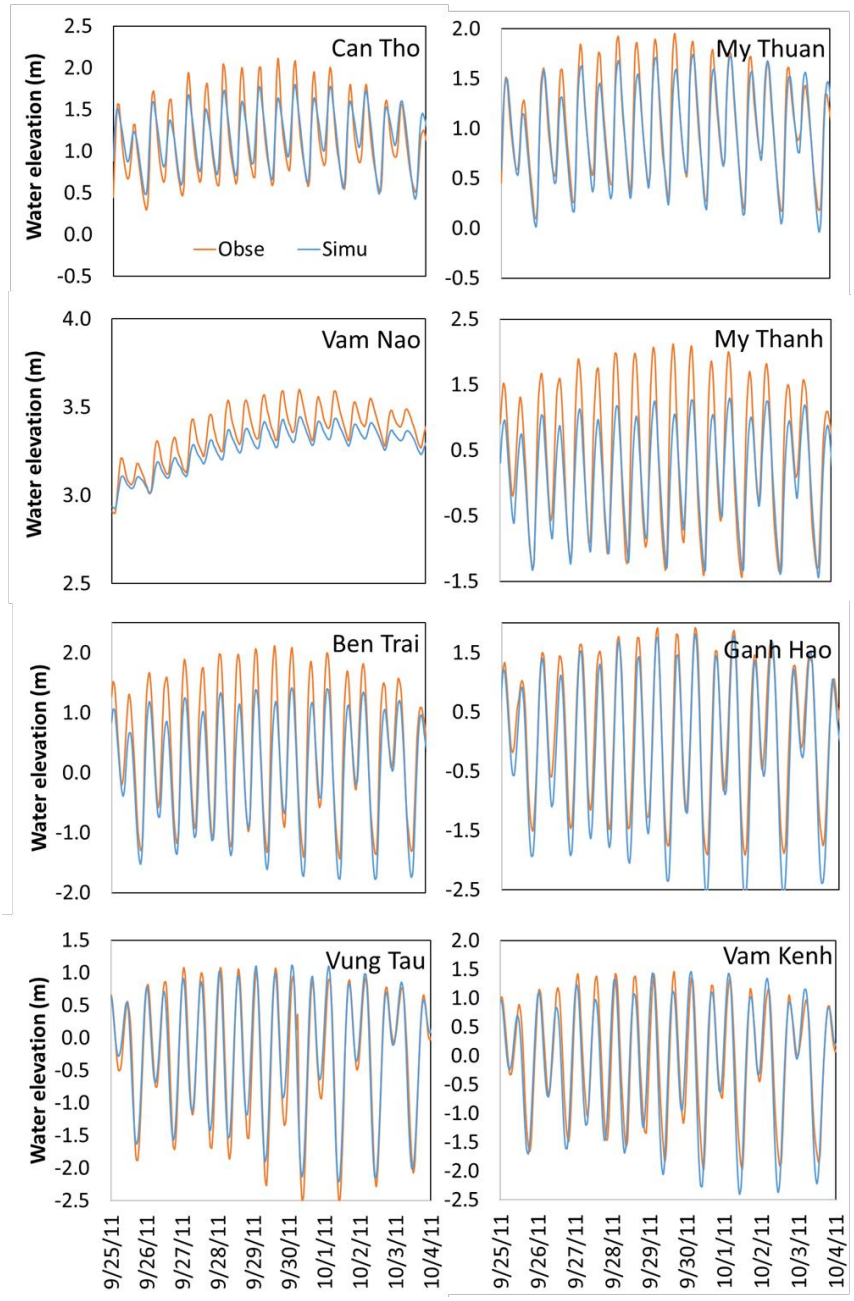

Fig. 4.8. Model validation. The red lines present the measured data and the blue lines present the simulated one.

Table 4.3. Hydrodynamic model validation

No.	Station	Calibration 10 - 19 Sept 2011			Validation 25 Sept – 4 Oct 2011		
		NSE (%)	MAE (m)	RMSE (m)	NSE (%)	MAE (m)	RMSE (m)
1	Can Tho	74.69	0.178	0.203	87.48	0.136	0.163
2	My Thuan	82.95	0.830	0.273	92.52	1.116	0.303
3	Vam Nao	74.04	0.004	0.131	60.29	0.008	0.143
4	My Thanh	87.14	0.263	0.316	76.99	0.391	0.487
5	Ben Trai	79.98	0.249	0.292	82.16	0.360	0.429
6	Ganh Hao	90.83	1.472	0.272	88.49	1.726	0.366
7	Vung Tau	87.26	0.225	0.275	93.04	0.192	0.249
8	Vam Kenh	92.97	0.175	0.211	84.96	0.292	0.365

4.4.2 Sediment transport

The daily measured SSC data is only available in Can Tho and My Thuan stations, thus these stations are selected for validating sediment transport simulation. The time periods for sediment transport validation are same as hydrodynamic simulation, 10 - 19 September and 25 September - 4 October 2011. Three parameters of sediment properties, used for model validation are particle size, settling velocity and fraction of each size class (see Table 4.4).

Table 4.4. Particle size and settling velocity in SISYPHE

No.	Particle size (µm)	Settling velocity (m/s)	Fraction (%)
1	10	2.10^{-6}	40
2	20	2.10^{-4}	30
3	50	1.10^{-3}	20
4	250	1.10^{-2}	10

The model validations in Can Tho and My Thuan stations are shown in Fig. 4.9 and Fig. 4.10 with R^2 error of 0.76 and 0.85; 0.53 and 0.63, respectively. The R^2 error formula used here is shown below:

$$R^2 = \frac{n\left(\sum_{i=1}^{n} SSC_{simu,i} SSC_{obs,i}\right) - \left(\sum_{i=1}^{n} SSC_{simu,i}\right)\left(\sum_{i=1}^{n} SSC_{obs,i}\right)}{\sqrt{\left[n\sum_{i=1}^{n} SSC_{simu,i}^2 - \left(\sum_{i=1}^{n} SSC_{simu,i}\right)^2\right]\left[n\sum_{i=1}^{n} SSC_{obs,i}^2 - \left(\sum_{i=1}^{n} SSC_{obs,i}\right)^2\right]}} \quad (4.12)$$

where $SSC_{obs,i}$ is the observed SSC at time t = $i\Delta$t and $SSC_{simu,i}$ is the numerically simulated SSC at time t = i Δt, n being the total number of time steps.

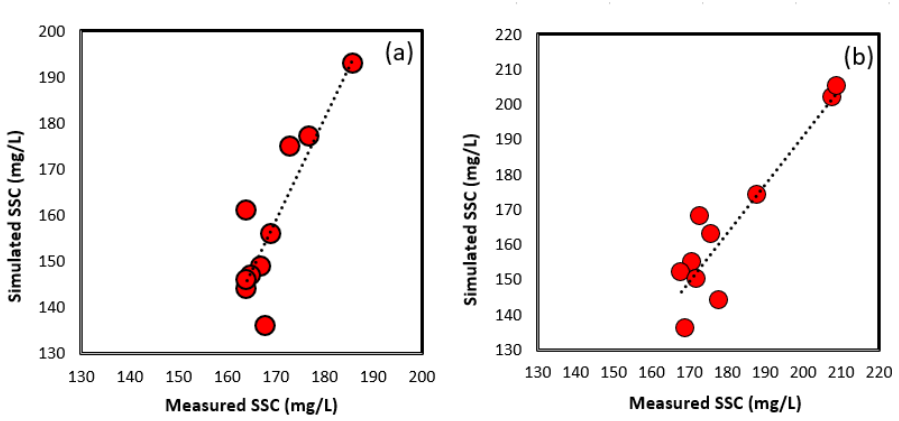

Fig. 4.9. Model calibration (a) and validation (b) of SSC at Can Tho. The dots present the measured SSC in ebb tide and the red lines present the simulated SSC.

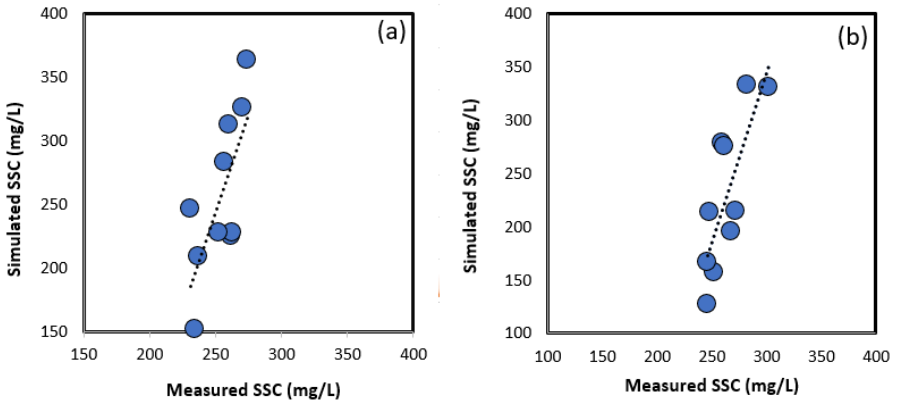

Fig. 4.10. Model calibration (a) and validation (b) of SSC at My Thuan. The dots present the measured SSC in ebb tide and the blue lines present the simulated SSC.

4.5 Results

4.5.1 Hydrodynamics

Flooding in the VMD is normally caused by two ways: (1) upstream floods and (2) the tidal-induced floods triggered by the tidal regimes from the East and West Seas (Balica et al., 2014). Thus, the period 25 - 30 October 2011 is selected to simulate the extreme flood dynamics in the VMD, because the

maximum water level in 2011 was higher than that of the historic flood event in 2000 (Dung et al., 2013, Apel et al., 2016). Indeed, a late flood peak in October 2011 in coincidence with a spring tide period (Triet et al., 2017) caused the highest water level observed so far in the VMD.

Inundation level and area

Fig. 4.11 shows that water levels in the upper VMD that are always higher than downstream, especially in the PoR and LXQ basin, which are considered as two flood-prone areas of the VMD. Water level in the PoR is higher than 1.8 m, evenly reaching 4.0 m in some locations. Water level in the LXQ basin is higher than 1 m but limited by the Cai San channel, which redistributes the flow in the VMD by discharging floodwater to the Gulf of Thailand in order to protect local residents and crops. Thanks to the multi-channel network, inundation areas between Tien and Hau rivers with water levels > 1.0 m are limited to the upstream of Can Tho and My Thuan. It confirms the effects of the multi-channel network, which do not only influence the hydrodynamics of each single branch, but also propagate flood signal in the other branches, through the hydraulic links in the channel system.

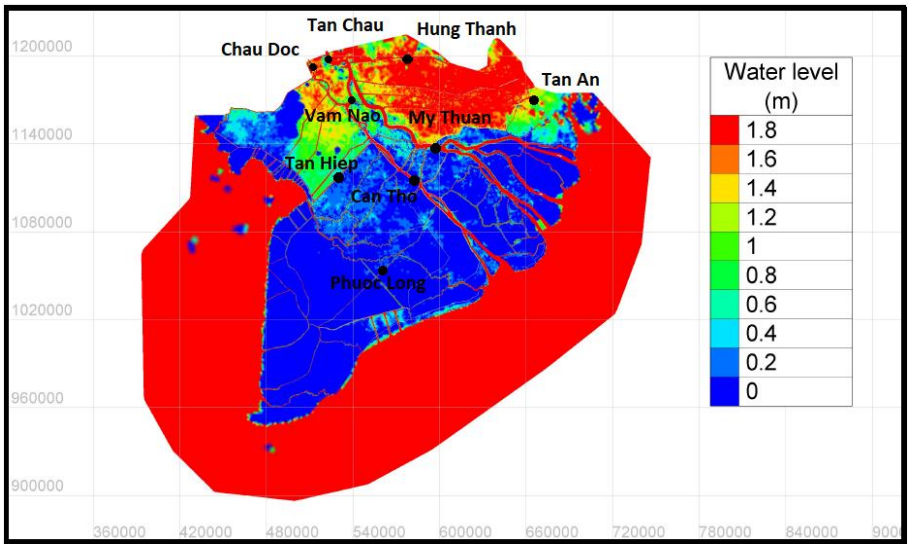

Fig 4.11. Inundation area and water level in the VMD in the Scenario 1 on 30 October 2011

The inundation area is calculated as the area exposed to flood level higher than 0.5 m. When water depth exceeds 0.5 m over the land surface, it indeed results in noticeable damages and severe limitations for cultivation (Van et al. 2012 and Balica et al., 2014). The total inundation area in Scenario 1 is 11.710 km^2, accounting for 29 % of the whole VMD area, which agrees with the studies by Hoa et al. (2008) and Renaud and Kuenzer (2012).

Flow velocity

To assess the influences of the multi-channel network on the flow dynamics of the VMD, the hourly flow velocity is extracted at several stations in each river basin (locations of the stations are shown in Fig. 4.11).

Fig. 4.12 (a) shows the flow velocity at the upstream station of the Hau River (Chau Doc). It is rather constant with value of 0.75 m/s. At Vam Nao conjunction, the flow velocity increases to 0.82 m/s because of the flow balance mechanism between the Tien River and Hau River (Thanh et al., 2020). In Can Tho, under the tidal regimes, the flow velocity oscillates, between 0.46 and 1.2 m/s, with a mean value of 0.8 m/s. Two time series extracted from the channels of the Hau River at Tan Hiep station (33 km from the main river) and Phuoc Long station (88 km from the main river) show mean values of 0.5 m/s and 0.3 m/s, respectively.

Fig. 4.12 (b) presents the flow velocity in the upstream station of the Tien River (Tan Chau) is rather constant value, as in Chau Doc of the Hau River, but with a magnitude quite higher 1.16 m/s. The fluctuation of the flow velocity in My Thuan is higher than in Can Tho, ranging from 0.66 to 2.24 m/s, with a mean value of 1.45 m/s. Because the semidiurnal tidal amplitude from the East Sea mainly influencing the Tien River is stronger than the diurnal tide from the Gulf of Thailand (Manh et al., 2014, Thanh et al., 2020). Velocities in Hung Thanh station (35 km from the main river) and Tan An station (25 km from the main river) exhibit mean values of 0.1 m/s and 0.3 m/s, respectively.

Generally, the flow velocity in the channel system reduces by the distance from the main rivers. In the upper part of the VMD (Chau Doc, Tan Chau and Vam Nao), it is dominantly affected by the river flow, whereas the middle part (Can Tho and My Thuan) is under the effects of tidal propagation.

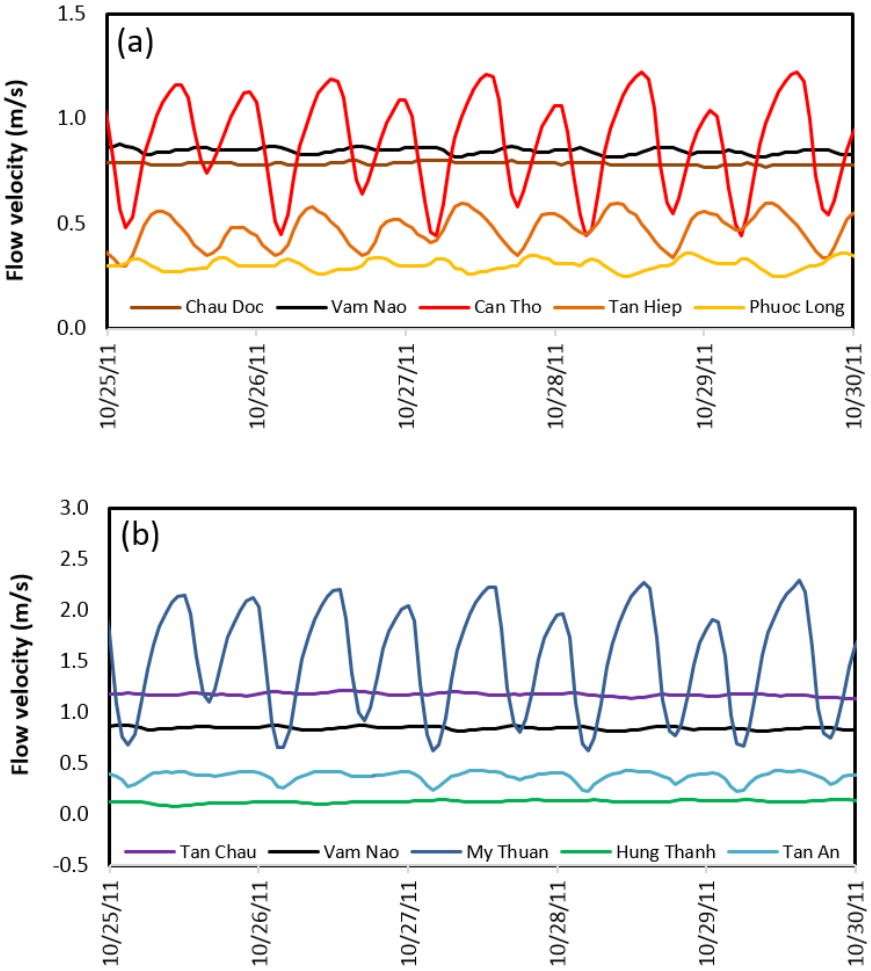

Fig. 4.12. Flow velocity in Hau river (a) and Tien river (b) from the upstream to downstream and distances to main branches

4.5.2 Sediment dynamics

Similar to hydrodynamics, the sediment dynamics in the floodplain of the VMD also relies on three mechanisms: the flood from the Mekong River, overflow among compartments surrounded by dyke system and the tidal backwater effects. In the upper VMD, the sediment transport is controlled mostly by the Mekong River flow. In the middle areas and lower estuaries, it is strongly influenced by both effects of river discharge and tidal propagation.

On the muddy continental shelf, ocean forcing by waves and currents is the driven mechanisms of sediment resuspension, which can later diffuse inland in the estuary through tidal pumping and density current mechanism, leading to the formation of fluid mud layers (Marchesiello et al., 2019).

The Mekong River is considered as a carrier of mostly fine particles. However, sand also plays a gradual role in the particle components of the Mekong (Le et al., 2020a). Thus, the grain size distribution features a mixture of populations, corresponding to distinct transport processes. Fine sediments are transferred as pseudo washload and strong suspension modes in the upper layers; while sand may transit as low suspension mode or bedload mode in the near-bottom layer of sediment.

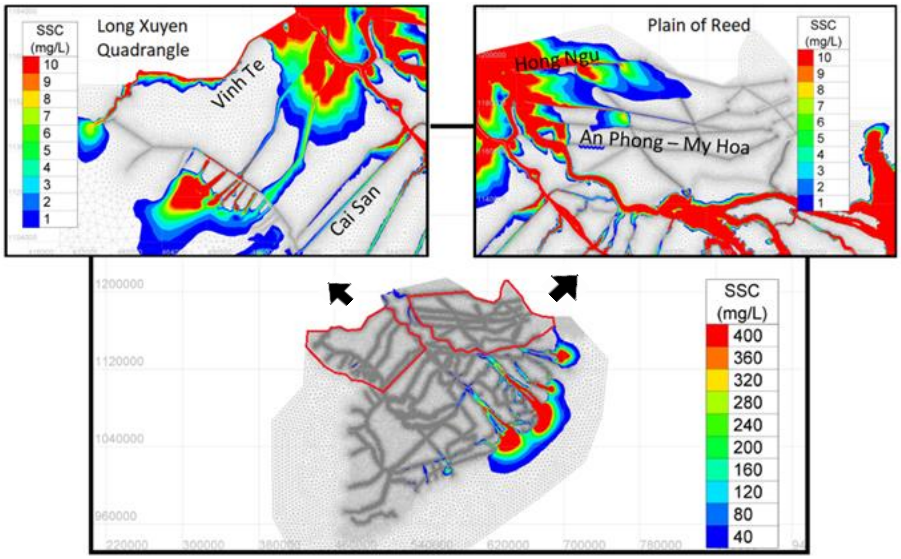

Fig. 4.13. Spatial SSC from Scenario 1 at the end of wet season 2011

In Scenario 1, a proportion of sediment distributes in the channels, another small proportion settles in the floodplain, especially in the PoR basin and the LXQ basin with distances lower than 20 km from the main rivers. A large proportion of sediment discharges downward (see Fig. 4.13).

At the end of the wet season, SSC shows higher values in the coastal area than in the upper part. SSC in Can Tho and My Thuan can reach up to 100 mg/L.

It is because of the mixture of flood flow downwards and the tidal effects upwards causing a zone of maximum turbidity.

Along the Mekong delta coast, in the wet season, the weak southwest monsoon winds (Eidam et al., 2017) in combination with strong flood flows cause most of the fluvial sediment discharging seaward. Suspended sediments settle in the delta front zone and in the estuaries, at approximately 35 km from the shorelines with SSC of 50 mg/L, that explains the formation of the Ca Mau Peninsula for thousand years (Zoccarato et al., 2018). The sediment flux patterns reflect the interactions of riverine flow and coastal currents, showing by high SSC in the southwest direction of the front zone.

SSC variation along the Tien and Hau rivers

Fig. 4.14 (a, b, c) presents the modelled SSC variation along the Hau and the Tien rivers in October 2011. SSC are taken at four stations along each river to see the SSC variation from the upstream to downstream. Obviously, SSC increases sharply along rivers and varies with the tidal regimes. Daily SSC in the upper Hau River and Tien River are stable with a value of 58 - 92 mg/L, respectively. While in the seaward direction, the maximum values can reach to 800 mg/L to 1000 mg/L in the Hau and the Tien rivers estuaries, respectively.

SSC variation by the multi-channel network

In the multi-channel network, SSC exhibits an exponentially decreasing trend with distances from the main rivers (see Fig. 4.15), which are in line with flow velocity, as presented in section 5.1.2 above. The mean values in the Hau River and Tien River are 60 mg/L and 100 mg/L, respectively. The mean SSC in the channels is approximately 25 mg/L. In general, at a distance beyond 20 km from the main rivers, no notable SSC (< 5 mg/L) can be observed. One exception is the An Phong – My Hoa channel, a conjunction with a small channel at a distance of 20 km from the Tien River that receives an additional sediment source. These figures also present a temporary reduction of SSC in both tributaries and from the upper to the lower channels.

SSC in the PoR basin is higher than in the LXQ basin (15 - 45 mg/L and 5 - 10 mg/L, respectively), because (1) SSC in the Tien River is higher than the

one in the Hau River, (2) flow in the LXQ basin directly discharges to the Gulf of Thailand while floodwater is kept in the PoR basin for a short time before discharging to the East Sea, (3) the multi-channel network in the LXQ basin has higher density than the one in the PoR basin, which means in the less developed bank of the floodplain, SSC is higher than the developed one.

Within the compartments, SSC is much lower than in the channels, < 5 mg/L. This is because the levees can work as vertical walls preventing coarser sediment entering the paddy compartments, whereas only finer particles near the surface of the water body can enter by the overflow.

Generally, in comparison with the main rivers, the SSC in the multi-channel network and the floodplain is much lower (see Fig. 4.14 and Fig. 4.15). The source of sediment in the channels is from the main rivers. The channels work as a sediment conveyor, it plays an important role in the sediment dynamics of the VMD. However only a small part of suspended sediment is deposited in the compartments whilst a large part is discharged to the delta front zone after a flood season by the channel system, then under the cycles of resuspension/deposition processes principally by waves forcing (Marchesiello et al., 2019). It can be deduced that the construction and operation of the multi-channel network cause reduction in sediment supplying to floodplain, which can result in lower agricultural production and exacerbate deltaic sinking.

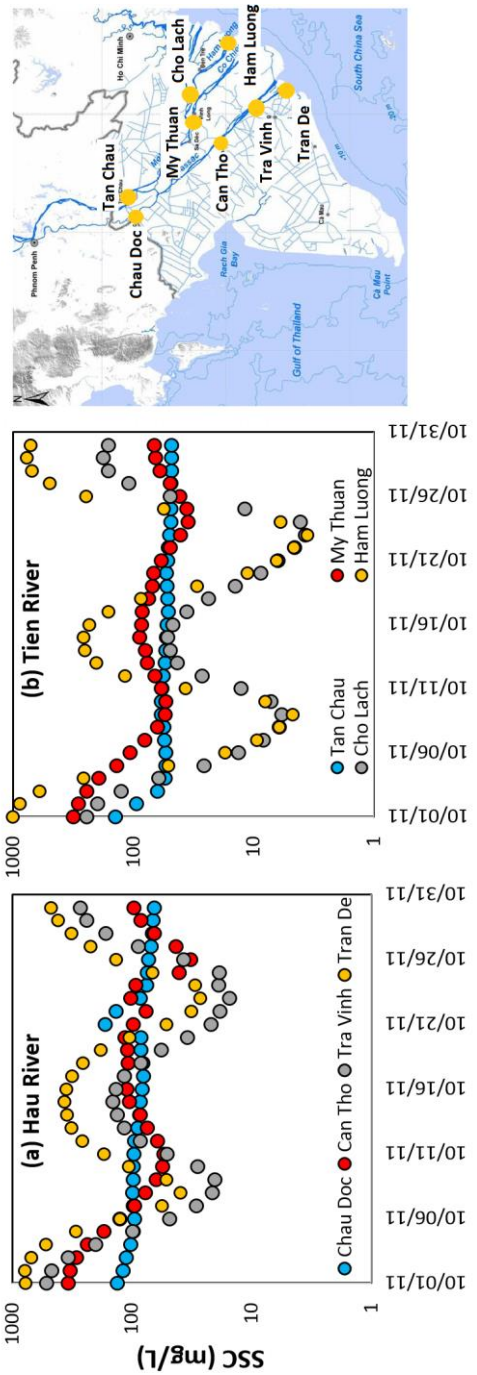

Fig 4.14. SSC variation along the Hau River (a) and the Tien River (b)

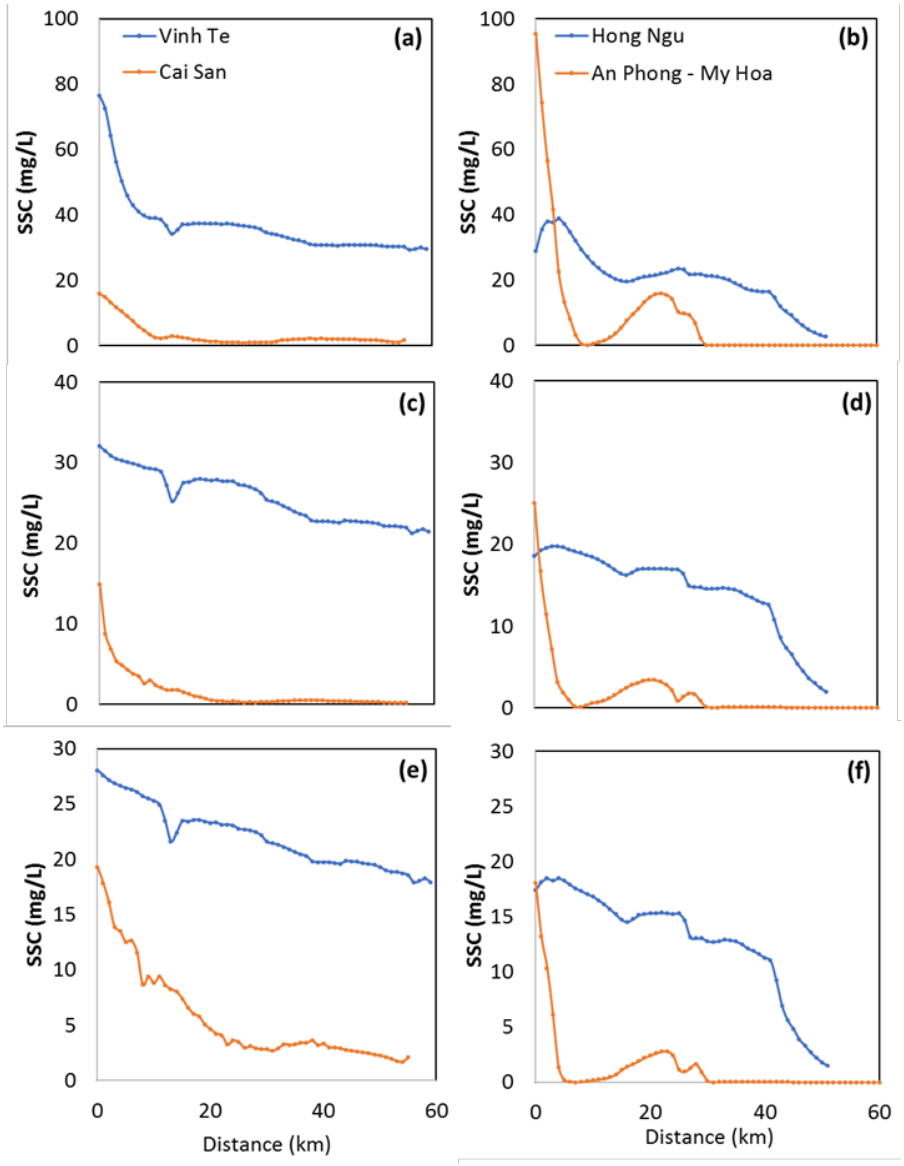

Fig 4.15. SSC in the channels of the Hau river (a, c, e) and the Tien river (b, d, f) on 1, 15 and 30 October 2011. The blue dots show SSC in upper channels and the red dots show SSC in downstream channels

4.6 Discussion

Scenario 2 is simulated and compared with results from Scenario 1 in order to assess the impacts of the current multi-channel networks on the flow and sediment dynamics in the VMD.

4.6.1 Flood dynamics

Inundation level and area

In the Scenario 2 ("pre-development period"), the average inundation level in the PoR basin and LXQ basin is approximately 1.0 m, in some local areas it reaches 2.0 m (see Fig. 4.16); whereas the results from the Scenario 1 (the full network scenario) show the maximum water level of the PoR can reach up to 4.0 m. In this scenario, the total inundation area with water levels of > 0.5 m in Scenario 2 reaches 25.918 km^2, accounting for 65 % of the VMD area in comparison with 29 % of Scenario 1. Lower water levels and larger inundation areas from Scenario 2 indicate that the channel system is a substantial driver of the hydraulic scheme in the VMD. It works efficiently to drain flood waters from the LXQ basin and the PoR basin to the Gulf of Thailand and to the Vam Co River, before discharging to the East Sea, respectively (Thanh et al., 2020).

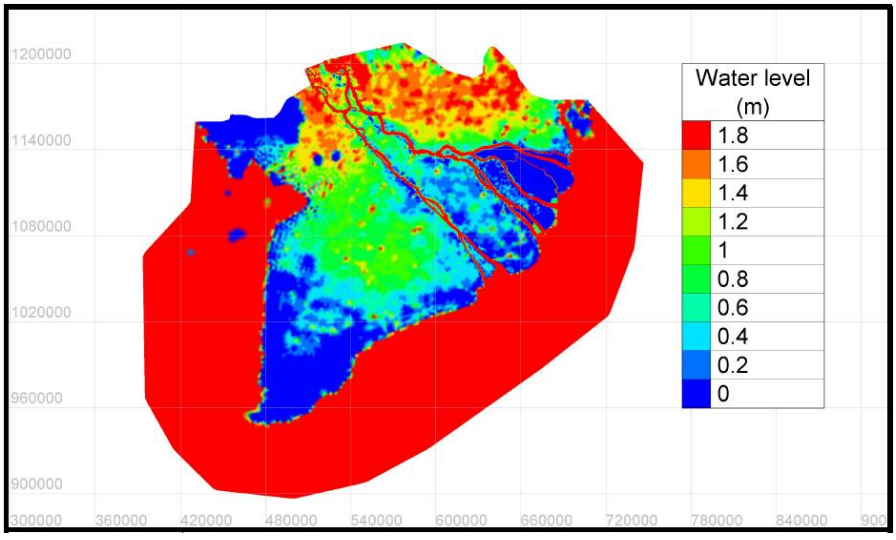

Fig 4.16. Inundation area and water level in the VMD in the Scenario 2

Water elevation and discharge at Can Tho and My Thuan stations

Two main stations (Can Tho and My Thuan) are selected to reevaluate the impacts of the complex channel system on the hydrodynamics in the VMD (see Fig. 4.17). These stations correspond to two important cities in this region, with high population density (about 1000 people/km^2), intensive agricultural production and key economic hotspots.

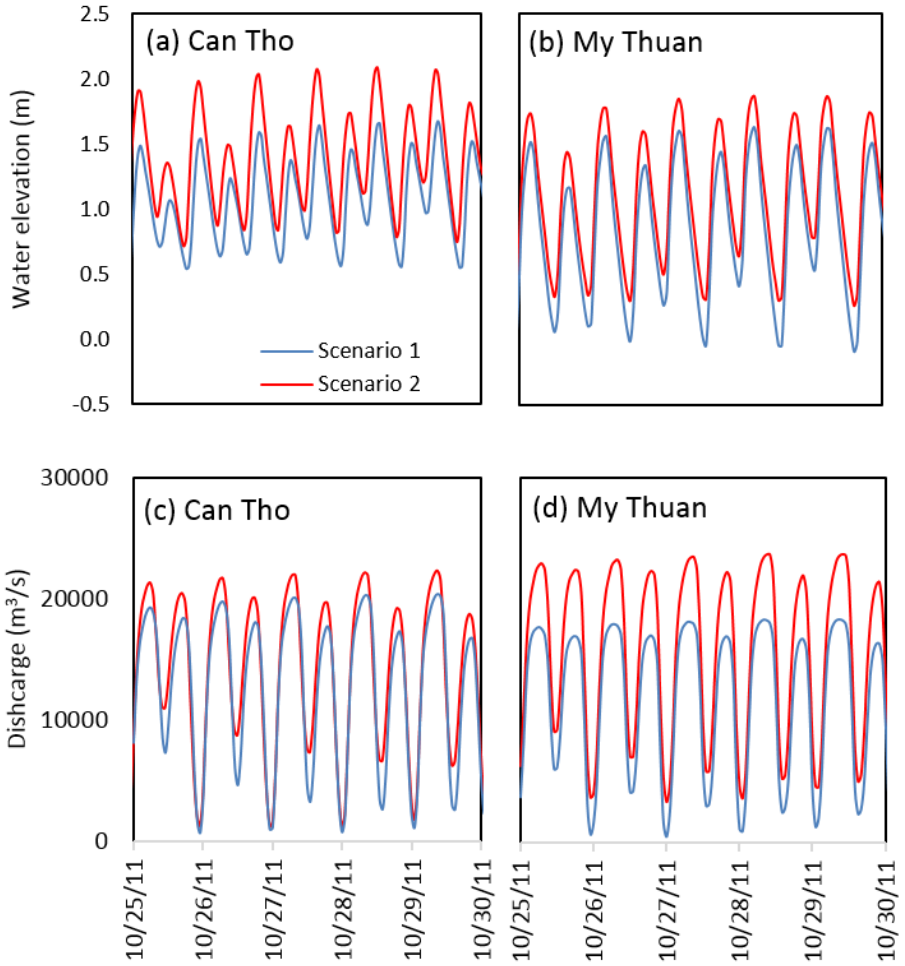

Fig. 4.17. Water level and discharge at Can Tho (a, c) and My Thuan (b, d) between two scenarios

At these stations, the tidal signal is clearly visible even during the highest flood event (Hung et al., 2012 and Eslami et al., 2019). Water elevation increases 0.11 - 0.43 m in Can Tho and 0.18 - 0.45 m in My Thuan in comparison with those in Scenario 1. Discharge at Can Tho station does not change significantly between the two scenarios (about 2000 m^3/s). While discharge at My Thuan station increases about 5400 m^3/s, and reaches approximately 24,000 m^3/s. Because the PoR habours the largest volume of floodwater in the VMD (Thanh et al., 2020), thus overland flow from the PoR results stronger effects on My Thuan station than the effects of LXQ basin on Can Tho station.

The effects of the multi-channel systems in floodwater elevation reduction

The historical flood year 2011 caused a large inundation area in the VMD (see Fig. 4.11 and Triet et al., 2017). The maximum simulated floodwater elevation at the main stations in both scenarios are extracted to compare with the Vietnam flooding alarm elevation No. 1 (Alarm No. 1) to define the flooded area and assess the impacts of the channel network on flood protection (see Fig. 4.18).

Water elevations at almost all stations in the upper VMD are higher than the Alarm No. 1 in both scenarios, because the upstream flood plays a dominant influence on the flow dynamics, especially the PoR basin and the LXQ basin. These region acts as a water storage in wet season and a water supplying source in dry season for the whole VMD.

The coastal area experiences less influence of the upstream flow, thus the water elevation in this area is lower than the Alarm No. 1 (Phung Hiep, Tra Vinh, My Tho and Dai Ngai). In some locations of the estuarine area (Vam Kenh and Hoa Binh) under stronger effects of the semi-diurnal tide from the East Sea, water elevation is higher than the Alarm No. 1.

Water elevations in Scenario 1 are lower than those in Scenario 2 because the channel network works effectively as a water conveyor from the VMD to the seas. Thus, water levels in Can Tho and My Thuan in Scenario 1 are approximately the Alarm No.1. We confirm the effect of the multi-channel network on flood reduction, especially in the coastal areas and key cities of the VMD

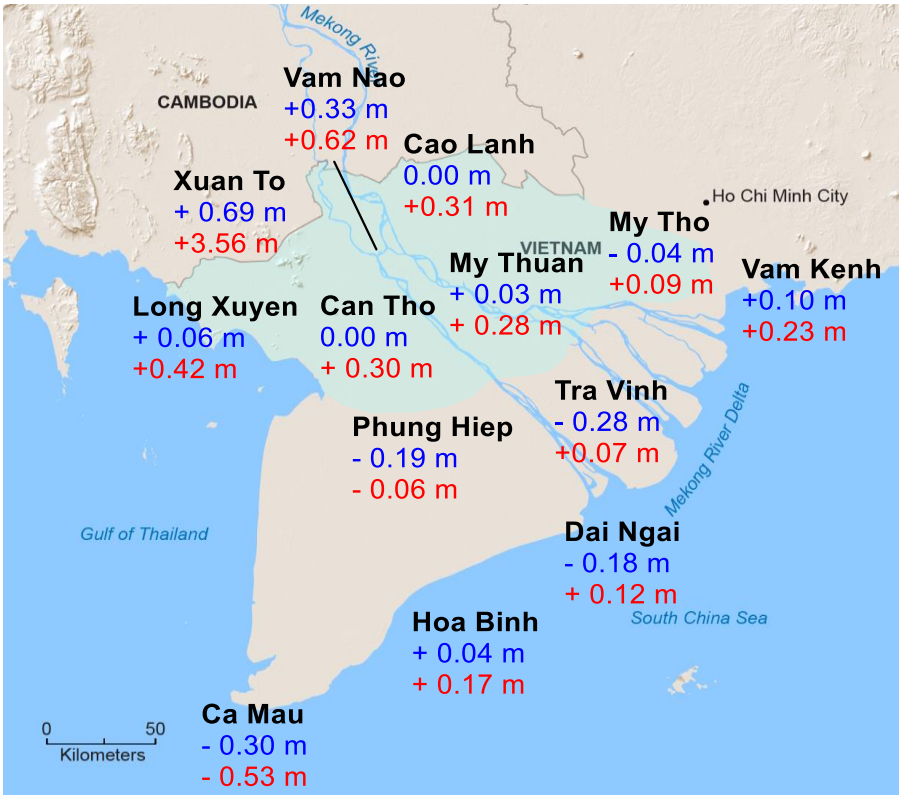

Fig. 4.18. The highest water elevations at main stations in comparison with the Vietnam alarm elevation No. 1. Blue texts show the results from Scenario 1, red texts present the results from Scenario 2. Positive values mean the water elevation at the station higher than the Vietnam alarm elevation No. 1, negative values mean the water elevation lower than the Vietnam alarm elevation No. 1. The light blue area assumes the inundation area in both scenarios.

.

4.6.2 Sediment dynamics

In Scenario 1 and Scenario 2, the main source of sediment in the delta is from the two rivers. In Scenario 1 (see Fig. 4.13 and Fig. 4.15), SSC shows a high spatial variability in the floodplain due to the interplay of the complex networks, river system, tidal regimes and human regulation. Within the delta, the embankments and channels protect the land from flooding, but at the same time, they cease the natural sediment deposition by obstructing the overflow. Oppositely, in Scenario 2 (see Fig. 4.19), SSC prevails within the two main

rivers. Thus, mean SSCs in Scenario 2 are higher than those in Scenario 1, 40 mg/L in the upper part and 100 mg/L in the coastal area, evenly up to 1000 mg/L in the estuaries. The area with SSC > 50 mg/L is extended to 3 - 4 km along two sides of each main tributaries because of overland flow. Suspended sediment discharges further offshore, about 40 km and along 200 km of the coastline (see Fig. 4.19).

This issue raises a concern about sediment budget reduction in the VMD by infrastructure construction in combination with other drivers such as more upstream hydropower dams, uncontrolled sand mining along rivers, overexploitation of groundwater and climate change. All these drivers will thus aggravate the on-going erosion of the delta (Anthony et al., 2015).

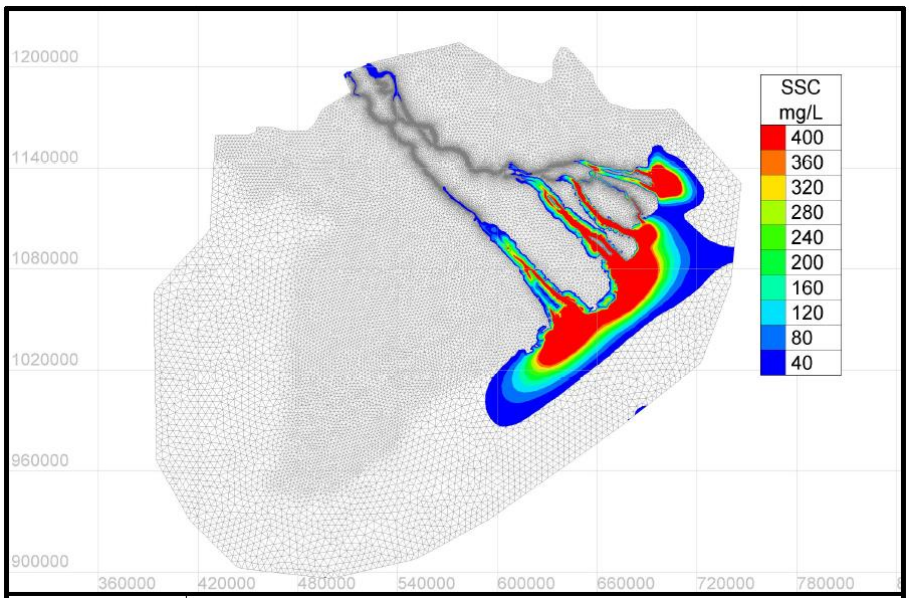

Fig 4.19. SSC from Scenario 2 at the end of the wet season 2011

SSC at Can Tho and My Thuan stations

Fig. 4.20 shows SSC in Can Tho and My Thuan from Scenario 1 and Scenario 2. In comparison with Scenario 1, SSC in Scenario 2 increases between 1.7 and 1.9 times in both stations. The maximum SSC increases from 550 mg/L to 1005 mg/L in Can Tho and from 600 mg/L to 1060 mg/L in My Thuan. Sediment load rise from 2.96 Mtons to 6.65 Mtons in Can Tho and from 3.43

Mtons to 7.69 Mtons in My Thuan. Thus, the total sediment load in October 2011 from the Tien River and Hau River in Scenario 2 is 2.34 times higher than in Scenario 1, from 6.39 Mtons to 14.34 Mtons. The sediment load which flows to the sea via the Hau River and the Tien River accounts for 46 % and 56 % of the total load, respectively. This result is similar to the statistical results conducted by Ha et al. 2018.

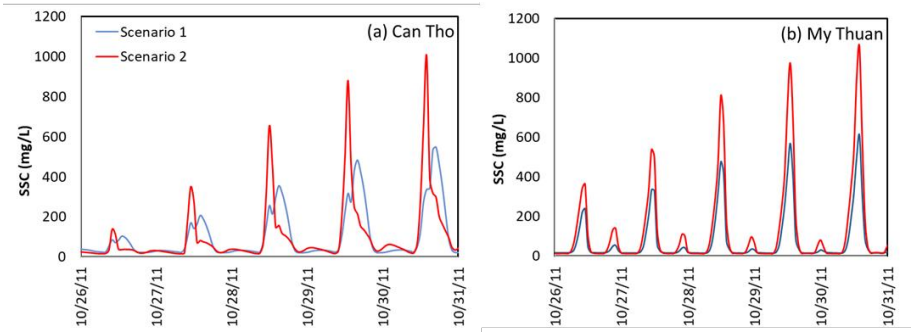

Fig. 4.20. Comparison between SSC from Scenario 1 and 2 in Can Tho (a) and My Thuan (b)

4.6.3 Uncertainties

As observed in Fig. 4.7 - 4.8, the phase of validation shows some discrepancies, in particular, some noticeable underestimation of water elevation in the stations of Vam Nao, My Thanh and Ben Trai stations. However, the general agreement between measures and model are satisfying in most stations.

As being presented in the section 4.2, the VMD is a wide and complex domain; i.e., a low-lying area where small topography effects interact with meteo-hydrological regimes and tidal forcings. Moreover, the VMD is being clearly modified by ongoing anthropogenic stresses and climate changes. For these reasons, it is virtually impossible to capture all the modifications. An exact simulation of the current status of the VMD is not the real objective but the model is designed to help consequently policy makers and stakeholders in their understanding of the hydrodynamics of the VMD. The model has tried to integrate main drivers and utilize robust input data sources, especially an original bathymetry, because the bathymetry appears to control the hydrodynamics of the coastal areas (Blumberg et al., 2008). The most

underestimated simulation is found in Vam Nao, where the morphological conditions altered significantly and severe incision and erosion occurred as reported by Brunier et al. (2014) and Binh et al (2020). Excessive sand mining (Best et al., 2019 and Hackney et al., 2020), land-use changes (Minderhoud et al., 2017) and over-exploitation of groundwater (Minderhoud et al., 2019) activities induced river bed lowering and instability in the LMB, especially in the VMD (Minderhoud et al., 2017). All these supplemental causes contribute to the underestimation of water elevations and model uncertainties.

In addition, the VMD also experiences a partitioning of its floodplain topography due to the density of the multi-channel networks, dyke systems and compartments as well as the presence of vegetation. It makes the flow distribution between the floodplain and the channel system very complex, causing possible underestimation of the water elevation in the floodplain. However, the model can reproduce the flow generated by the tidal regime in a satisfying way (Ganh Hao, Vung Tau and Vam Kenh stations). Thus, results are considered as acceptable and show that it is possible to predict water levels and inundation extents (as shown in Fig. 4.18) as well as SSC in the delta. In order to improve the simulation of the hydrodynamics in such a complex domain, it would be necessary to have updated bathymetry data, information about engineering's infrastructure and better estimates of vegetation roughness. This would certainly result in a reduction of model uncertainties.

4.7 Conclusion

This study confirms the capacity of a full 2D model to simulate flood and sediment dynamics on a large-scale domain under many drivers such as man-made structures and natural conditions (flood events, tidal motions and wind stress). We believe that our study results can provide original information regarding the shift of hydrodynamics on the extreme flooding pattern in the VMD in the current status and perspectives. Such information may be useful for the local residents and policy makers to assess risks and adopt appropriate prevention measures.

The results also shed light on the link between hydrodynamic alterations and human interventions in the VMD. The inundation area in the VMD in 2011

was calculated to be approximately 12,000 km^2 with water level of 0.5 – 4.0 m. The construction of the channel network belittles flooding areas, helping local communities to lessen flood-driven damage and increases agricultural production area. Without the multi-channel network, the inundation area may extend to approximately 26,000 km^2, causing serious damages and human suffering (Hoa et al., 2008).

With the reduction on the floodwater level and inundation area, the multi-channel network also causes lower SSC in the floodplain, especially in the PoR basin and the LXQ basin (approximately 50 %), which are two intensive agricultural production areas in the VMD, leading to instability in the VMD and degradation of soil quality for agricultural production.

In the light of this study, we can confirm that more sustainable development and operation of the multi-channel system will bring a better regulation of water cycles and sediment transport patterns in the VMD. By doing this, the system may reduce flooding but also increase SSC in the floodplain, that will contribute to improve agricultural productivity and compensate serious erosion in the delta.

The VMD is also more vulnerable to climate change, especially to the relative sea level rise and storm surges (Wassman et al., 2004, Hoa et al., 2007, Van et al., 2012, Smajgl et al., 2015, Nhan et al., 2016, Hoang et al. 2016, Dang et al., 2018a), which likely put additional pressures on the water-related safety and sustainability of this region. For future studies, numerical simulations should be conducted to predict the flood heights and duration in the VMD caused by the combined impact of alternated upstream flows, tides, storm surges, sea level rise and engineering structures. The flow distributions and saltwater intrusion in dry season would be addressed in forthcoming works.

Chapter 5 Conclusions and perspectives

5.1 Conclusions

This work has been conducted following the concept of sustainable science: it strengthens the link between well-known academic institutions from North and South countries. Results and recommendations developed in the manuscript could be useful for both academics and policy makers involved in the management of this transboundary basin, where the knowledge of hydrodynamics is still not comprehensively documented. Due to its large-scale and the complexity of the domain, finding a suitable methodology is not a straightforward task. In this work, both field and model investigation methods are applied simultaneously. In this work, both field and model investigation methods are applied simultaneously.

The outcome of this thesis are a better understanding of flow and sediment dynamics in the Lower Mekong Basin, particularly sediment properties along the river, periodic watering and dewatering process in the Tonle Sap and the effects of the multi-channel system on the flow and sediment transport in the Vietnamese Mekong Delta. This information may be useful to assess forthcoming modifications by natural drivers and human activities, then adopt appropriate prevention measures.

5.1.1 Sediment properties along the Lower Mekong Basin

The Chapter 2 has assessed the behavior of sediment properties along the Lower Mekong Basin at three representative conditions from fluvial to

estuarine environments. This objective is conducted by implementing field surveys and laboratory analysis by various advanced equipment and techniques, especially SCAF (System for the Characterization of Aggregates and Flocs). Consequently, the sediment properties and flocculation process of each environment are investigated. In addition, it is the first time that flocculation index is applied in a large tropical river, demonstrating its capacity on predicting flocculation capacity by particle sizes and their settling velocities. This study also determines a threshold SSC, which promotes the formation of so-called fluid mud layers near the bottom in the Mekong Delta. In the light of this study, we have some recommendations for the Mekong Delta management in the aspect of hydro-sedimentary changes.

In the Lower Mekong River, as in many other large hydrosystems under tropical climates, we may anticipate that particle populations (and its consequences) fluctuate seasonally and yearly. As designed, this study cannot catch all these variations, however, we ensure that it describes a general pattern that could be helpful when establishing some monitoring strategies in similar large tropical hydrosystems in Southeast Asia.

5.1.2 The periodic watering and dewatering process in the Tonle Sap lake

The Tonle Sap is the largest freshwater lake in Southeast Asia and one of the most vibrant ecosystems in the world. As well, it also experiences an unique hydrological regime with seasonally bi-directional flows. Therefore, a good simulation of flow patterns in the Tonle Sap is critical and ordeal for modelers. Our work attempts to model the watering and dewatering process in the Tonle Sap lake by applying an existing wetting – drying algorithm in two space dimensions and implemented in SLIM. This algorithm consists of a threshold value of fluid depth for a thin layer and a blending parameter in order to guarantee positive values of the water depth, while preserving local mass conservation and the well-balanced property at wet/dry interfaces. A special point of this algorithm is to solve the shallow water equations in a fully implicit way, where large time steps can be used. Thus, computational time is significantly reduced and allows long - time simulations. The resulting model

reasonably handles backwater flows during the rainy season and simulates the propagations of wet and dry interfaces without numerical instability.

The model is a powerful tool to simulate a specific flow regime of the Tonle Sap system, help understanding the relationship between the Tonle Sap lake and the Lower Mekong Basin. It also proves to be an effective source providing robust data of discharge and water level at locations which lack of monitored hydrological data. This information may be beneficial for authorities in establishing developing plans and analyzing potential risks in the event of flooding and drought. Furthermore, it can be conveniently applied to larger river basins.

The limitation of our work is the application of three wetting–drying parameters (ε_1, ε_2, ε_3) that have to be calibrated. We hope to improve our algorithm in SLIM in order to convert these parameters into dimensionless ones that would be valid for a large range of applications.

5.1.3 Flow and sediment dynamics of the Vietnamese Mekong Delta and the effect of the multi-channel systems

This section concerns a very important and the most sensitive part of the Lower Mekong Basin. The simulation of hydrodynamics and sediment transport in the Vietnamese Mekong Delta is really a challenge task because of the complicated channel and dyke systems. In this work, TELEMAC – 2D model coupled with SISYPHE sediment transport module successfully simulates the flow and sediment dynamics in this complex domain. The advantage of our simulation is the utilization of measured data from our field survey campaigns for the model inputs.

This work confirms the capacity of a full 2D model to simulate flood dynamics and sediment transport on a large scale domain under many drivers such as man-made constructions and natural conditions (flood events, tidal motions and wind stress). It also sheds light on the link between flow alterations and man-made constructions in the Vietnamese Mekong Delta.

The computed results reveal that the multi-channel system is able to reduce flooding area (water level and discharge) in the central and coastal part of the Vietnamese Mekong Delta, however it also causes a gradual fall of SSC in the

floodplain, that may cause damages in food production. Thus, more sustainable development and operation of the system is extremely needed in the region.

The most important difficulty in our simulations is the limited access to up-to-date and reliable data sources, especially concerning bathymetry and SSC, that plays essential roles in hydrodynamic simulations. As presented in Chapter 4, bathymetry and topography in the VMD vary significantly because of human and natural drivers. According to SSC assessment, monitoring stations are only located in the mainstreams and several short-term data series are found in the floodplains, that cause difficulties for model validation.

5.2 Perspectives

As being mentioned above, the Cambodia floodplain and the Mekong Delta have a close hydraulic connectivity, strongly depending on the Mekong River. Using the existing models, conducting full 2D simulations for this combined region would be a preliminary step for further researches to assess impacts of human interventions on the transboundary domain. Some detailed objectives below can be implemented:

- The assessment of the combined impacts of the natural condition in the Cambodia floodplain and local man-made structures in the Vietnamese Mekong Delta on the hydrodynamics is still limited. The obtained results from such a research could lead to define operational recommendations for the sustainable development and management of the water regulating structures in the region.
- Saltwater intrusion is becoming more critically. Adapting to it becomes a top priority from the downstream countries' governments. Thus, the accurately modelling and predicting saltwater intrusion in dry season is essential in the coastal area, especially in the context of climate change and relative sea level rise. It may help reduction of economic losses, ecological damages and residential livelihoods.

- The simulated results by hydrodynamic models can be more robust when comparing with satellite images to understand the evolution of the Mekong floodplain for a long period and its perspectives. Such comparisons could be further developed.

SLIM has proven its capacity to simulate of the watering and dewatering phases in the Tonle Sap. At present, the Tonle Sap Lake is rapidly filling with sediment from its catchment (Kummu et al., 2008b). It would have serious implications for the floodwater storage and threaten the lake ecosystem (Piman et al., 2017), that requires a deep assessment of this issue. We think that the development of SLIM could pay attention on sediment transport by taking into account the existence of particle size distribution and corresponding settling velocity as well as their temporary variations due to the flocculation and breakup processes of suspended sediment. These processes cause mass exchanges between different classes and result in erosion and deposition from the bottom of the lake.

The Vietnamese Mekong Delta also faces with environmental degradation related to increased suspended sediment load by anthropogenic activities. With a better knowledge of sediment properties along the Lower Mekong Basin, achieved from this thesis, further studies may pay attentions on the consequences of sediment characteristics on pollutant transport. This issue should be performed by a comprehensive study, including field surveys, laboratory analysis and modelling by inheriting available TELEMAC-SISYPHE coupled model. The outcomes could identify high contaminated locations, then assess environmental risks caused by water pollution and sediment on human and ecosystems.

References

1. ADB (2009a). The economics of climate change in Southeast Asia: a regional review. Asian Development Bank, Manila, Philippine. Available at https:// ww.adb.org/sites/default/files/publication/29657/ economics-climate-change-se-asia.pdf.
2. ADB (2009b). Cambodia: Preparing the Water Resources Management (Sector) Project. Water Resources Management Sector Development Project Technical Annex on Integrated Water Resources Management (IWRM). Ministry of Water Resources and Meteorology, Royal Government of Cambodia and Asian Development Bank, Phnom Penh. Available at https://www.adb.org/sites/default/files/project-document/ 64081/38558-01-cam-tacr.pdf.
3. Anthony, E. J., & Gratiot, N. (2012). Coastal engineering and large-scale mangrove destruction in Guyana, South America: Averting an environmental catastrophe in the making. *Ecological Engineering, 47*, 268-273.
4. Anthony, E. J., Brunier, G., Besset, M., Goichot, M., Dussouillez, P., & Nguyen, V. L. (2015). Linking rapid erosion of the Mekong River delta to human activities. *Scientific reports, 5*, 14745.
5. Anthony, E.J. (2015). Wave influence in the construction, shaping and destruction of river deltas: A review. *Marine Geology, 361*, 53-78.
6. Antoine, G., Cazilhac, M., Monnoyer, Q., Jodeau, M., Gratiot, N., Besnier, A. L., ... & Le Brun, M. (2015, April). Lateral and vertical heterogeneity of flow and suspended sediment characteristics during a dam flushing event, in high velocity conditions. In *EGU General Assembly Conference Abstracts* (Vol. 17).
7. Apel, H., Trepat, O. M., Hung, N. N., Merz, B., & Dung, N. V. (2016). Combined fluvial and pluvial urban flood hazard analysis: concept development and application to Can Tho city, Mekong Delta, Vietnam. *Natural Hazards & Earth System Sciences, 16*(4).
8. Azhikodan, G., & Yokoyama, K. (2018). Sediment transport and fluid mud layer formation in the macro-tidal Chikugo river estuary during a

fortnightly tidal cycle. *Estuarine, Coastal and Shelf Science, 202*, 232-245.

9. Azrulhisham, E. A., & Azri, M. A. (2018, February). Application of LISST instrument for suspended sediment and erosive wear prediction in run-of-river hydropower plants. In *2018 IEEE International Conference on Industrial Technology (ICIT)* (pp. 886-891). IEEE.
10. Bachmann, R. W., Hoyer, M. V., Vinzon, S. B., & Daniel Jr, E. C. (2005). The origin of the fluid mud layer in Lake Apopka, Florida. *Limnology and Oceanography, 50*(2), 629-635.
11. Baldwin D.S., Mitchell A.M. (2000). The effects of drying and reflooding on the sediment and soil nutrient dynamics of lowland river floodplain systems: a synthesis. *Regulated Rivers: Research & Management, 16*(5):457-467.
12. Balica, S., Dinh, Q., Popescu, I., Vo, T. Q., & Pham, D. Q. (2014). Flood impact in the MD, Vietnam. *Journal of Maps, 10*(2), 257-268.
13. Balzano A (1998) Evaluation of methods for numerical simulation of wetting and drying in shallow water flow models. *Coastal Engineering 34*(1-2):83-107.
14. Barbier, E.B. (1987). The concept of sustainable economic development. *Environmental Conservation 14*(2), 101-110.
15. Begnudelli L., Sanders B.F. (2006). Unstructured grid finite-volume algorithm for shallow-water flow and scalar transport with wetting and drying. *Journal of Hydraulic engineering, 132*(4), 371-384.
16. Berg M., Stengel C., Trang P.T.K., Viet P.H., Sampson M.L., Leng M., Samreth S., Fredericks D. (2007). Magnitude of arsenic pollution in the Mekong and Red River Deltas - Cambodia and Vietnam. *Science of The Total Environment, 372*(2-3), 413-425.
17. Best, J. (2018). Anthropogenic stresses on the world's big rivers. *Nature Geoscience, 12*, 7-21.
18. Bianchi, T.S. (2016). *Deltas and humans: A long relationship now threatened by global change*. Oxford University Press.
19. Binh, V.D., Kantoush, S., & Sumi, T. (2020). Changes to long-term discharge and sediment loads in the Vietnamese Mekong Delta caused by upstream dams. *Geomorphology*, 353, 107011.

20. Blumberg, A. F., & Georgas, N. (2008). Quantifying uncertainty in estuarine and coastal ocean circulation modeling. *Journal of Hydraulic Engineering*, 134(4), 403-415.
21. Brackenridge, G.R. (2011, August 24). The Flood Observatory. University of Colorado-Boulder. Accessed August 25, 2011. Retrieved from https://earthobservatory.nasa.gov/images/51913/flooding-along-the-mekong-river.
22. Bradford S.F., Sanders B.F. (2002). Finite-volume model for shallow-water flooding of arbitrary topography. *Journal of Hydraulic Engineering, 128*(3), 289-298.
23. Bravard, J. P., Goichot, M., & Tronchère, H. (2014). An assessment of sediment-transport processes in the Lower Mekong River based on deposit grain sizes, the CM technique and flow-energy data. *Geomorphology, 207*, 174-189.
24. Brunier, G., Anthony, E. J., Goichot, M., Provansal, M., & Dussouillez, P. (2014). Recent morphological changes in the Mekong and Bassac river channels, Mekong delta: The marked impact of river-bed mining and implications for delta destabilisation. *Geomorphology*, 224, 177-191.
25. Brunier, G., Anthony, E. J., Gratiot, N., & Gardel, A. (2019). Exceptional rates and mechanisms of muddy shoreline retreat following mangrove removal. *Earth Surface Processes and Landforms, 44*, 1559 - 1571.
26. Burt T.P. (1996) The hydrological role of floodplains within the drainage basin system. In: *Haycock NE, Burt TP, Goulding KWT, Piney G (ed) Buffer zones: their processes and potential in water protection*, Haycock Associated Limited, UK, pp 21-32.
27. Buschmann, J., Berg, M., Stengel, C., Winkel, L., Sampson, M. L., Trang, P. T. K., & Viet, P. H. (2008). Contamination of drinking water resources in the Mekong delta floodplains: Arsenic and other trace metals pose serious health risks to population. *Environment International, 34*(6), 756-764.
28. Camenen, B., & van Bang, D. P. (2011). Modelling the settling of suspended sediments for concentrations close to the gelling concentration. *Continental Shelf Research, 31*(10), 106-116.
29. Camenen, B., Le Coz, J., Dramais, G., Peteuil, C., Fretaud, T., Falgon, A., ... & Moore, S. A. (2014). A simple physically-based model for predicting sand transport dynamics in the LMB. In *Proceeding River Flow conference*, Lausanne, Switzerland, 8pp.

30. Campbell I.C., Say S., Beardall J. (2009) Tonle Sap Lake, the heart of the lower Mekong. In: *Campbell I.C. (ed) The Mekong, 1st ed*, Academic Press, New York, pp 251-272.
31. Candy, A. S. (2017). An implicit wetting and drying approach for non-hydrostatic baroclinic flows in high aspect ratio domains. *Advances in Water Resources, 102*, 188-205.
32. Casulli V. (2009) A high resolution wetting and drying algorithm for free - surface hydrodynamics. *International Journal for Numerical Methods in Fluids, 60*(4), 391-408.
33. Casulli, V., and Stelling, G. S. (1998). Numerical simulation of 3D quasi-hydrostatic, freesurface flows. *Journal of Hydraulic Engineering, 124*(7), 678-686.
34. Comba, S., & Sethi, R. (2009). Stabilization of highly concentrated suspensions of iron nanoparticles using shear-thinning gels of xanthan gum. *Water Research, 43*(15), 3717-3726.
35. Craig J.F., Halls A.S., Barr J.J.F., Bean C.W. (2004) The Bangladesh floodplain fisheries. *Fisheries Research, 66*(2-3), 271-286.
36. Dang, T. D., Cochrane, T. A., Arias, M. E., Van, P. D. T., & de Vries, T. T. (2016). Hydrological alterations from water infrastructure development in the Mekong floodplains. *Hydrological processes, 30*(21), 3824-3838.
37. Dang, T. D., Cochrane, T. A., & Arias, M. E. (2018). Future hydrological alterations in the Mekong Delta under the impact of water resources development, land subsidence and sea level rise. *Journal of Hydrology: Regional Studies, 15*, 119-133.
38. D'alpaos L., Defina A. (2007). Mathematical modeling of tidal hydrodynamics in shallow lagoons: A review of open issues and applications to the Venice lagoon. *Computers & Geosciences, 33*(4), 476-496.
39. Darby, S. E., Hackney, C. R., Leyland, J., Kummu, M., Lauri, H., Parsons, D. R., ... & Aalto, R. (2016). Fluvial sediment supply to a mega-delta reduced by shifting tropical-cyclone activity. *Nature, 539*, 276 - 279.
40. De Brye B., Schellen S., Sassi M., Vermeulen B., Kärnä T., Deleersnijder E., Hoitink T. (2011). Preliminary results of a finite-element, multi-scale model of the Mahakam Delta (Indonesia). *Ocean Dynamics, 61*(8),1107-1120.

41. Dresback K.M., Kolar R.L., Dietrich J.C. (2002). Impact of the form of the momentum equation on shallow water models based on the generalized wave continuity equation. *Development in Water Science, 47*, 1573-1580.
42. Droppo, I. G., Nackaerts, K., Walling, D. E., & Williams, N. (2005). Can flocs and water stable soil aggregates be differentiated within fluvial systems?.*Catena, 60*(1), 1-18.
43. Duc Tran, D., Halsema, G. V., Hellegers, P. J., Phi Hoang, L., Quang Tran, T., Kummu, M., & Ludwig, F. (2018). Assessing impacts of dike construction on the flood dynamics of the Mekong Delta. *Hydrology and Earth System Sciences, 22*(3), 1875-1896.
44. Duong, T. A., Hoang, L. P., Bui, M. D., & Rutschmann, P. (2018). Modelling seasonal flows alteration in the Vietnamese Mekong Delta under upstream discharge changes, rainfall changes and sea level rise. *International Journal of River Basin Management, 17*(4), 435-449.
45. Duong, T. A., Hoang, L. P., Bui, M. D., & Rutschmann, P. (2018). Simulating Future Flows and Salinity Intrusion Using Combined One-and Two-Dimensional Hydrodynamic Modelling—The Case of Hau River, Vietnamese Mekong Delta. *Water, 10*(7), 897.
46. Duy Vinh, V., Ouillon, S., Van Thao, N., & Ngoc Tien, N. (2016). Numerical simulations of suspended sediment dynamics due to seasonal forcing in the Mekong coastal area. *Water, 8*(6), 255.
47. Dyer, K. R., Bale, A. J., Christie, M. C., Feates, N., Jones, S., & Manning, A. J. (2002). The turbidity maximum in a mesotidal estuary, the Tamar Estuary, UK: I. Dynamics of suspended sediment. In *Proceedings in Marine Science* (Vol. 5, pp. 203-218). Elsevier.
48. Dyer, K. R., Bale, A. J., Christie, M. C., Feates, N., Jones, S., & Manning, A. J. (2002b). The turbidity maximum in a mesotidal estuary, the Tamar estuary, UK: II. The floc properties. In *Proceedings in Marine Science* (Vol. 5, pp. 219-232). Elsevier.
49. Dung, N.V., Merz, B., Bárdossy, A., Apel, H. (2013). Flood hazard in the Mekong Delta -a probabilistic, bivariate, and non-stationary analysis with a short-termed future perspective. *Natural Hazards and Earth System Sciences Discussion, 1*, 275-322.
50. Eastham, J., F. Mpelasoka, M. Mainuddin, C. Ticehurst, P. Dyce, G. Hodgson, R. Ali and M. Kirby (2008). *Mekong River Basin Water Resources Assessment: Impacts of Climate Change*. CSIRO: Water for a Healthy Country National Research Flagship.

51. Eidam, E. F., Nittrouer, C. A., Ogston, A. S., DeMaster, D. J., Liu, J. P., Nguyen, T. T., & Nguyen, T. N. (2017). Dynamic controls on shallow clinoform geometry: Mekong Delta, Vietnam. *Continental Shelf Research, 147*, 165-181.
52. European Space Agency – ESA (2007). Envisat images of the Mekong Delta in Vietnam. Retrieved from https://www.esa.int/ESA_Multimedia/Images/2007/04/Envisat_image_of_the_Mekong_Delta_in_Vietnam
53. Eslami, S., Hoekstra, P., Kernkamp, H., Trung, N.N., Duc, D.D., Quang, T. T., ... Vegt, M.V.D. (2019). Flow Division Dynamics in the Mekong Delta: Application of a 1D-2D Coupled Model. *Water, 11*(4), 837.
54. Farrell, E. J., & Sherman, D. J. (2013). Estimates of the Schmidt Number for vertical flux distributions of wind-blown sand. *Journal of Coastal Research, 65*(sp2), 1289-1295.
55. Fennessy, M. J., Dyer, K. R., & Huntley, D. A. (1994). Size and settling velocity distributions of flocs in the Tamar Estuary during a tidal cycle. *Netherland Journal of Aquatic Ecology, 28*(3-4), 275-282.
56. Fettweis, M., Francken, F., Pison, V., & Van den Eynde, D. (2006). Suspended particulate matter dynamics and aggregate sizes in a high turbidity area. *Marine Geology, 235*(1-4), 63-74.
57. Fu, K., Su, B., He, D., Lu, X., Song, J., & Huang, J. (2012). Pollution assessment of heavy metals along the Mekong River and dam effects. *Journal of Geographical Sciences, 22*(5), 874-884.
58. Fujii H., Garsdal H., Ward P., Ishii M., Morishita K., Boivin T. (2003). Hydrological roles of the Cambodian floodplain of the Mekong River. *International Journal of River Basin Management, 1*(3):253-266.
59. Fujihara, Y., Hoshikawa, K., Fujii, H., Kotera, A., Nagano, T., & Yokoyama, S. (2016). Analysis and attribution of trends in water levels in the Vietnamese Mekong Delta. *Hydrological Processes, 30*(6), 835-845.
60. Furukawa, K., & Wolanski, E. (1996). Sedimentation in mangrove forests. *Mangroves and Salt Marshes, 1*(1), 3-10.
61. Furukawa, K., Wolanski, E., & Mueller, H. (1997). Currents and sediment transport in mangrove forests. *Estuarine, Coastal and Shelf Science, 44*(3), 301-310.

62. Gabioux, M., Vinzon, S. B., & Paiva, A. M. (2005). Tidal propagation over fluid mud layers on the Amazon shelf. *Continental Shelf Research, 25*(1), 113-125.
63. Garschagen M., Diez J.R., Nhan D.K., Kraas F. (2012) Socio-Economic Development in the Mekong Delta: Between the Prospects for Progress and the Realms of Reality. In: Renaud F., Kuenzer C. (eds) *The Mekong Delta System*. Springer Environmental Science and Engineering. Springer, Dordrecht.
64. General Statistics of Vietnam (2016). *Statistical Yearbook of Vietnam 2016*. Statistical Publishing House, Hanoi, Vietnam
65. Goudie, A. S. (2018). *Human impact on the natural environment*. John Wiley & Sons.
66. Gourgue O., Deleersnijder E., White L. (2007). Toward a generic method for studying water renewal, with application to the epilimnion of Lake Tanganyika. *Estuarine, Coastal and Shelf Science, 74*(4):628-640.
67. Gourgue O., Comblen R., Lambrechts J., Kärnä T., Legat V., Deleersnijder E. (2009). A flux limiting wetting - drying method for finite-element shallow-water models, with application to the Scheldt Estuary. *Advances in Water Resources, 32*(12):1726-1739.
68. Gourgue O., Baeyens W., Chen M.S., de Brauwere A., de Brye B., Deleersnijder E., Elskens M., Legat V. (2013). A depth-averaged two-dimensional sediment transport model for environmental studies in the Scheldt Estuary and tidal river network. *Journal of Marine Systems, 128*, 27-39.
69. Gratiot, N., Manning, A.J. (2004). An experimental investigation of floc characteristics in a diffusive turbulent flow. *Journal of Coastal Research, S1 41*, 105–113.
70. Gratiot, N., Gardel, A. and Anthony, E.J., 2007. Trade-wind waves and mud dynamics on the French Guiana coast, South America: input from ERA-40 wave data and field investigations. *Marine Geology, 236*, 15-26.
71. Gratiot, N., Coulaud, C., Legout, C., Mercier, B., Mora, H., & Wendling, V. (2015). Unit for measuring the falling speed of particles in suspension in a fluid and device comprising at least one measuring unit and one automatic sampler. *Patent - Publication number WO2015055963 A, 1*.
72. Gratiot, N., & Anthony, E. J. (2016). Role of flocculation and settling processes in development of the mangrove-colonized, Amazon-

influenced mud-bank coast of South America. *Marine Geology, 373*, 1-10.

73. Gratiot, N., Bildstein, A., Anh, T. T., Thoss, H., Denis, H., Michallet, H., & Apel, H. (2017). Sediment flocculation in the Mekong River estuary, Vietnam, an important driver of geomorphological changes. *Comptes Rendus Geoscience, 349*(6-7), 260-268.
74. Gugliotta, M., Saito, Y., Nguyen, V. L., Ta, T. K. O., & Tamura, T. (2019). Sediment distribution and depositional processes along the fluvial to marine transition zone of the Mekong River delta, Vietnam. *Sedimentology, 66*(1), 146-164.
75. Gupta, A., & Liew, S. C. (2007). The Mekong from satellite imagery: A quick look at a large river. *Geomorphology, 85*(3-4), 259-274.
76. Gupta, A., Hock, L., Xiaojing, H., Ping, C., 2002. Evaluation of part of the Mekong River using satellite imagery. *Geomorphology, 44*(3-4), 221–239.
77. Ha, D.T., Ouillon, S., & Van Vinh, G. (2018). Water and suspended sediment budgets in the lower Mekong from high-frequency measurements (2009–2016). *Water, 10*(7), 846.
78. Hackney, C. R., Darby, S. E., Parsons, D. R., Leyland, J., Best, J. L., Aalto, R., Nicholas, A.P. & Houseago, R. C. (2020). River bank instability from unsustainable sand mining in the lower Mekong River. *Nature Sustainability*, 1-9.
79. Hanington, P., To, Q. T., Van, P. D. T., Doan, N. A. V., & Kiem, A. S. (2017). A hydrological model for interprovincial water resource planning and management: a case study in the Long Xuyen Quadrangle, Mekong Delta, Vietnam. *Journal of Hydrology, 547*, 1-9.
80. Hapuarachchi, H.A.P., Takeuchi, K., Zhou, M., Kiem, A.S., Georgievski, M., Magome, J., Ishidaira, H. (2008). Investigation of the Mekong River basin hydrology for 1980–2000 using the YHyM. *Hydrological Processes, 22*(9), 1246-1256.
81. Hai, P. T., Masumoto, T., & Shimizu, K. (2008). Development of a two-dimensional finite element model for inundation processes in the Tonle Sap and its environs. *Hydrological Processes: An International Journal, 22*(9), 1329-1336.

82. Heniche M, Secretan Y, Boudreau P, Leclerc M (2000) A two-dimensional finite element drying-wetting shallow water model for rivers and estuaries. *Advances in Water Resources, 23*(4):359-372
83. Hoa, L.T.V., Shigeko, H., Nhan, N.H., Cong, T.T. (2008). Infrastructure effects on floods in the Mekong River Delta in Vietnam. *Hydrological Processes, 22*(9), 1359-1372.
84. Hoang, L.P., Lauri, H., Kummu, M., Koponen, J., van Vliet, M., Supit, I., ... Ludwig, F. (2016). Mekong River flow and hydrological extremes under climate change. *Hydrology and Earth System Sciences, 20*(7), 3027-3041.
85. Hung, N.N., Delgado, J.M., Tri, V.K., Hung, L.M., Merz, B., Bárdossy, A., Apel, H. (2012). Floodplain hydrology of the Mekong Delta, Vietnam. *Hydrological Processes, 26*(5), 674-686.
86. Hung, N.N., Delgado, J.M., Güntner, A., Merz, B., Bárdossy, A., Apel, H. (2014). Sedimentation in the floodplains of the Mekong Delta, Vietnam. Part I: suspended sediment dynamics. *Hydrological Processes, 28*(7), 3132-3144.
87. Hung, N. N., Delgado, J. M., Güntner, A., Merz, B., Bárdossy, A., & Apel, H. (2014). Sedimentation in the floodplains of the Mekong Delta, Vietnam Part II: deposition and erosion. *Hydrological Processes, 28*(7), 3145-3160.
88. Huong, H. T. L., & Pathirana, A. (2013). Urbanization and climate change impacts on future urban flooding in Can Tho city, Vietnam. *Hydrology and Earth System Sciences, 17*(1), 379.
89. Huu-Thoi, N., & Gupta, A.D. (2001). Assessment of water resources and salinity intrusion in the Mekong Delta. *Water International, 26*(1), 86-95.
90. Ji X, Li Y, Luo X, He D (2018) Changes in the Lake Area of Tonle Sap: Possible Linkage to Runoff Alterations in the Lancang River?. *Remote Sensing, 10*(6):866-886.
91. Kantoush, S., Binh, D. V., Sumi, T., & Trung, L. V. (2017). Impact of Upstream Hydropower Dams and Climate Change on Hydrodynamics of Vietnamese Mekong Delta. *Journal of Japan Society of Civil Engineers, Ser. B1* (Hydraulic Engineering), 73.
92. Käkönen, M. (2008). Mekong Delta at the crossroads: more control or adaptation?. *AMBIO: A Journal of the Human Environment, 37*(3), 205-213.

93. Kärnä T., De Brye B., Gourgue O., Lambrechts J., Comblen R., Legat V., Deleersnijder E (2011). A fully implicit wetting - drying method for DG-FEM shallow water models, with an application to the Scheldt Estuary. *Computer Methods in Applied Mechanics and Engineering, 200*(5-8), 509-524.
94. Kesserwani G., Liang Q. (2012). Dynamically adaptive grid based discontinuous Galerkin shallow water model. *Advances in Water Resources, 37*, 23-39.
95. Kineke, G. C., Sternberg, R. W., Trowbridge, J. H., & Geyer, W. R. (1996). Fluid-mud processes on the Amazon continental shelf. *Continental Shelf Research, 16*(5-6), 667-696.
96. Kite, G. (2001). Modelling the Mekong: hydrological simulation for environmental impact studies. *Journal of Hydrology, 253*(1-4), 1-13.
97. Knight, D. W. (1981). Some field measurements concerned with the behaviour of resistance coefficients in a tidal channel. *Estuarine, coastal and shelf science, 12*(3), 303-322.
98. Kondolf, G. M., Rubin, Z. K., & Minear, J. T. (2014). Dams on the Mekong: Cumulative sediment starvation. *Water Resources Research, 50*(6), 5158-5169.
99. Kondolf, G.M., Schmitt, R.J., Carling, P., Darby, S., Arias, M., Bizzi, S., Castelletti, A., Cochrane, A.T., Gibson, S., Kummu, M., Oeurng, C., Ru bin, Z., Wild, T., 2018. Changing sediment budget of the Mekong: Cumulative threats and management strategies for a large river basin. *Science of The Total Environment, 625*, 114–134.
100. Kulp, S. A., and Strauss, B. H. (2019). New elevation data triple estimates of global vulnerability to sea-level rise and coastal flooding. Nature communications, 10(1), 1-12.
101. Kummu, M. and Varis, O. (2007). Sediment-related impacts due to upstream reservoir trapping, the Lower Mekong Basin. *Geomorphology, 85*, 275 – 293.
102. Kummu, M., and Sarkkula, J. (2008a). Impact of the Mekong River flow alteration on the Tonle Sap flood pulse. *AMBIO, 37*(3), 185-193.
103. Kummu, M., Penny, D., Sarkkula, J., & Koponen, J. (2008b). Sediment: curse or blessing for Tonle Sap Lake?. *AMBIO: A Journal of the Human Environment, 37*(3), 158-163.

104. Kummu M., Tes S., Yin S., Adamson P., Jozsa J., Koponen J., Richey J., Sarkkula J. (2014). Water balance analysis for the Tonle Sap Lake - floodplain system. *Hydrological Processes, 28*(4):1722-1733.
105. Lambrechts J., Humphrey C., McKinna L., Gourge O., Fabricius K.E., Mehta A.J., Lewis S., Wolanski E. (2010). Importance of wave-induced bed liquefaction in the fine sediment budget of Cleveland Bay, Great Barrier Reef. *Estuarine, Coastal and Shelf Science, 89*(2), 154-162.
106. Le, H. A., Gratiot, N., Santini, W., Ribolzi, O., Tran, D., Meriaux, X., ... & Soares-Frazão, S. (2020a). Suspended sediment properties in the Lower Mekong River, from fluvial to estuarine environments. *Estuarine, Coastal and Shelf Science, 233*, 106522.
107. Le, H. A., Lambrechts, J., Ortleb, S., Gratiot, N., Deleersnijder, E., & Soares-Frazão, S. (2020b). An implicit wetting–drying algorithm for the discontinuous Galerkin method: application to the Tonle Sap, Mekong River Basin. *Environmental Fluid Mechanics*, 1-29.
108. Le Hir, P., Roberts, W., Cazaillet, O., Christie, M., Bassoullet, P., & Bacher, C. (2000). Characterization of intertidal flat hydrodynamics. *Continental shelf research, 20*(12-13), 1433-1459.
109. Le, T. V. H., Nguyen, H. N., Wolanski, E., Tran, T. C., & Haruyama, S. (2007). The combined impact on the flooding in Vietnam's Mekong River delta of local man-made structures, sea level rise, and dams upstream in the river catchment. *Estuarine, Coastal and Shelf Science, 71*(1-2), 110-116.
110. Legout, C., Droppo, I.G., Coutaz, J., Bel, C., Jodeau, M., 2018. Assessm ent of erosion and settling properties of fine sediments stored in cobble bed rivers: the Arc and Isère alpine rivers before and after reservoir flushing. *Earth Surface Processes and Landforms, 43*(6), 1295–1309.
111. Lee, B. J., Fettweis, M., Toorman, E., & Molz, F. J. (2012). Multimodality of a particle size distribution of cohesive suspended particulate matters in a coastal zone. *Journal of Geophysical Research: Oceans, 117*(C3).
112. Lovelock, C. E., Cahoon, D. R., Friess, D. A., Guntenspergen, G. R., Krauss, K. W., Reef, R., ... & Saintilan, N. (2015). The vulnerability of Indo-Pacific mangrove forests to sea-level rise. *Nature, 526*, 559- 563.
113. Lu X., Kummu M., Oeurng C. (2014). Reappraisal of sediment dynamics in the LMB, Cambodia. *Earth Surface Processes and Landforms, 39(14)*:1855-1865.

114. Malarkey, J., Baas, J. H., Hope, J. A., Aspden, R. J., Parsons, D. R., Peakall, J., ... & Bass, S. J. (2015). The pervasive role of biological cohesion in bedform development. *Nature communications, 6*, 6257.
115. Molden, D. (2013). Water for food water for life: A comprehensive assessment of water management in agriculture. Routledge.
116. Manh, N.V., Dung, N.V., Hung, N.N., Merz, B., & Apel, H. (2014). Large-scale quantification of suspended sediment transport and deposition in the Mekong Delta. *Hydrology and Earth System Sciences Discussions, 11*(4).
117. Manh, N.V, Dung, N. V., Hung, N. N., Kummu, M., Merz, B., & Apel, H. (2015). Future sediment dynamics in the Mekong Delta floodplains: Impacts of hydropower development, climate change and sea level rise. *Global and Planetary Change, 127*, 22-33.
118. Manning, A. J., Friend, P. L., Prowse, N., & Amos, C. L. (2007). Estuarine mud flocculation properties determined using an annular mini-flume and the LabSFLOC system. *Continental Shelf Research, 27*(8), 1080-1095.
119. Manning, A. J., Baugh, J. V., Spearman, J. R., & Whitehouse, R. J. (2010). Flocculation settling characteristics of mud: sand mixtures. *Ocean dynamics, 60*(2), 237-253.
120. Manning, A. J., Baugh, J. V., Soulsby, R. L., Spearman, J. R., & Whitehouse, R. J. S. (2011a). Cohesive sediment flocculation and the application to settling flux modelling. *Sediment Transport*, 91-116.
121. Manning, A. J., Baugh, J. V., Spearman, J. R., Pidduck, E. L., & Whitehouse, R. J. (2011b). The settling dynamics of flocculating mud-sand mixtures: Part 1—Empirical algorithm development. *Ocean Dynamics, 61*(2-3), 311-350.
122. Marchesiello, P., Nguyen, N.M., Gratiot, N., Loisel, H., Anthony, E.J. and Nguyen, T., 2019. Erosion of the coastal Mekong Delta: Assessing natural against man induced processes. *Continental Shelf Research, 181*, 72-89.
123. Martins R., Leandro J., Djordjevic S. (2018). Wetting and drying numerical treatments for the Roe Riemann scheme. Journal of Hydraulic Research, 56(2), 256-267.
124. May R., Jinno K., Tsutsumi A. (2011). Influence of flooding on groundwater flow in central Cambodia. *Environmental Earth Sciences, 63*(1), 151-161.

125. Mchannelly, W. H., Friedrichs, C., Hamilton, D., Hayter, E., Shrestha, P., Rodriguez, H., ... & ASCE Task Committee on Management of Fluid Mud. (2007). Management of fluid mud in estuaries, bays, and lakes. I: Present state of understanding on character and behavior. *Journal of Hydraulic Engineering, 133*(1), 9-22.
126. McLachlan, R. L., Ogston, A. S., & Allison, M. A. (2017). Implications of tidally - varying bed stress and intermittent estuarine stratification on fine-sediment dynamics through the Mekong's tidal river to estuarine reach. *Continental Shelf Research, 147*, 27-37.
127. Medeiros S.C., Hagen S.C. (2013). Review of wetting and drying algorithms for numerical tidal flow models. *International Journal for Numerical Methods in Fluids, 71*(4), 473-487.
128. Mehta, A. J. (1991). Understanding fluid mud in a dynamic environment. *Geo-Marine Letters, 11*(3-4), 113-118.
129. Minderhoud, P. S. J., Coumou, L., Erban, L. E., Middelkoop, H., Stouthamer, E., & Addink, E. A. (2018). The relation between land use and subsidence in the Vietnamese Mekong delta. *Science of The Total Environment, 634*, 715-726.
130. Minderhoud, P. S. J., Coumou, L., Erkens, G., Middelkoop, H., & Stouthamer, E. (2019). Mekong delta much lower than previously assumed in sea-level rise impact assessments. *Nature communications, 10*(1), 1-13.
131. Molden, D. (2013). *Water for food water for life: A comprehensive assessment of water management in agriculture*. Routledge.
132. MRC website, available at http://www.mrcmekong.org/.
133. MRC (2004). *Progress In Water Management at the River Basin Level: Mekong River Basin*. Available at https://www.riob.org/en/file/264414/download?token=bzMrPwUO.
134. MRC (2005). *Overview of the Hydrology of the Mekong Basin*, *Tech. Rep*; MRC, Vientiane, Laos. Available at http://www.mekonginfo.org/assets/midocs/0001968-inland-waters-overview-of-the-hydrology-of-the-mekong-basin.pdf.
135. MRC (2009). *Flow of the Mekong. MRC Management Information booklet series No. 2*. Available at http://www.mrcmekong.org/assets/Publications/report-management-develop/MRC-IM-No2-the-flow-of-the-mekong.pdf.

136. MRC (2013). *2013 Lower Mekong Regional Water Quality Monitoring Report*. MRC Technical Paper No. 51. Mekong River Commission, Vientiane, 63 pp.
137. MRC (2015). *Annual Mekong Flood Report 2011*, Mekong River Commission, Phnom Phenh.
138. MRC (2015). *Development of Guidelines for Hydropower Environmental Impact Mitigation and Risk Management in the Lower Mekong Mainstream and Tributaries*. Mekong River Commission, 88pp.
139. MRC (2017). *The Mekong River Commission*. Vientiane: Lao PDR, http://www.mrcmekong.org/topics/flood-and-drought/, accessed 1 Aug. 2017.
140. MRC (2018). *State of the Basin*. Mekong River Commission. Available at http://www.mrcmekong.org/assets/Publications/SOBR-v8_Final-for-web.pdf.
141. Mikkelsen, O. A., Hill, P. S., & Milligan, T. G. (2006). Single-grain, microfloc and macrofloc volume variations observed with a LISST-100 and a digital floc camera. *Journal of Sea Research, 55*(2), 87-102.
142. Milliman, J. D., & Meade, R. H. (1983). World-wide delivery of river sediment to the oceans. *Journal of Geology, 91*(1), 1-21.
143. Nash, J.E. and Sutcliffe, J.V. (1970). River flow forecasting through conceptual models - Part I—A discussion of principles. *Journal of Hydrology, 10*(3), 282-290.
144. Nguyen, A.D. and Savenije, H.H.G. (2006). Salt intrusion in multi-channel estuaries: a case study in the Mekong Delta, Vietnam. *Natural Hazards and Earth System Sciences, 3*(2), 499-527.
145. Nguyen, T. T., Némery, J., Gratiot, N., Garnier, J., Strady, E., Tran, V. Q., ... & Aimé, J. (2019). Phosphorus adsorption/desorption processes in the tropical Saigon River estuary (Southern Vietnam) impacted by a megacity. *Estuarine, Coastal and Shelf Science, 227*, 106321.
146. Nhan, N. H. (2016). Tidal regime deformation by sea level rise along the coast of the Mekong Delta. *Estuarine, Coastal and Shelf Science, 183*, 382-391.
147. Nielsen C., Apelt C. (2003). Parameters affecting the performance of wetting and drying in a two-dimensional finite element long wave hydrodynamic model. *Journal of Hydraulic Engineering, 129*(8), 628-636.

148. Nikuradse, J. (1950). *Laws of flow in rough pipes* (p. 1292). Washington: National Advisory Committee for Aeronautics.
149. Nittrouer, C. A., DeMaster, D. J., Eidam, E. F., Nguyen, T. T., Liu, J. P., Ogston, A. S., & Phung, P. V. (2017). The Mekong continental shelf: The primary sink for deltaic sediment particles and their passengers. *Oceanography, 30*(3), 60-70.
150. Oeurng, C., Cochrane, T. A., Chung, S., Kondolf, M. G., Piman, T., & Arias, M. E. (2019). Assessing climate change impacts on river flows in the Tonle Sap Lake Basin, Cambodia. *Water, 11*(3), 618.
151. Parsons, D. R., Schindler, R. J., Hope, J. A., Malarkey, J., Baas, J. H., Peakall, J., ... & Aspden, R. J. (2016). The role of biophysical cohesion on subaqueous bed form size. *Geophysical research letters, 43*(4), 1566-1573.
152. Penny D. (2006). The Holocene history and development of the Tonle Sap, Cambodia. *Quaternary Science Reviews, 25*(3-4), 310-322.
153. Peteuil, C., Frétaud, T., Wirz, C., Camenen, B., Guertault, L., Le Coz, J., & Dramais, G. (2014). Importance of field observation for managing sediment fluxes in hydropower projects design and operation. In *Proceedings of the 19th IAHR-APD Congress*, Hanoi, Vietnam.
154. Piman, T., & Shrestha, M. (2017). *Case study on sediment in the Mekong River basin: Current state and future trends*. UNESCO and Stockholm Environment Institute (SEI).
155. Pham Van C., de Brye B., Deleersnijder E., Hoitink A.J.F., Sassi M., Spinewine B., Hidayat H., Soares-Frazão S. (2016). Simulations of the flow in the Mahakam river – lake- delta system, Indonesia. *Environmental Fluid Mechanics, 16*(3), 603-633.
156. Rauen, W. B., Lin, B., & Falconer, R. A. (2009). Modelling dynamic bed roughness associated with bed form development. In *Advances in Water Resources and Hydraulic Engineering* (pp. 865-870). Springer, Berlin, Heidelberg.
157. Remacle J.F. and Lambrechts J. (2018). Fast and robust mesh generation on the sphere Application to coastal domains. *Computer-Aided Design, 103*, 14-23.
158. Renaud, F. G., & Kuenzer, C. (Eds.). (2012). *The Mekong Delta system: Interdisciplinary analyses of a river delta*. Springer Science & Business Media.

159. Ribolzi, O., Evrard, O., Huon, S., Rouw, A. De, Silvera, N., Latsachack, O., Soulileuth, B., Lefèvre, I., Pierret, A., 2017. From shifting cultivation to teak plantation: effect on overland flow and sediment yield in a montane tropical catchment. *Scientific Reports, 7*, 1–12.
160. Rijn, L. C. V. (1984). Sediment transport, part II: suspended load transport. *Journal of Hydraulic Engineering, 110*(11), 1613-1641.
161. Royal Haskoning, Deltares, UNESCO - IHE (2010). *The Flood Management and Mitigation Programme, Component 2: Structural Measures and Flood Proofing in the Lower Mekong Basin, Final Report*, *Volume 6C Integrated Flood Risk Management Plan for the West Bassac area in Cambodia*. Mekong River Commission, Phnom Phenh.
162. Rouse, H. (1937). Modern conceptions of the mechanics of fluid turbulence. *Trans ASCE, 102*, 463-505.
163. Santini, W., Camenen, B., Coz, J. L., Vauchel, P., Guyot, J. L., Lavado, W., ... & Espinoza Villar, R. (2019). An index concentration method for suspended load monitoring in large rivers of the Amazonian foreland. *Earth Surface Dynamics, 7*(2), 515-536.
164. Schindler, R. J., Parsons, D. R., Ye, L., Hope, J. A., Baas, J. H., Peakall, J., ... & Paterson, D. M. (2015). Sticky stuff: Redefining bedform prediction in modern and ancient environments. *Geology, 43*(5), 399-402.
165. Schmitt, R. J. P., Rubin, Z., & Kondolf, G. M. (2017). Losing ground-scenarios of land loss as consequence of shifting sediment budgets in the Mekong Delta. *Geomorphology, 294*, 58-69.
166. Schmitt, R. J. P., Bizzi, S., Castelletti, A., Opperman, J. J., & Kondolf, G. M. (2019). Planning dam portfolios for low sediment trapping shows limits for sustainable hydropower in the Mekong. *Science Advances, 5*(10), eaaw2175.
167. Schelske, C. L. (2006). Comment on the origin of the “fluid mud layer” in Lake Apopka, Florida. *Limnology and Oceanography, 51*(5), 2472-2480.
168. Seah, K. C., Qasim, G. H., Hong, Y. S., Kim, E., Kim, K. T., & Han, S. (2017). Assessment of colloidal copper speciation in the Mekong River Delta using diffusive gradients in thin film techniques. *Estuarine, Coastal and Shelf Science, 188*, 109-115.
169. Sequioa. LISST-Portable|XR User's Manual Version 1.2 (2016).

170. Sime, L. C., Ferguson, R. I., & Church, M. (2007). Estimating shear stress from moving boat acoustic Doppler velocity measurements in a large gravel bed river. *Water Resources Research, 43*(3).
171. Simmons, B., Woog, R., Dimitrov, V. (2007). Living on the edge: A Complexity-Informed exploration of the human–water relationship. *World Futures, 63*(3-4), 275-285.
172. Smagorinsky, J. (1963). General circulation experiments with the primitive equations: I. The basic experiment. *Monthly weather review, 91*(3), 99-164.
173. Smardon, R. (2009). Restoration of the Tram Chim National Wildlife Preserve, Vietnam. *Sustaining the World's Wetlands*, 153–178.
174. Sottolichio, A., Hurther, D., Gratiot, N., Bretel, P., 2011. Acoustic turbulence measurements of near-bed suspended sediment dynamics in highly turbid waters of a macrotidal estuary. *Continental Shelf Research, 31*, 36-49.
175. Spearman, J., & Manning, A. J. (2008). On the significance of mud transport algorithms for the modelling of intertidal flats. In *Proceedings in Marine Science* (Vol. 9, pp. 411-430). Elsevier.
176. Stokes, G. G. (1857). On the effect of wind on the intensity of sound. *Brit. Assoc. Report,* 22.
177. Syvitski, J. P., Kettner, A. J., Overeem, I., Hutton, E. W., Hannon, M. T., Brakenridge, G. R., ... & Nicholls, R. J. (2009). Sinking deltas due to human activities. *Nature Geoscience, 2*(10), 681-686.
178. Ta, T. K. O., Nguyen, V. L., Tateishi, M., Kobayashi, I., Tanabe, S., & Saito, Y. (2002). Holocene delta evolution and sediment discharge of the Mekong River, southern Vietnam. *Quaternary Science Reviews, 21*(16-17), 1807-1819.
179. Takagi, H., Thao, N. D., & Esteban, M. (2014). Tropical cyclones and storm surges in Southern Vietnam. *In Coastal Disasters and Climate Change in Vietnam* (pp. 3-16). Elsevier.
180. Takagi, H., Thao, N. D., & Anh, L. T. (2016). Sea-level rise and land subsidence: impacts on flood projections for the Mekong Delta's largest city. *Sustainability, 8*(9), 959.
181. Tamura, T., Horaguchi, K., Saito, Y., Nguyen, V.L., Tateishi, M., Ta, T.K.O., ... Watanabe, K. (2010). Monsoon-influenced variations in morphology and sediment of a mesotidal beach on the Mekong River delta coast. *Geomorphology, 116*(1-2), 11-23.

182. Thacker W.C. (1981). Some exact solutions to the nonlinear shallow-water wave equations. *Journal of Fluid Mechanics, 107*, 499-508.
183. Thanh V.Q., Reyns J., Wackerman C., Eidam E.F., Roelvink D. (2017). Modelling suspended sediment dynamics on the subaqueous delta of the Mekong River. *Continental Shelf Research, 147*, 213-230.
184. Toorman, E.A., Anthony, E., Augustinus, P.G.E.F., Gardel, A., Gratiot, N., Homenauth, O., Huybrechts, N., Monbaliu, J., Moseley, K., Naipal, S. 2018. Interaction of mangroves, coastal hydrodynamics and morphodynamics along the coastal fringes of the Guianas. *Coastal research library series*, Springer book, pp 429-473.
185. Tran Anh, D., Hoang, L., Bui, M., Rutschmann, P. (2018). Simulating future flows and salinity intrusion using combined one-and two-dimensional hydrodynamic modelling—the case of Hau River, Vietnamese Mekong Delta. *Water 10*(7), 897.
186. Tran, D. D., Van Halsema, G., Hellegers, P. J., Hoang, L. P., Tran, T. Q., Kummu, M., & Ludwig, F. (2018). Assessing impacts of dike construction on the flood dynamics of the Mekong Delta. *Hydrology and Earth System Sciences, 22*(3).
187. Tran, T.D., Chorda, J., Laurens, P., Cassan, L. (2016). Modelling nature-like fishway flow around unsubmerged obstacles using a 2D shallow water model. *Environmental Fluid Mechanics, 16*(2), 413-428.
188. Tri, V. K. (2012). Hydrology and hydraulic infrastructure systems in the Mekong Delta, Vietnam. In *The Mekong Delta System* (pp. 49-81). Springer, Dordrecht.
189. Triet, N.V.K., Nguyen, V.D., Fujii, H., Kummu, M., Merz, B., Apel, H. (2017). Has dyke development in the Vietnamese Mekong Delta shifted flood hazard downstream?. *Hydrology and Earth System Sciences, 21*(8), 3991.
190. Truong, S.H., Ye, Q., and Stive, M.J.F. (2017). Estuarine mangrove squeeze in the Mekong Delta, Vietnam. *Journal of Coastal Research, 33*(4), 747–763.
191. Udo, K., & Mano, A. (2011). Application of Rouse's Sediment Concentration Profile to Aeolian Transport: Is the suspension system for sand transport in air the same as that in water?. *Journal of Coastal Research, S1 64*, 2079-2083.

192. UN Vietnam (2020, March 25). Drought and Saltwater Intrusion in the Mekong Delta – Flash Update No. 3. Retrieved from https://vietnam.un.org/index.php/en/38962-flash-update-no-3-drought-and-saltwater-intrusion-mekong-delta
193. Uncles, R. J., Stephens, J. A., & Law, D. J. (2006). Turbidity maximum in the macrotidal, highly turbid Humber Estuary, UK: Flocs, fluid mud, stationary suspensions and tidal bores. *Estuarine, Coastal and Shelf Science, 67*(1-2), 30-52.
194. Vallaeys V., Kärnä T., Delandmeter P., Lambrechts J., Baptista A.M., Deleersnijder E., and Hanert E. (2018). Discontinuous Galerkin modeling of the Columbia Rivers coupled estuary plume dynamics. *Ocean Modelling, 124*, 111-124.
195. Van, L. A., & Van Bang, D. P. (2013). Hindered settling of sand–mud flocs mixtures: From model formulation to numerical validation. *Advances in Water Resources, 53*, 1-11.
196. Van, P.D.T., Popescu, I., Van Griensven, A., Solomatine, D.P., Trung, N.H., Green, A. (2012). A study of the climate change impacts on fluvial flood propagation in the Vietnamese Mekong Delta. *Hydrology and Earth System Sciences, 16*(12), 4637–4649.
197. Van Leussen, 1994. Estuarine macroflocs and their role in fine-grained sediment transport. Ph.D. thesis, University of Utrecht, The Netherlands.
198. Vanoni, V. A. (1946). Transportation of suspended sediment by water. *Trans. of ASCE, 111*, 67-102.
199. Varis, O., Kummu, M., & Salmivaara, A. (2012). Ten major rivers in monsoon Asia-Pacific: An assessment of vulnerability. *Applied Geography, 32*(2), 441-454.
200. Vater S, Beisiegel N, Behrens J (2015) A limiter-based well-balanced discontinuous Galerkin method for shallow-water flows with wetting and drying: One-dimensional case. *Advances in Water Resources, 85*,1-13.
201. Västilä, K., Kummu, M., Sangmanee, C., Chinvanno, S. (2010). Modelling climate change impacts on the flood pulse in the Lower Mekong floodplains. *Journal of Water and Climate Change, 1*(1), 67-86.
202. Villaret, C., Hervouet, J.M., Kopmann, R., Merkel, U., Davies, A.G. (2013). Morphodynamic modeling using the Telemac finite-element system. *Computers & Geosciences, 53*, 105-113.
203. Vincent D., Karatekin O., Vallaeys V., Hayes A.G., Mastrogiuseppe M., Notarnicola C., Dehant V., Deleersnijder E. (2016). Numerical study of

tides in Ontario Lacus, a hydrocarbon lake on the surface of the Saturnian moon Titan. *Ocean Dynamics, 66*(4), 461-482.

204. Vörösmarty, C. J., McIntyre, P. B., Gessner, M. O., Dudgeon, D., Prusevich, A., Green, P., ... & Davies, P. M. (2010). Global threats to human water security and river biodiversity. *Nature, 467*(7315), 555.
205. Vu, T.T., Nguyen, P.K., Chua, L.H., Law, A.W. (2015). Two-dimensional hydrodynamic modelling of flood inundation for a part of the Mekong River with TELEMAC-2D. *International Journal of Environment and Climate Change, 5*(2), 162-175.
206. Walling, D. E. (2009). The sediment load of the Mekong River. In *The Mekong* (pp. 113-142). Academic Press.
207. Warner J.C., Defne Z., Haas K., Arango H.G. (2013). A wetting and drying scheme for ROMS. *Computers & Geosciences, 58*, 54-61.
208. Ward J.V., Tockner K., Schiemer F. (1999). Biodiversity of floodplain river ecosystems: ecotones and connectivity. *River Research and Applications, 15*(13), 125-139.
209. Warmink, J. J., Van der Klis, H., Booij, M. J., & Hulscher, S. J. (2011). Identification and quantification of uncertainties in a hydrodynamic river model using expert opinions. *Water resources management*, 25(2), 601-622.
210. Wassmann, R., Phong, N. D., Tho, T. Q., Hoanh, C. T., Khoi, N. H., Hien, N. X., ... & Tuong, T. P. (2019). High-resolution mapping of flood and salinity risks for rice production in the Vietnamese Mekong Delta. *Field Crops Research, 236*, 111-120.
211. Wendling, V., Gratiot, N., Legout, C., Droppo, I. G., Coulaud, C., & Mercier, B. (2015). Using an optical settling column to assess suspension characteristics within the free, flocculation, and hindered settling regimes. *Journal of Soils and Sediments, 15*(9), 1991-2003.
212. Wheater H., Evans E. (2009). Land use, water management and future flood risk. *Land Use Policy, 26*, 251-264.
213. Windt, C., Ebrahimian, A., & Traver, R. Flow Characterization of Stormwater Runoff in Philadelphia. In *World Environmental and Water Resources Congress 2017* (pp. 365-371).
214. Winterwerp, J. C. (2002). On the flocculation and settling velocity of estuarine mud. *Continental Shelf Research, 22*(9), 1339-1360.

215. Winterwerp, J. C. (2011). Fine sediment transport by tidal asymmetry in the high-concentrated Ems River: indications for a regime shift in response to channel deepening. *Ocean Dynamics, 61*(2-3), 203-215.
216. Wolanski, E., Huan, N. N., Nhan, N. H., & Thuy, N. N. (1996). Fine-sediment dynamics in the Mekong River estuary, Vietnam. *Estuarine, Coastal and Shelf Science, 43*(5), 565-582.
217. Wolanski, E., Nhan, N. H., & Spagnol, S. (1998). Sediment dynamics during low flow conditions in the Mekong River estuary, Vietnam. *Journal of Coastal Research, 14*(2), 472-482.
218. World Bank (2019). *Vietnam: Toward a Safe, Clean and Resilient Water System*. Washington DC. Available at https://openknowledge.worldbank.org/handle/10986/31770.
219. Wright, L. D. (1978). River deltas. In *Coastal sedimentary environments* (pp. 5-68). Springer, NY.
220. WUP-JICA (2004) Vol. II: *Supporting Report, Paper IV: Development of Hydro-Hydraulic Model for the Cambodian Floodplains. Final report*. JICA, Japan.
221. Xing, F., Meselhe, E. A., Allison, M. A., & Weathers III, H. D. (2017). Analysis and numerical modeling of the flow and sand dynamics in the lower Song Hau channel, Mekong Delta. *Continental Shelf Research, 147*, 62-77.
222. Xue, Z., Liu, J.P., DeMaster, D., Van Nguyen, L., Ta, T.K.O., 2010. Late Holocene evolution of the Mekong subaqueous delta, southern Vietnam. *Marine Geology 269*(1-2), 46–60.
223. Yamazaki, D., Sato, T., Kanae, S., Hirabayashi, Y., & Bates, P. D. (2014). Regional flood dynamics in a bifurcating mega delta simulated in a global river model. *Geophysical Research Letters, 41*(9), 3127-3135.
224. Yuan D., Lin B., Falconer R. (2008). Simulating moving boundary using a linked groundwater and surface water flow model. *Journal of Hydrology, 349*(3-4), 524-535.
225. Zoccarato, C., Minderhoud, P. S., & Teatini, P. (2018). The role of sedimentation and natural compaction in a prograding delta: insights from the mega Mekong delta, Vietnam. *Scientific reports, 8*(1), 11437.